The Dissertation Committee for Min Naing Lwin
certifies that this is the approved version of the following dissertation:

Model-Based Dynamic Relaying for Power System Protection Under Uncertainty

Committee:

Surya Santoso, Supervisor

Ross Baldick

Jonathan Valvano

Joydeep Ghosh

Eric Bickel

Model-Based Dynamic Relaying for Power System Protection Under Uncertainty

by

Min Naing Lwin, B.S.; M.S.E.

DISSERTATION

Presented to the Faculty of the Graduate School of

The University of Texas at Austin

in Partial Fulfillment

of the Requirements

for the Degree of

DOCTOR OF PHILOSOPHY

THE UNIVERSITY OF TEXAS AT AUSTIN

May 2017

Dedicated to my wife Teresa and my son William.

Acknowledgments

I wish to thank the numerous people who have helped me throughout my career. First and foremost, I would like to express my gratitude to my supervisor Professor Surya Santoso for his advice, mentorship, and dedication to improving my critical thinking, presentation and writing skills. I would also like to thank Dr. Ross Baldick for his valuable guidance and all my committee members, Dr. Jonathan Valvano, Dr. Joydeep Ghosh, and Dr. Eric Bickel, for agreeing to serve on my committee and providing their important suggestions and input. I am also grateful to Dr. Ned Dimitrov for his guidance and input on my research.

I am fortunate to have had the opportunity to collaborate with great colleagues during my academic career including Dr. Anamika Dubey, Dr. Swagata Das, Dr. Saurabh Kulkarni, Dr. Pisitpol Chirapongsananurak, Dr. Duehee Lee, Dr. Tong Zhang, Jules Campbell, Jia Guo, Tuan Ngo, Kyung Woo Min, Harsha Padullaparti, Miguel Hernandez and Piyapth Siraponsophon.

I am also sincerely grateful to my family and friends for their continuous encouragement and support. In particular, I would like to thank my parents Yan and Yee Lwin for their sacrifices and dedication. I am especially grateful to my wife Teresa, who has been a source of unyielding support and encouragement.

Model-Based Dynamic Relaying for Power System Protection Under Uncertainty

Publication No. _____

Min Naing Lwin, Ph.D.
The University of Texas at Austin, 2017

Supervisor: Surya Santoso

Several major cascading outages have involved mis-operation or mis-coordination of protective relays during stressed system conditions that resulted in a vulnerable network. Such stressed conditions include concurrent high load demand, changes in circuit topology, equipment outages, and short-circuit faults. With levels of wind and photovoltaic (PV) generation projected to increase in the future, large-scale variable generation also presents an additional point of vulnerability to the existing protection system. In this work, a new framework is introduced that is built on model-based distributed relay intelligence. The framework integrates real-time measurements from adjacent buses and predictive circuit models embedded in relays. The data collected by the relay is input to circuit simulations in order to accurately predict possible fault conditions at the relay location. Settings can then be adapted in real-time based on prevailing system conditions. Several scenarios are evaluated

to demonstrate the effectiveness of this approach. This work further develops a probabilistic formulation of optimal relay characteristics that adapts to the randomness and uncertainty introduced by renewable generation. In this framework, the calculation of relay operating times is formulated as a stochastic optimization problem. In addition, at the system level, a mixed-integer linear program is developed for protective device and switch allocation considering intentional islanding with distributed generation in distribution systems.

Table of Contents

List of Tables

List of Figures

Chapter 1

Introduction

Protective relays play a critical role in the power system at all levels, including power generation, transmission, and distribution. Because these devices control the actuation of circuit breakers, relays must operate with high reliability and selectively isolate faulted sections. Furthermore, existing power systems are growing in complexity and are operating with more uncertainty due to increasing renewable generation. This chapter presents the motivation and background for leveraging increased computational power to enhance the reliability and security of protective relay operations. The chapter concludes with an outline of the research objectives and a description of the specific research approaches to address the objectives and their contributions.

1.1 Background and Motivation

The ability of protective relays to accurately identify and quickly isolate short-circuit faults is integral to maintaining a reliable and stable power system. However, it can be challenging to maintain coordination of remote backup protection, such as Zone 3 distance elements, in the presence of stressed system conditions. History has shown that several major cascading outages have involved mis-operation or

mis-coordination of protective relays [1–5]. For example, a Zone 3 mis-coordination ultimately triggered a massive cascading outage in 2003, the largest in the history of North America now called the Northeast blackout [6,7]. Similarly, in 2006, improper relay coordination was a key cause in initiating the largest blackout in Europe [8,9]. Table 1.1 and Fig. 1.1 summarize the scale of the recent major outages and the involvement of the protective relaying system as found in [10–12]. These outages demonstrate that coordination of remote backup zones in stepped-distance protection can be vulnerable during stressed conditions in which several events coincide, such as high load demand, changes in circuit topology, equipment outages, and short-circuit fault conditions. Furthermore, existing relay setting philosophies are generally biased to be more sensitive to any possible disturbances (high dependability). This approach can result in false positives (lower security) especially when the system is stressed [13]. An incorrect response by a relay during critical stressed conditions can further propagate a disturbance.

Additionally, during past major blackouts, variable generation from renewable energy resources was at a significantly lower level than at present. With levels of wind and photovoltaic (PV) generation projected only to increase in the future, e.g., 20% wind energy by the year 2030 [14–16], large-scale renewable energy generation can potentially introduce additional variation and uncertainty into system behavior. In conventional power networks, each generator's fault current contribution can be approximated as constant due to the controllable nature of the generators' output. This allows existing protection methodologies to calculate the appropriate response parameters of protective relays with high certainty in the expected worst-case fault conditions. Furthermore, because the worst-case system fault characteristics do not change significantly over time, relay settings can be static and do not need to be updated often once they have been set. However, wind and PV generation introduces

variability in power flows and short-circuit contributions not present in classical power networks. Wind and PV are characterized by variable output, minimal inertia, and fault current contribution that varies with the output [17–19]. Therefore, classical protection methodologies with static relay settings in the presence of high wind and PV penetration can lead to mis-coordination and unintended operations. Although state-of-the-art protection schemes utilizing phasor measurement units (PMUs) and adaptive relaying [4, 20] have made efforts to alleviate these issues, power system protection theory has lagged the pace of grid development and renewable integration. Furthermore, existing solutions aim at solving issues individually as they are encountered.

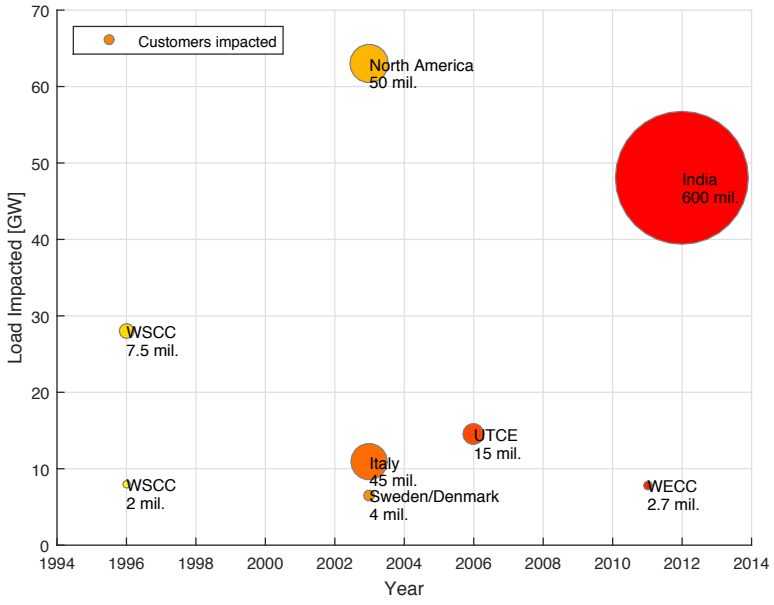

Figure 1.1: Scale of recent major outages worldwide in terms of load and customers impacted.

Table 1.1: Summary of protection system involvement in major outages

Location	Date	System Loading Prior to Outage	Event Trigger	Misoperation Type	Protective Element
Northeast	Nov. 9, 1965	Only a few lines heavily loaded	Load encroachment	Improper relay settings	Distance
WSCC	Jul. 2, 1996	High demand and large power flows due to hot weather	Tree contact	Zone 3	Distance
WSCC	Aug. 10, 1996	High demand and large power flows due to hot weather	Tree contact	Improper application	Directional phase overcurrent
North America	Aug. 14, 2003	Large power flows due to generator trip	Load encroachment	Zone 3	Distance
Sweden/Denmark	Sep. 23, 2003	Moderate loading of system	Trip of large power plant	N/A	N/A
Italy	Sep. 28, 2003	Critical lines heavily loaded	Tree contact	N/A	N/A
UTCE	Nov. 4, 2006	Critical lines heavily loaded	Load encroachment	Improper relay settings	Distance
WECC	Sep. 8, 2011	High loading during peak demand hours	Voltage instability	Coordination and Zone 3	Distance
India	Jul. 30/31, 2012	Large power flows due to unscheduled interchanges and forced outages	Load encroachment and Fault	Zone 3	Distance

Moreover, conventional power system protection approaches consider completely dispatchable generation, central management of static relay settings, and relays without capabilities for real-time awareness of system topology changes or large-scale generation swings [21, 22]. The primary purpose of protective relaying is to quickly detect faults in the protected zone and isolate the faulted section by opening a circuit breaker. There are several relay functions which help accomplish this goal, however, in this work, the focus will be on two of the most common: distance and overcurrent relays. Distance relays use local voltage and current measurements to calculate apparent impedance, allowing detection of faults in the complex impedance plane. The relay coverage is divided into zones and the coverage of each zone is calculated by a predetermined percentage of the line impedance, as shown in Fig. 1.2. Overcurrent relays respond to the magnitude of local current measurements. Coordination between overcurrent relays is achieved by an intentional time delay that is inversely proportional to the measured current.

Remote backup protection for distance relays, such as Zone 3, is only intended to operate in the case where the primary protective device at the remote end of an adjacent transmission line fails to clear a fault. However, load flowing through a

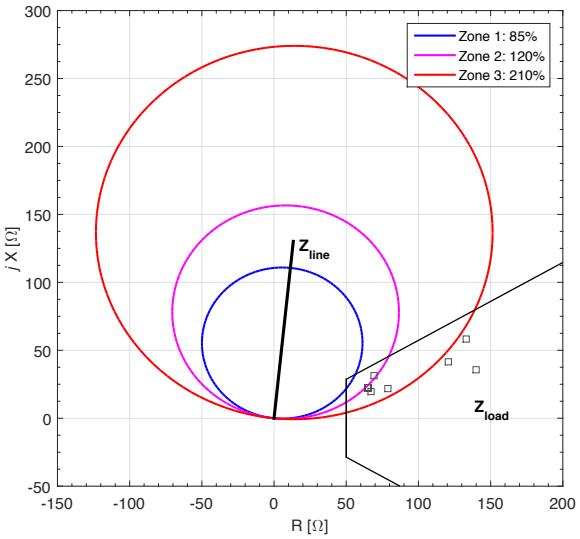

Figure 1.2: Example of relay coverage for three distance protection zones. The load encroachment is shown where the load region enters the relay's operating region.

transmission line also appears as impedance to the distance relay and is typically higher compared to the zone setting under normal loading conditions. When the network is heavily loaded, the apparent impedance can enter into the backup protection Zone 3 characteristic and trip the relay, causing an unwanted line outage. System conditions involving depressed voltages and high power flows have been a contributing cause of several major outages. Modern relays can implement specific functions to avoid tripping under conditions resembling faults (high power flows and depressed voltages), such as load encroachment blocking and power swing detection [23]. However, even with careful planning, these methods can still result in mis-coordination in complex protection schemes [13].

Recent efforts to improve remote backup protection involves utilizing wide-area measurements from phasor measurement units (PMUs). PMUs measure voltages and currents with accurate time stamping using a GPS time reference signal. These PMUs can be installed at critical locations across the power grid allowing for an operator to visualize the exact angular difference between locations in real-time and

can be used to assess system conditions such as frequency changes and power flows [4]. Some specific applications as stated in [4] include: state-estimation and real-time monitoring, voltage instability prediction, system model validation, adaptive relaying, and adaptive load shedding. PMUs can also be utilized for prevention of Zone 3 mis-operation under stressed power system conditions as shown in [20, 24].

In addition, because conventional protection relays employ static settings that are calculated from expected system conditions, settings may no longer be appropriate when distributed generation output changes, system topology changes, or fault conditions change. Therefore, adaptive relaying has been the practice of changing the relay's operating characteristics based on the present system condition. Applications of adaptive relaying utilizing phasor measurements such as adaptive out-of-step protection and the adaptive voting scheme have been reported in [20, 25] to discriminate between stable and unstable power swings. One commonly accepted method for adaptive relaying uses three relays in a voting scheme [12]. Building on this approach, [26] presents a decision tree based adaptive relaying scheme, which classifies system state using decision trees and predict the optimal security-dependability bias. These methods, however, rely on centralized analysis of system PMU measurements. This philosophy can be efficient for determining relay settings for a small number of protective devices, but a transmission network can consist of thousands of buses. In the distribution system, short-circuit faults are detected by relays that strictly measure fault current. Distributed generation can cause bidirectional power flow, resulting in mis-coordination between relays.

Determination of relay settings and coordination as part of an optimization framework was first introduced in [27]. In this formulation, the weighted sum of relay operation times in a given zone is minimized over the time-dial and pickup settings for directional overcurrent relays. Constraints are included for coordina-

tion between primary and backup relays, bounds for relay settings, and inverse-time characteristics. This framework is further developed in [28–31], where optimal settings for overcurrent relays is defined for minimum of the total sum of operating times. The problem formulation as presented in [31], is summarized below.

$$\text{Minimize} : J = \sum_{i=1}^{n} w_i t_i \tag{1.1}$$

where t_i is the time delay of relay i for a near-end fault and n is the number of relays. The weight w_i correspond to the likelihood a fault occurs in a given zone, with all weights typically set to one. The following constraint governs coordination between the primary and backup relays:

$$t_j - t_i \geq \text{CTI} \quad \forall (i,j) \in \Omega \tag{1.2}$$

where Ω is the set of primary/backup pairs of relays, with t_i and t_j being the operating times for the primary and backup relays respectively. The coordination time interval (CTI) provides the margin between primary and backup relay operating times and is typically a constant between 0.2 and 0.5 s. In general, the operating time of an overcurrent relay can be expressed as:

$$t_i = f_i(I_{fi}, I_{pui}) \times \text{TDS}_i \tag{1.3}$$

where f_i is a nonlinear function of I_{fi} and I_{pui}, I_{fi} is the fault current seen by the relay, I_{pui} is the pick-up setting of the relay, and TDS_i is the time-dial setting of the relay. A typical equation for f_i has the form:

$$f_i = \frac{1}{C}\left[\frac{A}{(\frac{I_{fi}}{I_{pui}})^2 - 1} + B\right] \times \text{TDS}_i \tag{1.4}$$

Although the above formulation and other similar methods allow for calculation of relay settings under an optimization framework, there are limitations. Their focus is to determine optimal device settings and improve upon automated approaches of the classical manual relay setting procedure. However, notably, the methods do not consider the stochastic nature of renewable energy sources or consider adaptation of settings based on real-time system conditions.

1.2 Objectives

The research presented in this dissertation aims to meet two key objectives: secure transmission protection in the presence of uncertainty introduced by stressed conditions and optimal distribution protection in the presence of renewable distributed generation. Each objective is described below.

Transmission Protection: Secure Relay Operation

The first objective focuses on secure transmission protection in the presence of uncertainty introduced by stressed conditions. The goal of this objective is to enhance security of the remote backup protection function by developing the following capabilities in individual relays: awareness of system state, real-time dynamic settings, and secure operation during stressed system conditions. With this scheme, the relay's trip or block decision is supervised and validated by real-time simulation results to maintain coordination with other relays when stressed system conditions are present. A conceptual overview of the proposed solution is illustrated in Fig. 1.3. Existing protection methods only interact between the physical, measurement, and decision layers. The proposed framework adds a supervisory relay intelligence layer to operate and supervise in real-time at the local relay level. Furthermore, the goal includes development of a prototype relay in hardware capable of implementing

the proposed protection framework.

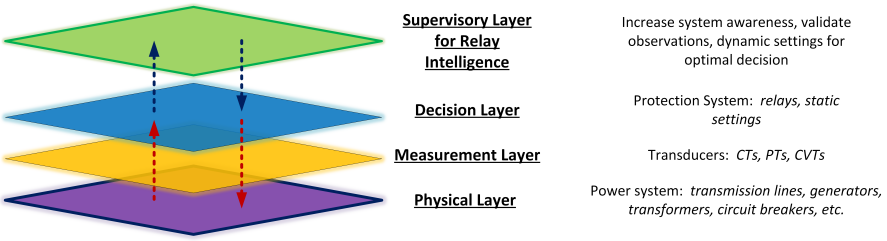

Figure 1.3: Conceptual illustration of a supervisory layer for relay intelligence.

Distribution Protection: Optimal Performance and Reliability

The second objective focuses on optimal distribution protection in the presence of renewable distributed generation. A high penetration of distributed generators (DGs) can affect fault current levels, contributing to protection coordination issues in fault detection and loss of selectivity. The first goal of this objective focuses on the device-level operating characteristics and the calculation of relay operating settings formulated as a stochastic optimization problem. The problem formulation defines a cost-based objective function that aims to minimize the impact of opening a circuit breaker given the uncertainty in the fault current observed at each relay, which can be impacted by fault location, fault resistance, breaker failure, and DG output. The optimization allows the relay to make the best possible decision based on known information (system structure and local measurements) and estimated values (non-local conditions). The second goal of this objective focuses on the system-level and the optimal allocation of protective devices in a distribution system considering intentional islanding with DGs.

1.3 Research Approach and Contributions

The specific research approaches taken to address the above objectives is organized into four areas. The first and second approaches address the objective of secure transmission protection and the third and fourth approaches address the objective of optimal distribution protection. Each approach and the associated contributions are described below.

1.3.1 Model-Based Distributed Intelligence Framework

Several major outages have been traced to the failure of remote backup protection elements in distance relays. Experience has shown that coordination of remote backup zones in stepped-distance protection can be vulnerable during stressed conditions. Furthermore, relay settings are typically biased for high dependability, resulting in lower security especially when several unexpected events coincide. An incorrect response by a relay during such a condition can trigger or propagate the disturbance. Therefore, a new framework for Model-Based Relaying is introduced to supervise and secure the operation of remote backup protection elements, such as Zone 3 [32–34].

The framework utilizes the fact that while a single relay can observe a 3-phase fault or stressed system condition with similar apparent impedances, other system parameters will be significantly different. Therefore, the framework proposes to include the capability in relays to quickly run circuit model simulations at the relay level. The proposed method aims to work in parallel with and supervise the conventional distance relay's zone 3 for discrimination between 3-phase faults and stressed conditions using the output of local circuit model simulations. Several case studies are evaluated to demonstrate that dependability is not degraded for true

fault conditions and security is enhanced for stressed system conditions.

1.3.2 Supervised Classification of Power Swings

Distance relay operation due to power swing conditions should be blocked in order to prevent unnecessary line trips leading to the formation of unplanned islands and the propagation of outages. A supervised classification approach is presented to improve the detection of symmetrical faults during power swing conditions in conventional distance relays [35]. The approach is intended to augment existing power swing blocking methods and trains a classifier with a focus on accuracy and interpretability. The contribution of the approach is the training of classifiers that maintain performance of other methods, while providing interpretable results. Training and test data is generated from time-domain simulations of the IEEE 9-Bus system for 17 280 scenarios. The following classifiers are compared and evaluated: support vector machine, random forest, gradient tree boosting, decision tree, and k-nearest neighbors. Utilizing mutual information for feature selection and only local measurements, the results show performance comparable to prior methods and provides the ability to view the decision boundary for greater understanding of the classifier output. Trade-offs between interpretability and performance are also assessed.

1.3.3 Optimal Overcurrent Relay Characteristics

The inverse-time operating characteristic of overcurrent relays is the primary protective element in distribution system protection schemes and has been utilized for several decades. As the distribution system becomes increasingly complex due to the growth of distributed generation, the protection task based on existing methodologies will become more difficult. Faster relay operating times while maintaining selectivity is critical. In this approach, a stochastic mixed-integer linear program is

formulated to minimize a relay's tripping time at discrete fault current intervals and considers the cost of tripping a relay as the objective function [36]. The formulation takes into account the probabilistic nature of the fault current observed at each relay, which can be impacted by fault location, fault resistance, device failure, and DG output. Monte Carlo simulation is used to determine the empirical probabilities of each relay observing a particular fault current. Probabilistic fault scenarios are simulated on the IEEE 34-Node test feeder. The proposed approach shows a decrease in expected energy loss due to faults up to 11.5% compared to conventional TCC curves for 10 000 Monte Carlo fault scenarios.

1.3.4 Optimal Protective Device Allocation

The location of protective devices, such as circuit breakers, reclosers, sectionalizers, and fuses, along with isolating switches in a distribution network is a key factor impacting the reliability performance. Furthermore, automatic restoration from intentional islanding with distributed generators (DGs) or from alternate feeders can reduce outage times. A mixed-integer linear program (MILP) formulation is proposed for protective device and switch allocation considering intentional islanding with distributed generation in distribution systems [37]. The specific impact of each protective device type and isolating switch is modeled, e.g., momentary interruptions caused by reclosers. Efficient graph search algorithms combined with a directed graph representation of the distribution system allows for pre-processing of the network data and facilitates the formulation of an MILP. The formulation is able to efficiently compute optimal device allocations for multiple scenarios, revealing key insights, e.g., the location and capacity of DGs providing the greatest reliability benefit for a fixed protection budget. Tests on realistic feeders and comparison with prior solutions shows improved allocations and lower objective function values.

Chapter 2

Model-Based Relaying Framework

Protective relaying is integral to maintaining power system reliability. However, it can be challenging to maintain coordination of remote backup protection zone 3 distance elements in the presence of stressed system conditions. Zone 3 misoperations occur during stressed system conditions where the measured impedance enters the operating characteristic and the relay is unable to discriminate between a 3-phase fault and a wide-area stressed condition. In part, the vulnerability lies in the fact that conventional relays only rely on local voltage and current measurements. Recent efforts in the literature have proposed using various types of wide area measurements to help make the zone 3 decision more secure. In [38], a scheme is presented where relay and breaker status of nearby lines are used to supervise zone 3. However, this requires that those remote devices operate securely. Synchrophasors are used in [39] and [40] to supervise relay decisions, however, these schemes require data to be streamed to a central location, where decisions can be directed to multiple devices. If a failure occurs at the central location, the scheme can be disabled for all relays.

In this chapter, a new framework is proposed for secure remote backup protec-

tion, utilizing only bus voltage magnitudes from adjacent buses to supervise the zone 3 decision. This is accomplished by comparing measured bus voltage magnitudes at adjacent buses and comparing with those during possible fault scenarios - with all computation done at the local relay level. The framework is termed Model-Based Distributed Intelligence (MBDI) because it integrates, at the relay level, real-time knowledge of the network structure and system state in the form of predictive circuit models. This approach takes advantage of advances in computing available to numerical relays today, such as improved processing power and communications capabilities. Under the MBDI framework, a solution is provided that can supervise relay decisions and prevent undesired relay operations. The calculation of relay operating settings is formulated with real-time measurements and the data collected by the relay is input to circuit model simulations in order to accurately predict real-time fault currents at the relay location. With this scheme, the relay's trip or block decision is supervised and validated by real-time simulation results to autonomously maintain coordination with other relays when stressed system conditions are present.

2.1 MBDI for Mitigation of Cascading Outages

Figure 2.1 presents a block diagram that compares existing methodologies to the one proposed. Under existing methodologies, the relays in Fig. 2.1a are set based on expected worse-case fault calculations that are done centrally. In Fig. 2.1b, relays are equipped with model-based distributed intelligence that reduces the uncertainty in each relay's assessment of the present system condition. It accomplishes this through the supervisory layer composed of a simulation circuit model and decision logic. The extent of the simulation model includes all adjacent buses to the relay, resulting in a total number of k buses modeled in the simulation circuit model. Any parts of the power system outside these k buses are modeled by their Thevenin

equivalent circuits. The objective of the supervisory layer is to confirm or reject the perceived system state (normal or fault) and determine optimal operating times. Measured system parameters are continuously streamed to the simulation circuit model. Under secure operation, the relay should only send a trip signal for true fault conditions in protected zones. The circuit model simulations provide an estimate of expected system values, such as voltages and power flows, at other buses in the presence of varying output. Because calculation of the relays settings are done in real-time at each individual relay under the proposed framework, the protection system can dynamically respond to changes in generation output.

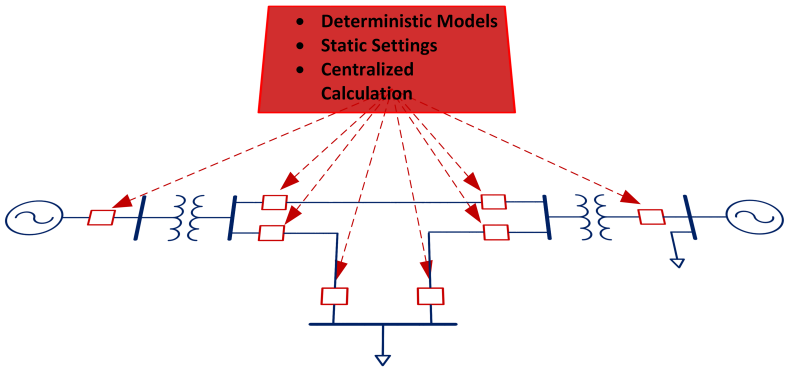

(a) centralized intelligence

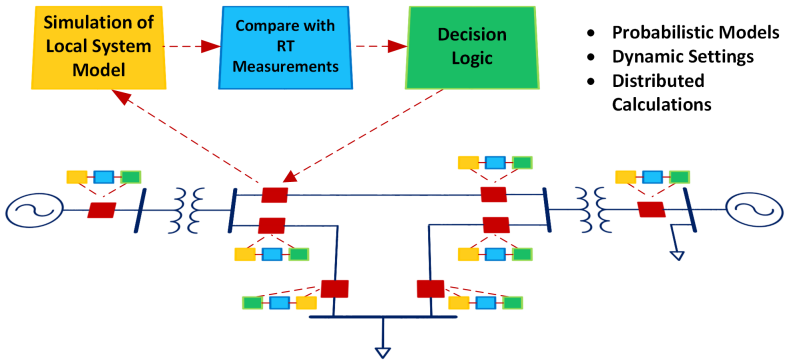

(b) distributed intelligence

Figure 2.1: Block diagrams comparing (a) centralized intelligence of existing protection schemes and (b) the proposed scheme with distributed intelligence and optimal supervisory decision logic.

In this section, the framework for integrating circuit structure information at the relay level is introduced and the results from several case studies are presented. Several fields of engineering and science have utilized system models to make decisions in real-time. For example, model-predictive control in control theory and model-based reasoning in artificial intelligence are well developed methods. In these schemes, models approximating the system are used to influence control decisions. In the area of power systems, protective relaying is a field that could immensely benefit from further development in this type of approach.

In existing protection methodologies, the backup protection element and time delay settings are determined based on the results of extensive fault studies computed on a model of the system in which the relay will be deployed. However, the system model is only a close representation of the actual system and relay settings are chosen to accommodate worst case fault scenarios and uncertainty in the model parameters [21, 22]. The proposed MBDI framework aims to decentralize or distribute the intelligence intrinsic to the system model and integrate it at the relay level to supervise remote backup protection operations. Incorporating knowledge of the circuit model at the relay level is important because circuit parameters do not change significantly across operating conditions, while power flows and voltage levels will vary with the system state (faults, stressed conditions, etc.).

Therefore, the key contribution of the MBDI framework for remote backup protection is the integration of circuit models at the relay and the ability to simulate possible fault scenarios locally using real-time measurements. MBDI further facilitates calculation of an expected system state as observed system parameters change. The simulation results for possible fault scenarios can then be compared against real-time system measurements to assess if there is a match within a specified tolerance. MBDI simulations can also include fault scenarios where relay or circuit breaker fail-

ures necessitate operation of the remote backup protection element. Subsequently, the MBDI framework is identical to existing standard industry practices for Zone 1 and Zone 2 setting, but makes use of real-time knowledge of the network structure and system state for Zone 3 operations.

A simplified flowchart of the full MBDI algorithm is presented in Fig. 2.2. For a system with N buses, let k be the bus where the MBDI relay is located, where $k \in \{1, ..., N\}$. The three-phase rms voltage and current measured at this bus is $\mathbf{V}_k$ and $\mathbf{I}_k$. Distance relays can operate on both line-to-ground or line-to-line impedances. In this study, only line-to-ground impedance is considered for simplicity and is calculated as

$$Z_{LG} = \frac{V_{phase}}{I_{phase} + kI_0} \tag{2.1}$$

where zero-sequence current $I_0 = \frac{1}{3}(I_a + I_b + I_c)$ and $k = \frac{Z_0 - Z_1}{Z_0}$ for zero-sequence and positive-sequence impedances, Z_0 and Z_1 respectively. When the MBDI relay identifies the apparent impedance entering Zone 3, the relay will start timing based on the specified time-delay setting. This part of the algorithm is the same as conventional methods, shown in the bottom left portion of Fig. 2.2a. However, potential fault scenarios are simulated using the MBDI circuit model in parallel, shown on the bottom right portion of Fig. 2.2a and Fig. 2.2b. Because Zone 3 is designed to operate for faults on the adjacent lines where primary protection has failed, MBDI first simulates faults on the adjacent line as the most likely candidate using the measured in impedance data. Note that this framework prioritizes simulation of relay or circuit breaker mis-operation scenarios to supervise Zone 3 operation.

The output of the MBDI simulations returns several parameters, however, for this study it is shown that the expected rms voltages at each Bus k, where $\hat{\mathbf{V}}_k = \left[\hat{V}_{a_k}\, \hat{V}_{b_k}\, \hat{V}_{c_k}\right]$, are sufficient to supervise Zone 3 operation. The MBDI framework

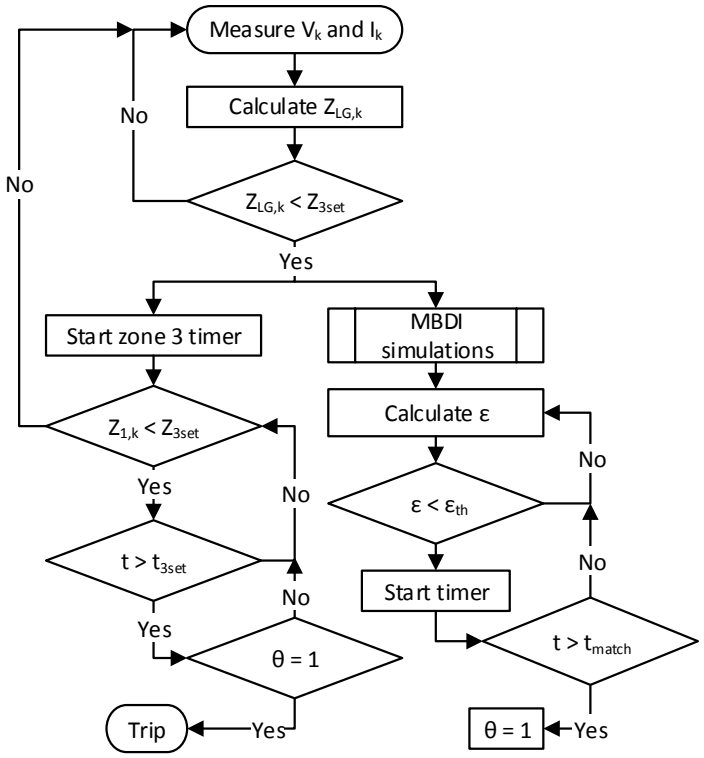

(a)

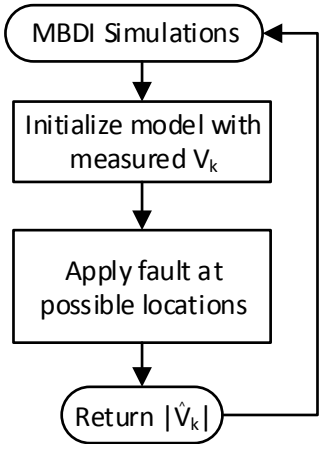

(b)

Figure 2.2: Overall flowchart of the MBDI algorithm shown in (a) and simulation subroutine in (b).

and even conventional relay setting methodologies assume the system model is a good representation of the actual system. Therefore, if Z_{LG} is observed within the Zone 3 setting, MBDI simulations of possible faults on the adjacent line should produce a match with measured bus voltages at nearby buses, $\mathbf{V}_k = [V_{a_k}\, V_{b_k}\, V_{c_k}]$, within a reasonable tolerance. The difference between the measured and expected voltages is calculated as

$$\boldsymbol{\epsilon} = \left| |\mathbf{V}_k| - |\hat{\mathbf{V}}_k| \right| \tag{2.2}$$

where $\boldsymbol{\epsilon}$ is the absolute error. The threshold or tolerance for absolute error is $\boldsymbol{\epsilon}_{th}$ and is set to 0.05pu voltage. The duration for $\boldsymbol{\epsilon}$ to be below the threshold is t_{match} and is set to 1 cycle. If these conditions are met, the flag θ is set to 1. If the bus voltages do not match or converge then $\theta = 0$ and this is an indication that observed impedance may not be a result of a fault and is possibly due to wide area stressed disturbance. Therefore, it may be wise to not trip and risk propagating the disturbance. The relay will wait momentarily until gets clearance from the MBDI module. An upper limit for the time delay associated with the MBDI module may be set such that the conventional Zone 3 logic can still operate.

2.2 Case Studies in a Small Transmission Network

2.2.1 Test System

To demonstrate the proposed scheme, a test system is developed in PSCAD/EMTDC to simulate various scenarios. The test system is chosen to allow for variety of faults and stressed condition simulations while being sufficiently simple. A proof-of-concept of the MBDI framework is achieved by running two models simultaneously in PSCAD while communicating with each other. The first model represents the

physical power system in which the MBDI relay operates. The second model represents the MBDI circuit model simulation and logic. The 5-bus test system is shown in Fig. 2.3 and consists of two generation buses (Bus 1 and Bus 3) and two load buses (Bus 2 and Bus 3). The two transformers in the system step up generation voltage from 15 kV to 345 kV for transmission. System parameters are from [41].

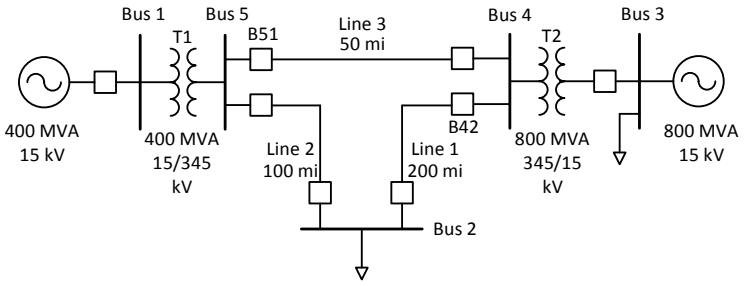

Figure 2.3: Single-line diagram of test system and validation fault scenarios.

The following assumptions are made for the MBDI algorithm above. The system structure, e.g., line configurations and impedances are considered to be fixed. Bus voltages and loads are considered variable and updated in real-time. Furthermore, it is assumed that the simulation model can determine fault location with reasonable accuracy. In this proof-of-concept, possible fault locations are determined by the apparent impedance phasor magnitude and phase angle. An intentional time delay of 3/5 cycles is added in order to model the expected delay due to the communication between adjacent buses; additional time delays are not intentionally added into the model.

2.2.2 Fault Scenarios

The test system demonstrates how an MBDI relay operates for actual faults. Only three-phase faults are applied because stressed system conditions are considered to affect three-phases simultaneously. In these scenarios, the relay is located at breaker

B51, shown in Fig. 2.3. Four fault scenarios, each a three phase-to-ground fault with negligible fault resistance, are simulated at different locations along Line 3 (5%, 50%, and 95% from Bus 5) and on Line 1 (10% from Bus 4). The locations are chosen to test operation of the MBDI framework for close-in faults, mid-line faults, faults just outside of the Zone 1 reach, and Zone 3 faults.

The validation results show that the MBDI framework correctly issues a confirmation signal for faults inside protected zones. The results for the Zone 3 fault are shown in Fig. 2.4 and 2.5. These, however, are also representative of the other fault scenarios. In Fig. 2.4a it is shown that the measured impedance enters into the Zone 3 characteristic. The MBDI relay at B51 senses the fault in Zone 3 and begins timing while simultaneously initiating the MBDI simulations shown in Fig. 2.4b. Using the measured impedance magnitude and phase angle, faults are simulated at possible locations on Line 1. In this case, because the apparent impedance magnitude is in Zone 3 with a phase angle along the transmission line, the simulated fault is applied on Line 1, between Bus 4 and Bus 2.

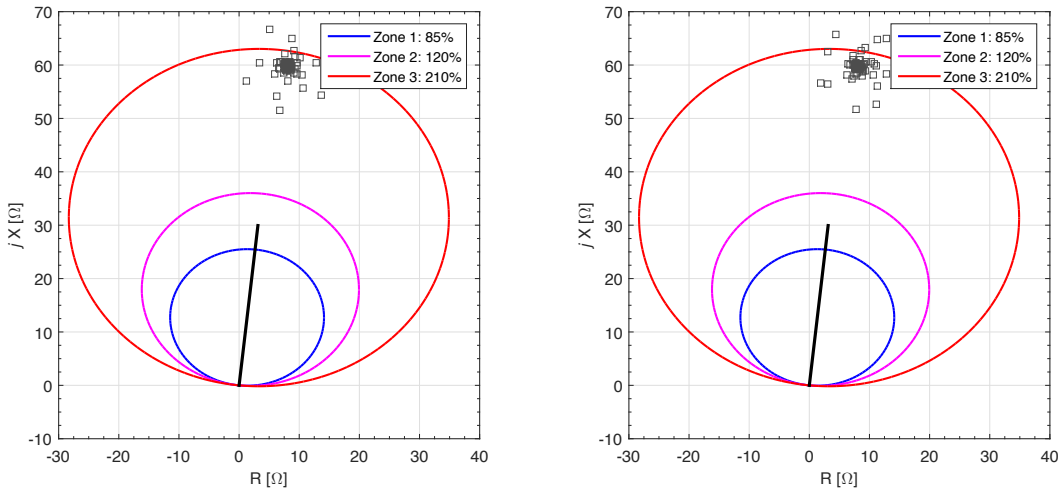

Figure 2.4: Apparent impedance comparison for Zone 3 fault scenario. MBDI simulation in (b) closely matches Zone 3 fault impedance in (a).

Figure 2.5a shows $\boldsymbol{\epsilon}$ for nearby buses 2, 4, and 5 as the simulation runs. It can be seen that the bus voltages converge below the threshold for longer than the required duration of 1 cycle as the MBDI simulation has provided a matching fault scenario. In Fig. 2.5b, Zone 3 detects a fault and picks up at approximately t = 0.22s. The MBDI simulations run in parallel and determine the correct location for the perceived fault and begins the fault simulation at approximately t = 0.23s. As the simulation progresses, the bus voltages from the simulated fault condition and measured bus voltages begin to converge. At t = 0.34s, $\boldsymbol{\epsilon}$ falls below the threshold value of 0.05 pu for longer than 1 cycle and confirms the fault condition. The MBDI module completes its assessment 130ms after Zone 3 picks up, well before a typical Zone 3 delay of 300ms.

In each of the three fault scenarios, the MBDI module is able to accurately supervise the relay's trip decision. In all cases, the differences between the measured and simulated bus voltages at Bus 2, Bus 4, and Bus 5 converge below the preset tolerance of 0.05 pu for at least 1 cycle. An important observation from the sequence of trip signals from each fault scenario is that additional time is required between the initial mho relay pickup and the MBDI module issuing a confirmation signal. The longest total duration between initial pickup and confirmation is approximately 0.23s for a mid-line fault and the shortest is 0.10s for a close-in fault. The total time duration before the supervisory layer issues the confirmation signal can be broken down into several components listed below:

- Communication time of measured values from k remote buses
- Simulation time of the circuit model
- Time to convergence between measured and simulated values below threshold
- Duration of time that convergence is maintained below threshold

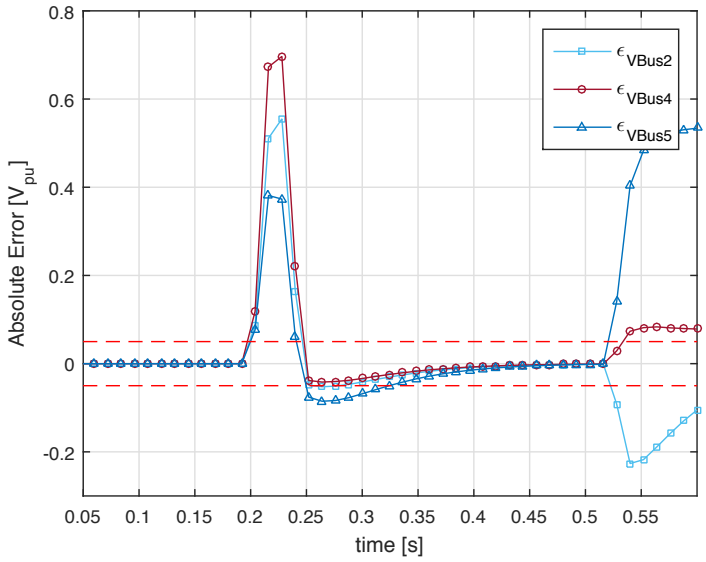

(a)

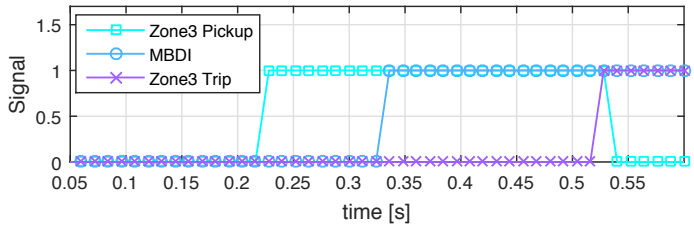

(b)

Figure 2.5: Zone 3 fault scenario: (a) Absolute error between measured and simulated bus voltages magnitudes and (b) and sequence of signals.

- Computation time in the MBDI logic

The PSCAD/EMTDC model inserts an intentional time delay in order to model the expected delay due to the communication between the relay and k adjacent buses. This is simulated in the PSCAD model as a 3/5 cycle delay between the power system model and MBDI simulation. The time delay components for circuit model simulation, convergence between measured and simulated values, and supervisory logic computation are captured as part of the PSCAD model implementation; additional time delays are not added into the model for these components. Lastly,

measured and simulated values must maintain convergence below the threshold for 1 cycle. This value is unchanged for all scenarios. Furthermore, the time durations discussed above are measured inside the PSCAD simulation. When this scheme is implemented in hardware, the time durations will also be dependent on the hardware components. In the next section, the proposed scheme will be evaluated for stressed system conditions. In those scenarios, the expected response of the supervisory layer will be to determine that a fault does not exist on the system and prevent incorrect relay trip. Differences between measured and simulated bus voltages are not expected to converge.

2.2.3 Case Studies for Stressed System Scenarios

In this section, the operation of the MBDI framework is demonstrated for stressed system conditions where conventional relays may mis-operate. Three scenarios are tested: load encroachment, voltage excursion, and high resistance fault. For each scenario, the goal is to first demonstrate how these conditions can cause a conventional relay to improperly trip. Then, the same scenario will be conducted with the relay equipped with the proposed supervisory scheme. It will be shown that a relay operating under the MBDI framework can effectively utilize simulation circuit models to supervise the relay's trip decision and provide secure operation. The section concludes with a summary of the results and a discussion of potential future work to further develop this concept.

Load Encroachment

Load encroachment has been often cited as a cause for several relay mis-operations. In general, apparent impedance at the local bus is reduced to within the operating characteristic, typically Zone 3, due to heavy loading on remote lines. In this case

study, the relay location is chosen at breaker B42 shown in Fig. 2.3. The zone reach settings for the relay at B42 are set at 85%, 120%, and 210% for Zone 1, Zone 2, and Zone 3, respectively. Load encroachment as observed by the relay at breaker B42 is simulated by incrementally increasing the load level at Bus 2. As a result, the voltage at Bus 2 decreases slowly to 0.636 pu and at Bus 4 to 0.959 pu. The depressed voltage at Bus 2 due to load encroachment is comparable to those reported in [5]. As the load draws more real power over Line 1, the apparent impedance seen at Bus 4 declines and begins to approach the Zone 3 characteristic. Note that because the load is more resistive than reactive, the apparent impedance approaches the Zone 3 characteristic with a smaller phaser angle than in the voltage excursion scenario. Load encroachment is also a long-term deviation, and again the apparent impedance enters the Zone 3 characteristic for longer than the set time delay (typically 1s or greater). A fault does not actually exist on the system, but the heavy loading on the line and reduced voltage will cause a conventional relay to trip, as shown in Fig. 2.6a.

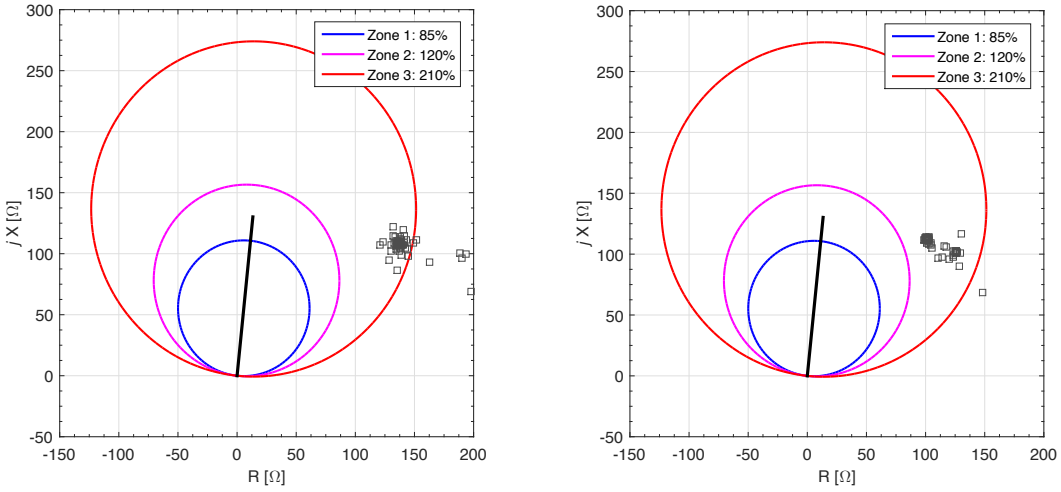

(a) (b)

Figure 2.6: Apparent impedance comparison for load encroachment scenario, with load encroachment impedance in (a) and MBDI fault simulation in (b).

The scenario is then run again with the same load encroachment condition applied at Bus 2. However, the MBDI scheme is now enabled. The overall results are shown in Figs. 2.6 and 2.7. Heavy loading on the line results in the apparent impedance entering the Zone 3 characteristic of relay distance element Fig. 2.6a and initiates the MBDI module. Impedance magnitude and phase information is used to determine possible fault locations in the simulation model. The closest match resulting from MBDI simulations is shown in Fig. 2.6b. The reactive component of the measured impedance estimates approximately the distance of the fault away from the relay and the resistive component estimates the fault resistance. In this case, the closest match occurs at a perceived fault location of 95% of Line 1, with a maximum resistance of 100 ohms. Note that an upper bound of 100 ohms provides a reasonable limit for simulated fault scenarios on a 345kV line.

Figure 2.7a shows ϵ for nearby buses 2, 4, and 5 as the simulation runs. It can be seen that, the bus voltages do not converge because the root causes of the low apparent impedances are not the same. In Fig. 2.7b, initially Zone 3 detects a fault and issues the initiation signal for MBDI simulations to run in parallel. The MBDI module determines the location for a perceived fault and begins the fault simulation at time 0.11s. As the simulation runs, the bus voltages from the simulated fault condition do not converge to the measured bus voltages because the root causes are different. As long as the load encroachment condition exists, the MBDI module will attempt to simulate possible faults that produce similar bus voltages. Consequently, a confirmatory signal is not issued. In this case, the relay operating under the MBDI framework effectively blocks an incorrect relay trip for a load encroachment at the remote bus. Tripping breaker B42 and opening Line 1 would have propagated the disturbance. However, by preventing an incorrect trip of Line 1, other relays or the operator can appropriately respond to the load encroachment and allow system

conditions to be restored.

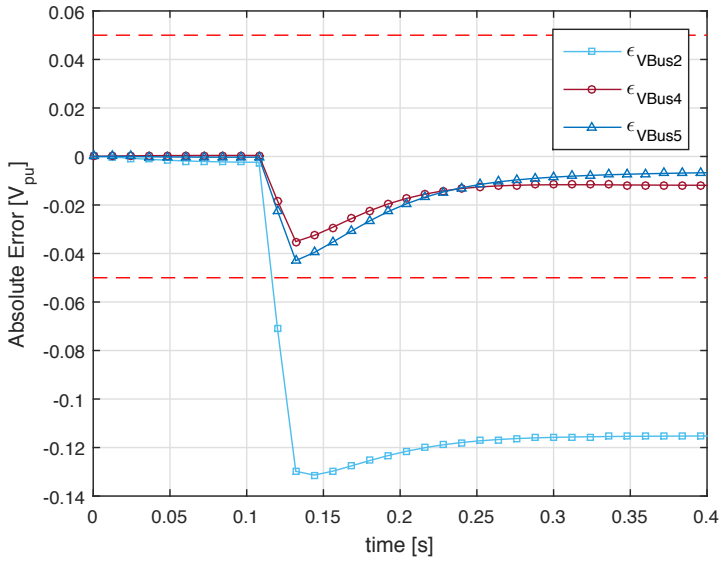

(a)

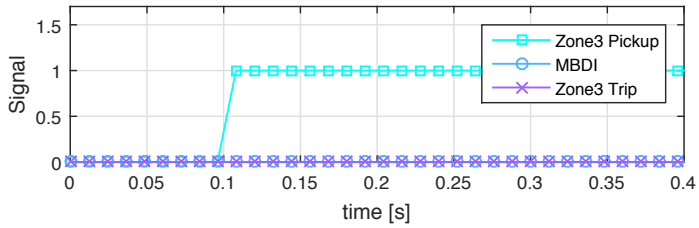

(b)

Figure 2.7: Load Encroachment scenario: (a) Absolute error between measured and simulated bus voltages magnitudes (b) and sequence of signals.

Voltage Excursion

In this case study, a voltage excursion at remote Bus 4 is simulated. Voltage excursions consist of long-term and short-term variations from nominal system voltage and can be a precursor to more serious issues such as voltage instability and voltage collapse. Voltage excursions generally occur at a bus when there is lack of sufficient reactive power support to match the load reactive power demand. Under high load-

ing conditions, a disturbance such as tripping of a line or generator can lead to a voltage excursion at a weak bus [23]. In this scenario, the zone reach settings for the relay at B51 are set at 85%, 120%, and 210% for Zone 1, Zone 2, and Zone 3, respectively. Note that because the length of the primary line (Line 3) is much smaller than the remote line (Line 1), the Zone 3 setting is conservatively chosen to only cover a portion of Line 1. In this way, the results from the simulated voltage excursion can also apply to situations where the remote line is a shorter length.

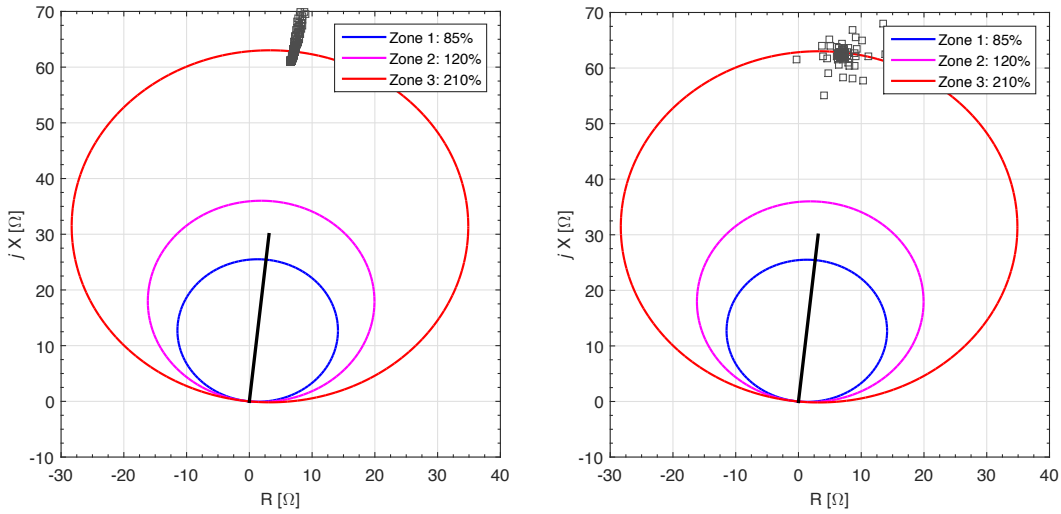

Figure 2.8: Apparent impedance comparison for voltage excursion scenario, with measured impedance in (a) and MBDI fault simulation in (b).

A voltage excursion is simulated at remote Bus 4 by slowly reducing the output from the upstream generator at Bus 3. This simulates a disturbance and lack of reactive power support a Bus 4, causing voltage at Bus 4 to slowly decline to 0.475 pu. As a result, the voltage at local Bus 5 slightly declines to 0.934 pu. This voltage excursion at Bus 4 results in reduced apparent impedance at the relay at Bus 5. Because the voltage excursion occurs as a long-term deviation, the apparent impedance enters the Zone 3 characteristic for longer than the set time delay (typi-

cally 1s or greater). Even though a fault does not actually exist on the system, the reduced apparent impedance causes the relay to trip. From the impedance plots in Fig. 2.8, it can be seen that the apparent impedance at the relay slowly approaches and ultimately enters the Zone 3 characteristic. The relay at B51 will identify the low impedance as a fault and incorrectly issues a trip signal to open the breaker.

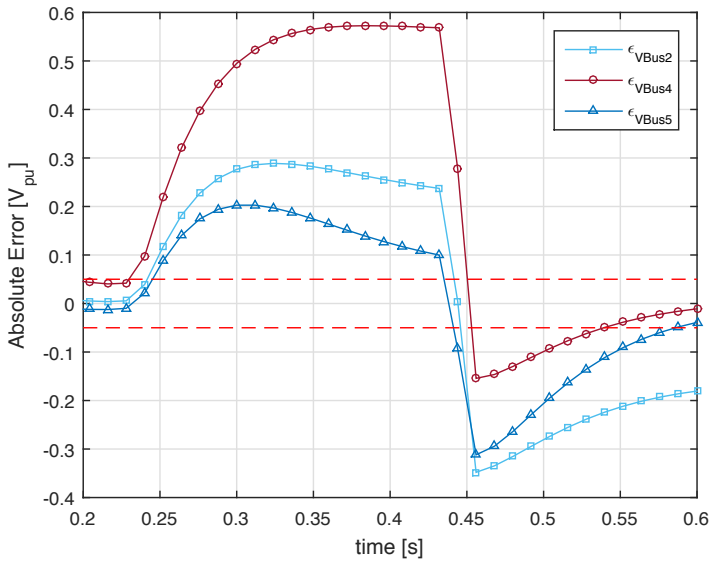

(a)

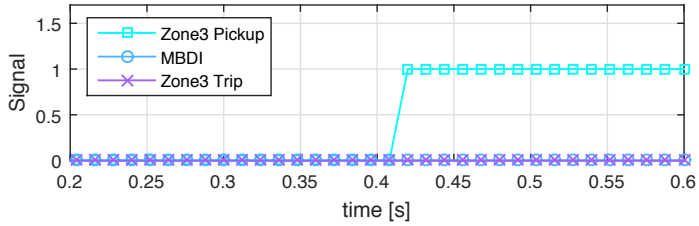

(b)

Figure 2.9: Absolute error between measured and simulated bus voltages magnitudes (a) and sequence of trip signals (b). The relay does not trip under voltage excursion because measured and simulated voltages do not converge.

The same voltage excursion is then applied at Bus 4 with the MBDI scheme enabled and the results are shown in Figs. 2.8 and 2.9. Similar to the previous sce-

nario, the reactive component of the measured impedance estimates approximately the distance of the fault away from the relay and the resistive component estimates the fault resistance. In this case, the MBDI module determines the perceived fault location to be on Line 1, between Bus 4 and Bus 2, and applies faults at possible locations. The plot in Fig. 2.8b shows the three-phase apparent impedance of the simulated fault with the closest match. The calculated $\boldsymbol{\epsilon}$ for nearby buses 2, 4, and 5 is shown in Fig. 2.9 as the simulation runs. As the simulation runs, the bus voltages from the simulated fault condition do not converge to the measured bus voltages because the root causes are different. Therefore, the MBDI module does not issue a confirmatory signal effectively blocks an incorrect relay trip at B51 for a voltage excursion at the remote Bus 4.

High Resistance Fault

In the prior case study, the power system experienced a load encroachment condition causing apparent impedance at the relay to enter the Zone 3 characteristic. The MBDI module, however, correctly detected that it was not a fault condition and blocked an incorrect trip. In practice, distance relays may be equipped with a load encroachment blocking feature, as discussed in Section 1.1. This feature effectively blocks a region of the impedance plane around the R-axis and prevents tripping in this region. However, a tradeoff with enabling the feature is that faults whose impedance falls in the load encroachment blocking region will not be detected by the relay. In this case study, it is first shown that a relay with traditional mho logic and load encroachment blocking may not detect faults with high fault resistance and then show how a relay operating with the proposed scheme can enable relays utilizing load encroachment blocking to detect high resistance faults. A single-line diagram illustrating the fault scenario of this case study is shown in Fig. 2.10.

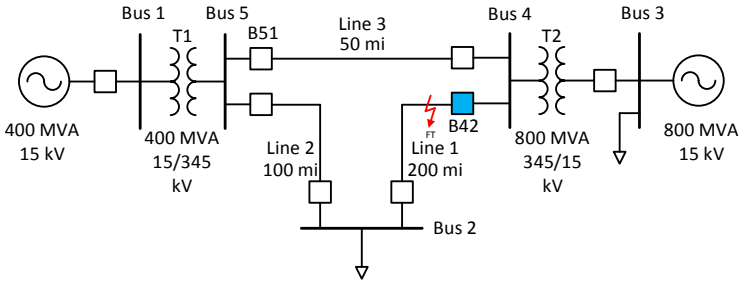

Figure 2.10: Single-line diagram of for high resistance fault scenario.

The relay for this scenario is located at circuit breaker B42 is a conventional distance relay that utilizes load encroachment blocking–with zone settings at 85%, 120%, and 210% for Zones 1, 2, and 3, repsectively. A high resistance fault of 80 Ω is simulated on Line 1 at approximately 20% of the line impedance away from the relay. The impedance trajectories for each phase, in Fig. 2.11a, are shown entering the Zone 3 characteristic. However, because the impedances are within the load encroachment blocking region, the relay will not trip for such a fault. This scenario demonstrates one tradeoff when utilizing load encroachment blocking. With this feature enabled, the relay is less susceptible to tripping due to load, however, it is unable to detect faults within the blocking region.

In previous case studies, the output from the MBDI module was used to discriminate stressed system conditions from a fault condition. In this case study, the true system state is a fault with impedance inside the load encroachment blocking region. The same high resistance fault scenario is run again with MBDI module enabled and results shown in Figs. 2.11 and 2.12. The MBDI algorithm is modified to validate impedances falling within both the load encroachment blocking region and any of the zone characteristics. Therefore, as soon as impedances enter any zone characteristic, the MBDI module determines possible fault locations and applies a high resistance fault in Line 1.

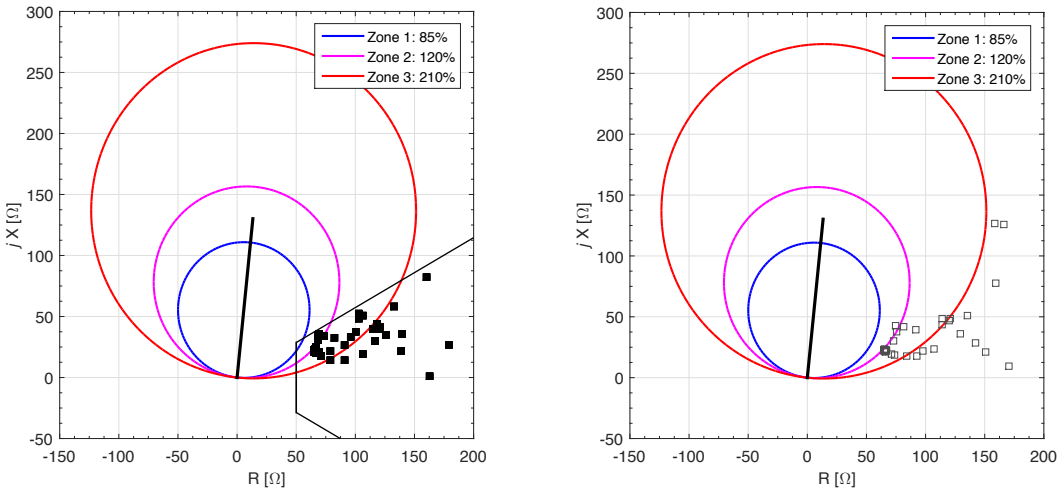

Figure 2.11: Apparent impedance comparison for high resistance fault scenario, with measured impedance in (a) and MBDI fault simulation in (b). Load encroachment blocking region is shown in (a).

Figure 2.12 shows the differences between measured and simulated bus voltages at Bus 2, Bus 4, and Bus 5. It can be seen that the high impedance fault occurs at t = 0.23 s and the relay detects an impedance within both the load encroachment blocking region and one of the zone characteristics. Immediately the bus voltage differences increase and can be seen in Fig. 2.12a between 0.23 and 0.25s. The MBDI module determines the correct location for the perceived fault and begins the fault simulation at approximately 0.25s. However, as the simulation runs, the measured and simulated bus voltages begin to converge. At time t = 0.27s, the bus voltage differences converge below the threshold value of 0.05 pu for longer than 1 cycle. The MBDI module determines the root causes between the measure and simulated system are the same and issues a confirmatory signal indicating a fault condition . This results in the load encroachment blocking being released and the relay is allowed to trip at t = 0.27s. In this case, the relay equipped with MBDI scheme effectively discriminates between load encroachment and a high resistance

fault, even though load encroachment blocking is enabled.

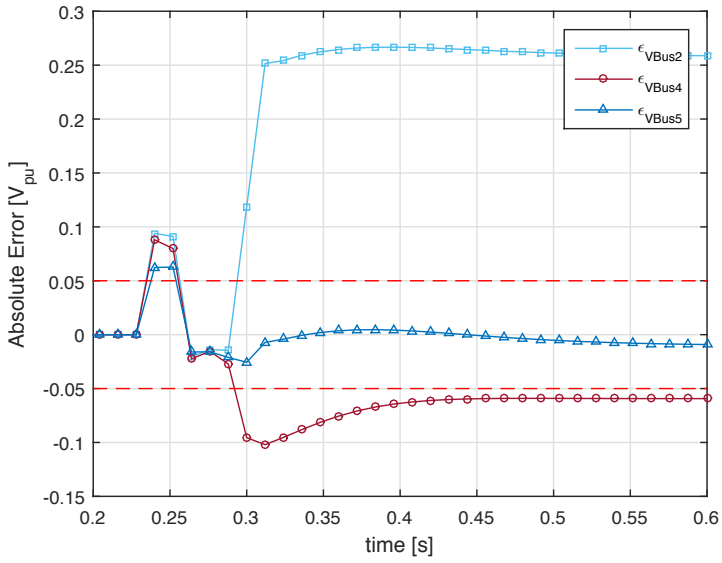

(a)

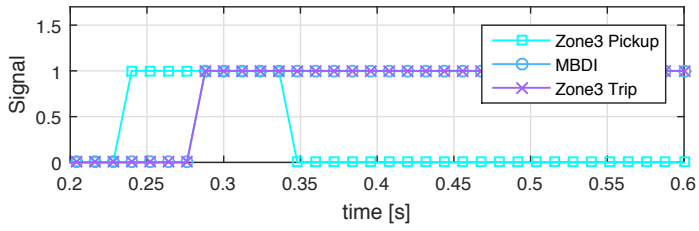

(b)

Figure 2.12: Absolute error between measured and simulated bus voltages magnitudes (a) and sequence of signals (b).

2.2.4 Conclusion from Case Studies

In each of the three case studies, the proposed MBDI scheme is able to supervise the relay's trip decision. For the voltage excursion and load encroachment scenario, the MBDI correctly prevents the relay from tripping when a fault is not present in the system. In these scenarios, security of the relay has been improved under stressed system conditions. In the high resistance fault scenario, MBDI is able detect a

fault inside the load encroachment blocking region. For this case study, the MBDI helps mitigate a tradeoff with the load encroachment blocking feature. It should also be noted that the MBDI framework does not rely on relay settings in the way traditional relays do. Therefore, it can prevent unwanted tripping in cases where the settings are incorrect. For example, a relay engineer can mistakenly set Zone 3 reach larger than intended. In a traditional relay, this incorrect setting extends the Zone 3 reach, making the relay more susceptible to load encroachment. However, with the MBDI framework, even with an incorrect Zone 3 setting, the logic would block relay operation because a fault is not present in the system. This inherent feature to the design of the scheme, further increases security under stressed conditions.

The result of testing the proposed supervisory scheme under various scenarios indicates that incorporating simulation circuit models in relays can improve security of remote backup protection under stressed system conditions. However, challenges and areas of future work remain which can further develop and improve the initial concept. These topics are presented in Section 4.

2.3 Summary

The MBDI framework is introduced to supervise and enhance security of remote backup protection and discriminate between 3-phase faults and stressed conditions. In true fault scenarios, the use of simulation circuit model output at the relay level is shown to accurately confirm the relay's trip decision well before the Zone 3 time delay expires. It is then shown for a load encroachment scenario that the proposed scheme correctly prevents the relay from tripping when a fault is not present in the system – thus improving the security.

Another important consideration is the time required for MBDI complete its assessment. In particular, for true fault scenarios, the MBDI output should confirm

a Zone 3 fault before the Zone 3 timer expires. It is shown that confirmation of the fault is provided within 100ms. Practical implementation of this scheme will also be dependent on the hardware components. The total time duration required can be broken down into several components such as, communication from remote buses, simulation time of the circuit model, time to convergence of the error ϵ below the threshold, and duration that convergence is maintained below the threshold. The results presented herein, however, demonstrate the potential viability of the MBDI framework and provide a basis for future development.

Chapter 3

Supervision of Power Swing Blocking Using MBDI

In chapter, an application of the MBDI framework is investigated, which was introduced in Chapter 2, applied to power swing blocking. It has been shown to supervise relay decisions and prevent undesired operation of remote backup elements during load encroachment and other slowly developing stressed system conditions. The power swing phenomenon can be characterized by oscillations in power flow between two areas of a power system due to an abrupt imbalance in mechanical and electrical power [42]. Initiating events that can result in a power swing include short-circuit faults, line switching, and large changes in generation or load – creating sudden differences in electrical power while mechanical power remains constant. The resulting oscillations in generator rotor angles can create extreme oscillations in power flows. Depending on the control system response, this phenomenon can lead to the eventual loss of synchronism between groups of generators.

Initiation of cascading outages are often characterized by stressed system conditions, including large power oscillations. Therefore, it is critical that relays operate securely under such conditions. During a power swing, load impedance can enter into Zone 1 or Zone 2 of a distance relay, appearing as a 3-phase fault and causing

an unintentional line trip. Although modern distance relays can provide a function for power swing blocking (PSB), the feature operates based on impedance rate of change and may fail to block if the impedance moves too fast during the swing [43]. The objective in this chapter is to investigate the efficacy of a relay equipped with MBDI to block tripping during power swings, presenting advantages and disadvantages of such a scheme. This chapter is organized as follows. Section 3.1 details the power swing phenomenon, discussing current practices to block relay operation and possible areas of improvement. Section 2.1 briefly describes the MBDI framework and how it is modified for power swing blocking. Section 3.2 presents case studies of power swing conditions in a 5-bus system and a discussion of results.

3.1 Conventional Impedance-based PSB Schemes

3.1.1 Impedance Measured by Distance Relay During Power Swings and Out-of-step Conditions

The analysis of the effect of power swings and out-of-step conditions on distance protection is discussed in [44]. During system disturbances, generators in a large interconnected power system form coherent groups of machines swinging with respect to each other. Under such conditions, a distance relay installed in the tie-line connecting the areas of two coherent groups of machines may observe impedance during the power swing as a three-phase fault when the positive sequence impedance trajectory enters its operating characteristic. In the following discussion, we provide an analysis for this phenomenon using a simple two-machine system.

Consider Fig. 3.1, where a distance relay A is installed at Bus A in the tie-line of a two-area system represented by two machines. The voltage and current seen by the relay at Bus A can be expressed as shown in (3.1) and (3.2), respectively.

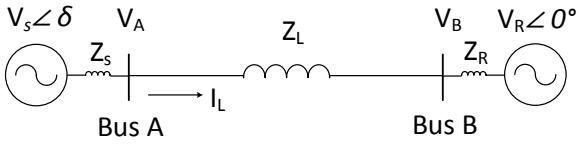

Figure 3.1: Tie-line connected between two areas. Distance relay A is installed at Bus A.

$$V_A = V_s\angle\delta - Z_S I_L \tag{3.1}$$

$$I_L = \frac{V_S\angle\delta - V_R}{Z_s + Z_L + Z_R} = \frac{V_S\angle\delta - V_R}{Z_T} \tag{3.2}$$

The positive sequence impedance seen by the relay is

$$Z_1 = \frac{V_A}{I_L} = -Z_S + Z_T\frac{V_S\angle\delta}{V_S\angle\delta - V_R} \tag{3.3}$$

Assuming the case when $|V_S| = |V_R|$ [23], the impedance trajectory as δ is varied and given by (3.4).

$$Z_1 = \left(\frac{Z_T}{2} - Z_S\right) - j\left(\frac{Z_T}{2}\cot\frac{\delta}{2}\right) \tag{3.4}$$

During the out-of-step (OOS) condition, when the generator voltages are 180° apart, the voltage at the middle of the line becomes zero. In other words, the distance relay perceives a three-phase fault at the middle of the line. In the case of a stable power swing, depending on the swing magnitude, the impedance locus may enter relay A's operating characteristic Zone 1, Zone 2, or Zone 3. The Zone

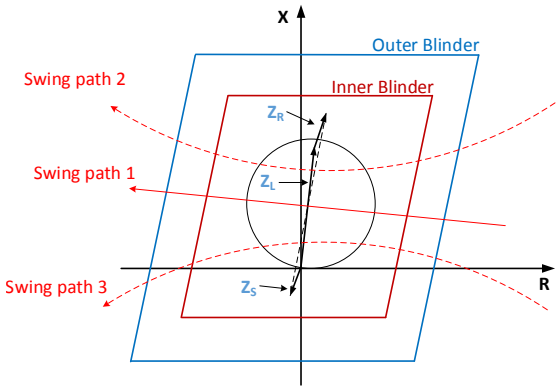

Figure 3.2: Trajectory of power swing in complex impedance plane and PSB scheme.

1 distance relay element, which typically has no intentional time delay, and backup protection elements may operate during both stable or unstable power swings [45].

3.1.2 Impedance-based PSB Schemes

The conventional power swing blocking (PSB) impedance-based methods rely on the principle that the oscillations are relatively slow during power swings due to system inertias. Subsequently, the apparent impedance seen by the relay moves in the complex plane with a slow trajectory compared to that during faults, where the apparent impedance switches to the fault location almost instantaneously. To measure the rate of change of impedance, these methods use two impedance measuring elements called blinders, shown in Fig. 3.2. A timer is started when the apparent positive-sequence impedance enters the outer blinder. If the impedance remains between the two blinders for a pre-determined time delay, a power swing is detected and selected distance zone elements are blocked for certain time period. While some relays use a single blinder, others can use double-blinders. Furthermore, the blinders can have quadrilateral, offset mho, or lenticular shapes [46].

3.1.3 Issues with Traditional Impedance-based PSB Methods

Although there are many power system quantities that can be measured, such as rate of change of power, phase angle difference across a transmission line, swing-center voltage, etc., most traditional power swing detection methods use rate of change of apparent positive sequence impedance. There are many issues associated with this method. One of the issues is the difficulty in the placement of the inner and outer blinders. The inner blinder must be placed outside the largest distance protection characteristic to ensure there is enough time to carry out blocking of the selected distance elements when the power swing is detected. The outer blinder must be placed away from the load region to prevent misoperation of power swing blocking because of load encroachment. This setting is difficult to accomplish especially in case of long lines with heavy loading where the line impedance is large compared to system impedances [23, 42].

Another issue is setting the impedance separation between the two blinder elements and the timer setting for effective differentiation between a power swing and a fault. As the rate of change of impedance is a function of system inertias and the accelerating torques, the blinder separation and timer delay settings need to be carefully chosen after performing system stability studies considering all possible operating conditions [23, 42, 44]. Furthermore, during out-of-step conditions, the slip frequency increases after the first slip cycle to subsequent cycles. As such, fixed impedance separation and fixed time delay settings may result in misoperation of power swing detection due to a faster rate of change of impedance after certain slip subcycles. These complexities illustrate the vulnerabilities in conventional impedance-based methods.

3.2 Case Studies

To demonstrate operation of conventional PSB schemes with MBDI logic, a test system is developed in PSCAD/EMTDC to simulate various scenarios. The test system is chosen to allow for variety of faults and power swing scenarios while being sufficiently simple. The MBDI framework is implemented by running two models simultaneously in PSCAD with communication between each other. The first model represents the physical power system in which the distance relay operates. The second model represents the MBDI circuit model simulation and logic. A single-line diagram of the 5-bus test system is shown in Fig. 2.3 and consists of two generation buses (Bus 1 and Bus 3) and two load buses (Bus 2 and Bus 3). The two transformers in the system step up generation voltage from 15 kV to 345 kV for transmission. System parameters and distance relay settings are modified from [41] and [32], respectively. The following scenarios demonstrate operation of a conventional PSB scheme in conjunction with the MBDI supervisory logic. The power swing is simulated by creating a mechanical torque input disturbance to the 800 MVA generator. For all scenarios, the relay is located at circuit breaker B51.

3.2.1 Scenario 1: Conventional Operation of PSB and MBDI

Slow Power Swing

Consider a slow power swing where the apparent impedance at the relay crosses through the blinders of the PSB scheme. The swing frequency is less than 2 Hz as observed in Fig. 3.3a and results in the PSB scheme to block operation of all distance elements for 2 s. As shown in Fig. 3.3c, the PSB signal goes high at 0.64 s and blocks operation of the distance elements correctly. Furthermore, the MBDI logic begins simulating possible faults as the apparent impedance enters Zone 3.

However, as shown in Fig. 3.3b, the adjacent bus voltages for simulated faults do not converge to the measured bus voltages within the specified threshold. The MBDI logic, therefore, also confirms that the observed impedance variation is not due to a fault condition.

Fault Scenario

Consider a Zone 2 fault at 90% of Line 3. Due to the fast change in apparent impedance, the PSB scheme does not detect a power swing and allows distance elements to trip. In parallel, the MBDI logic begins simulating possible faults after the impedance enters Zone 2 at 2.010s. The simulated and measured system bus voltages converge within 40 ms, and the MBDI logic confirms a Zone 2 fault before the timer expires and the Zone 2 distance element trips the breaker as intended. This scenario is shown in Fig. 3.4 and demonstrates that MBDI logic can correctly supervise true fault scenarios for backup distance elements, such as Zone 2 and Zone 3.

3.2.2 Scenario 2: Fast Power Swing

Conventional PSB schemes can fail if the observed power swing frequency is faster than anticipated. Choosing the appropriate timer setting can often be difficult due to challenges in modeling system inertias over several operating conditions. A typical upper bound for power swing frequency that is considered for PSB setting is 4-7 Hz [42]. In Scenario 2, a fast power swing occurs with a frequency of approximately 5 Hz, which is in this maximum range. If the PSB scheme is not set to detect this swing speed, the apparent impedance trajectory will appear as a fault, allowing the distance elements to operate. The PSB double blinder scheme is shown in Fig. 3.5 and it can be seen that the impedance trajectory enters Zones 2 and 3 during the

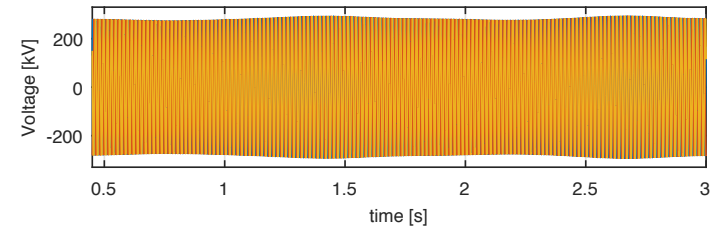

(a)

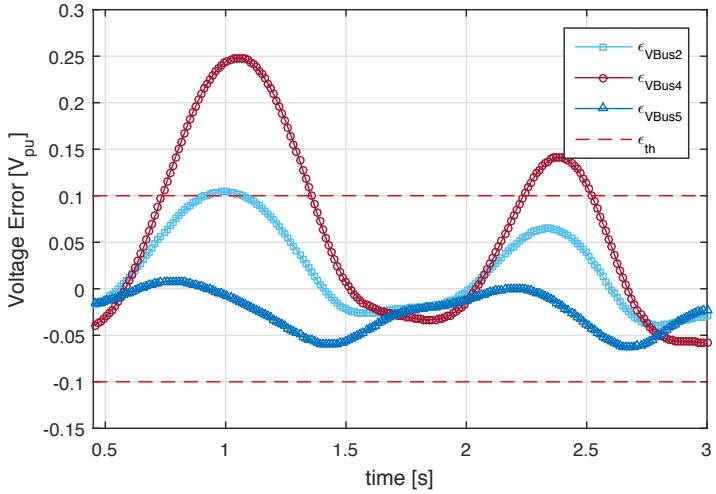

(b)

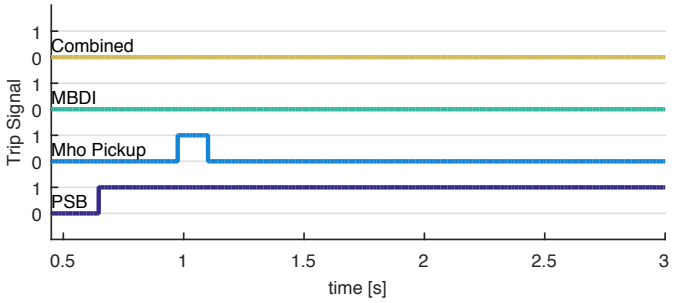

(c)

Figure 3.3: Scenario 1: Slow power swing where PSB correctly issues blocking signal and MBDI correctly does not issue trip.

swing. In Fig. 3.6c, it is observed that the PSB scheme does not detect the swing and the Zone 3 element is allowed to pick up.

The instantaneous voltage observed at the relay is shown in Fig. 3.6a and the

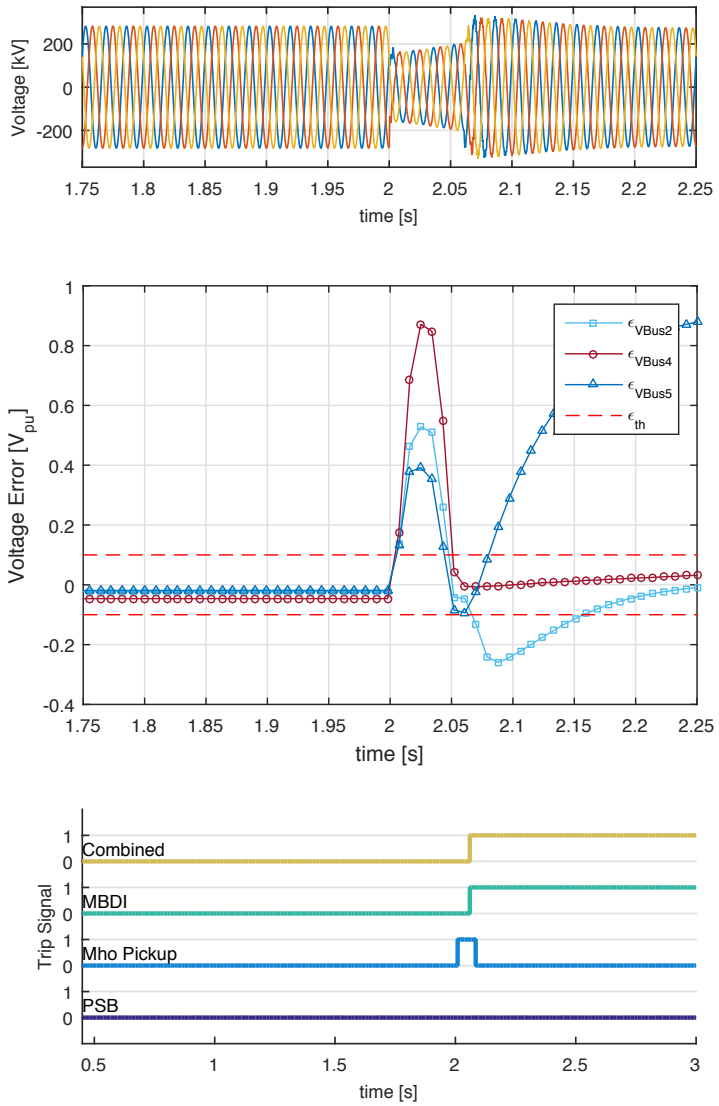

Figure 3.4: Scenario 1: Zone 2 fault where PSB does not block and MBDI correctly confirms a fault.

trip signals are shown in Fig. 3.6c. The PSB scheme does not issue a blocking signal for the power swing. The MBDI logic begins simulating possible Zone 3 faults at 1.12 s into the simulation. However, as shown in in Fig. 3.6b, the system bus voltages from the MBDI fault simulations do not converge with those measured and

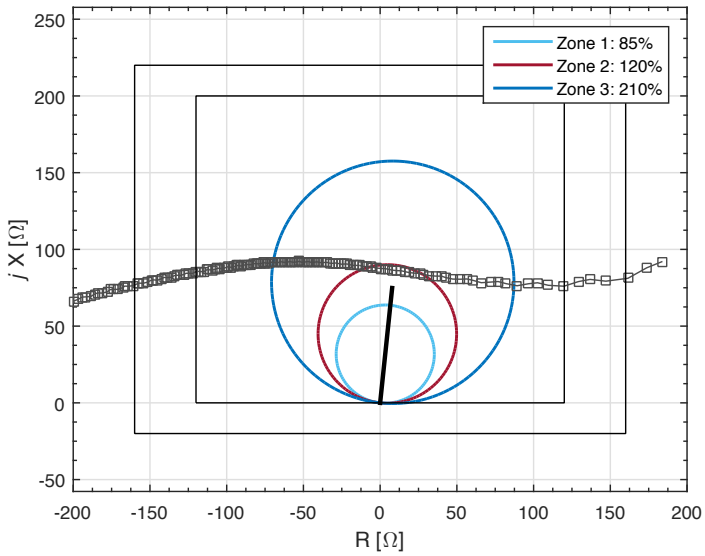

Figure 3.5: Scenario 2: Impedance trajectory of fast swing, moving left to right, showing impedance crossing Zones 2 and 3.

the MBDI logic does not issue a confirmatory trip signal. In this scenario, although the PSB scheme is unable to detect the power swing, the MBDI logic is able to block the distance elements and prevent a misoperation.

3.2.3 Scenario 3: Slow Power Swing and Three-Phase Fault

Another drawback of conventional PSB blinder schemes is that once a power swing is detected, the distance elements are blocked. If a three-phase fault occurs during this blocking interval, the response of the distance elements will be delayed. In Scenario 3, consider a slow power swing causing the PSB scheme to block distance elements from operating for a set time, similar to the slow power swing of Scenario 1. The apparent impedance observed by the relay is shown in Fig. 3.7. Initially, the impedance slowly crosses the double blinders and the distance elements are blocked from operating at 0.39 s when the PSB signal is issued, shown in Fig. 3.8c. While the blocking signal is active, a three-phase fault occurs in Zone 3 at 0.50 s. In this

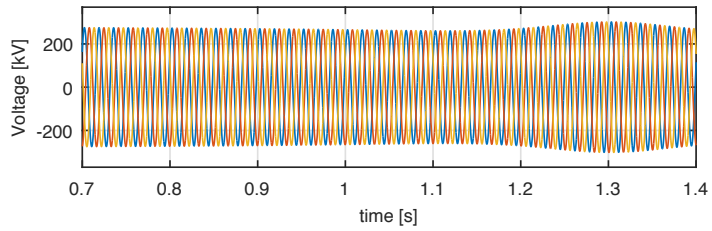

(a)

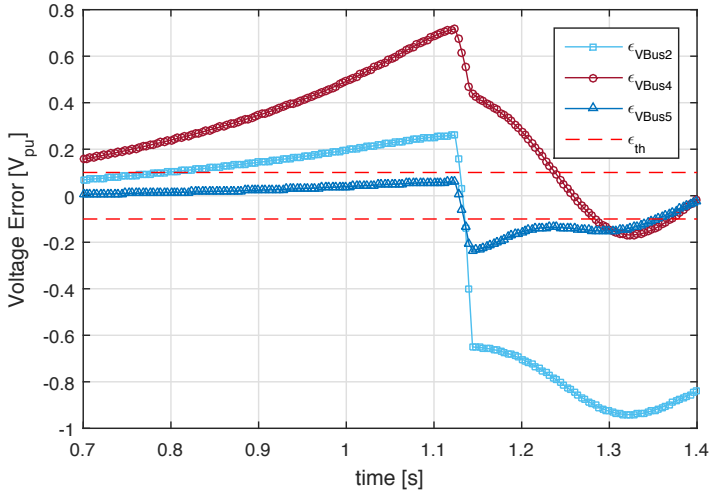

(b)

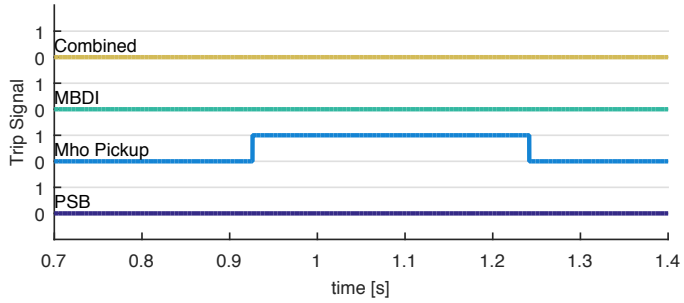

(c)

Figure 3.6: Scenario 2: PSB does not detect the swing due to fast slip frequency. MBDI logic does not confirm fault in Zone 3 and Zone 3 is blocked.

scenario, MBDI is able to confirm a fault condition while the PSB signal is active, allowing the fault to be cleared faster.

Under a conventional PSB scheme, the fault will exist in the system for at least

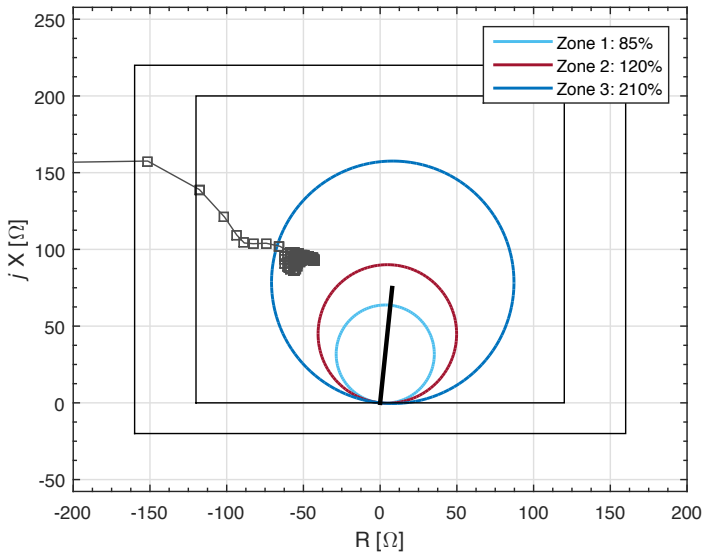

Figure 3.7: Scenario 3: Impedance trajectory shows fault in Zone 3 after PSB has issued blocking signal.

the duration of the PSB reset time if remote backup protection is required. However, the MBDI logic can supervise the PSB signal and confirm a fault condition. At 0.54 s, MBDI logic simulates possible Zone 3 faults and compares the simulated system bus voltages with those measured from adjacent buses. As observed in Fig. 3.8b, the bus voltage magnitudes converge to within the allowed tolerance and the MBDI logic issues a trip signal.

3.3 Summary

In this work, the MBDI framework is applied to supervise power swing blocking schemes in distance relays. The framework uses the output of circuit model simulations within the relay to accurately supervise conventional PSB schemes and prevent misoperations. In Scenario 1, it is shown that the MBDI logic supports conventional PSB operation and does not interfere with its blocking signal. In Scenarios 2 and

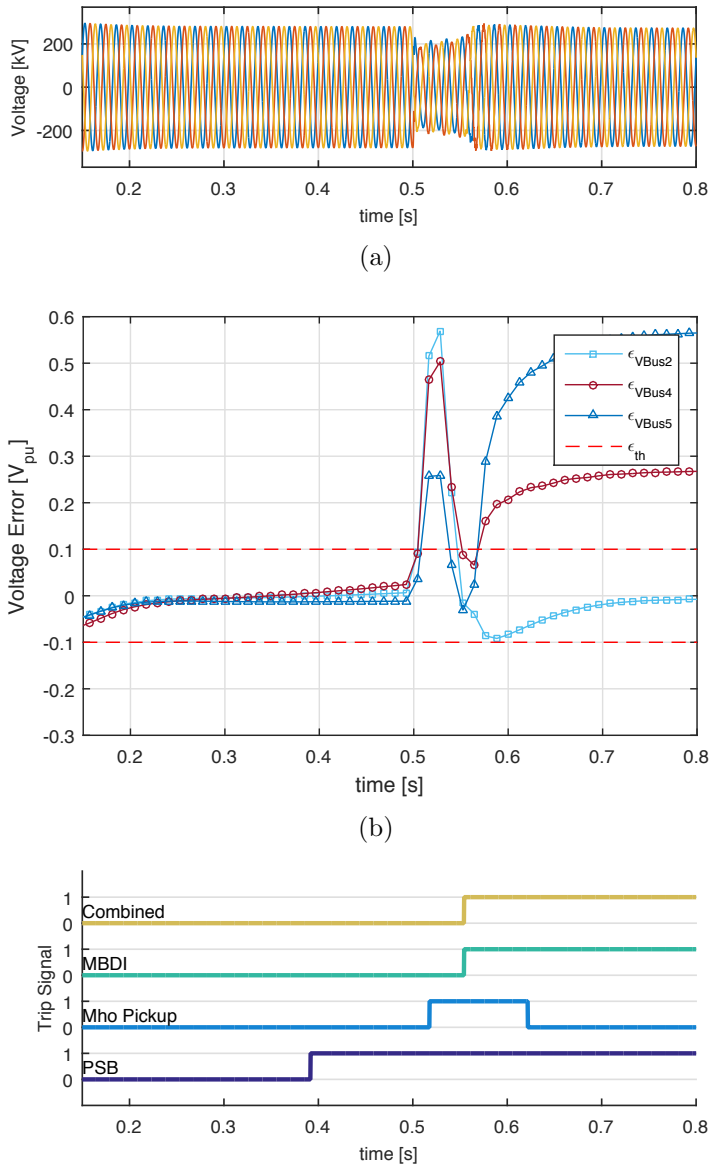

Figure 3.8: Scenario 3: A Slow swing is followed by a three-phase fault in Zone 3. PSB is blocking all zones, however, MBDI simulations confirm a Zone 3 fault.

3, MBDI logic is shown to supervise and provide the correct blocking or trip signal where conventional PSB schemes may fail. The results demonstrate the potential of the MBDI framework for supervising distance relays for enhanced security.

Chapter 4

Hardware Development and Design

In this section, the development and implementation of the initial MBDI concept is described. The performance of the proposed framework can be further evaluated with existing methods based on specified criteria, including the following: complexity, security, selectivity, dependability, cost of implementation, and maintainability. Another important consideration is the time required for MBDI complete its assessment. The nature of protective relaying necessitates that protection schemes be able to quickly and accurately detect and isolate faults in a given protected zone. Furthermore, coordination between relays relies heavily upon relay operating times. Therefore, a prototype relay capable of implementing the proposed protection framework is developed to demonstrate practical operation. The prototype relay will be tested for fault conditions on a power system test bed, described at the end of this section.

4.1 Prototype Design and Component Selection Basis

Numerical relays are the standard today for protective relay design [47] and can have a wide range of protection functions. However, the majority of relay functions, e.g. differential, over-current, and distance, operate based on local measurements of voltage and current (or derived quantities) of the fundamental frequency [48]. A block diagram illustrating major components for a typical numerical relay design is shown below in Fig. 4.1.

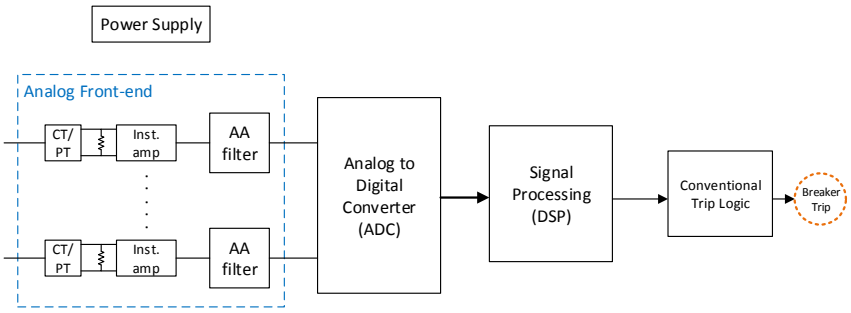

Figure 4.1: Typical numerical relay design.

The analog front end converts measured voltage and current to a differential voltage signal, which is amplified and then passed through an anti-aliasing filter prior to analog-to-digital conversion. Multiple channels may be required to measure different phases of voltage and current simultaneously. The analog-to-digital-converter (ADC) should be able to handle multiple channels with high resolution, high speed, and large input range. The output of the ADC is then passed to a processor chosen to have characteristics suited for digital signal processing (DSP) applications, as Fast Fourier Transform (FFT) calculation is required. The trip logic for the relay is also implemented by the processor. The following summarizes key criteria when choosing component specifications.

Speed Requirements Typically, fault conditions must be cleared as quickly as possible. Standards that govern relay response time include ANSI C37.90, IEC255-4, IEC60255-3. This requires that the relay hardware responds as fast as possible without sacrificing accuracy.

Accuracy Requirements The input signals (particularly current) have a large dynamic range as fault currents can be several times that of the load current; the relay is expected to operate accurately throughout this entire range. The analog front end of the system must be properly designed for high resolution (recommended minimum of 16-bit) [48] in order to achieve the following goals : high linearity, high stability, and low noise. The preferred type of ADC, therefore, is the successive-approximation register (SAR) which has characteristics of high linearity at high sampling rates.

Simultaneous Sampling Requirements Many protection functions, distance protection included, requires calculation of the phase angle between the measured voltage and current. This allows further calculation of real power, reactive power, power factor, impedance, and harmonics. The preferred way to synchronize the instantaneous voltage and current measurements is to simultaneously sample both signals, i.e., a simultaneous sampling ADC is required.

Controller Requirements In addition to performing FFT calculations for fundamental frequency components of voltage and current, the processor may be required to calculate other quantities such as impedance, harmonics, and active power. These calculated quantities can be used in the tripping logic of different protection algorithms. The processor should also have the necessary timers available to implement relay logic and connectivity to communicate with other devices. These requirements

suggest a controller with high performance, comparable to a DSP, and multiple peripherals.

Based on the above selection criteria, Fig. 4.2 shows a block diagram of a possible implementation for an MBDI relay prototype. Additional blocks needed for the MBDI framework are outlined in light blue. These include blocks for: circuit model simulations, MBDI logic, and comparison real-time (RT) measurements. These blocks will interact with conventional relay logic as described in Section 2.1 before arriving at a breaker trip decision. The Raspberry Pi 2 microcontroller is initially chosen to implement this part of the design. It is chosen for its performance characteristics (900 MHz ARM-cortex A7 and 1GB RAM), available peripherals (including 40 GPIO pins) and low cost. The TI-ADS8556 is chosen to meet the performance and simultaneous sampling requirements for the ADC.

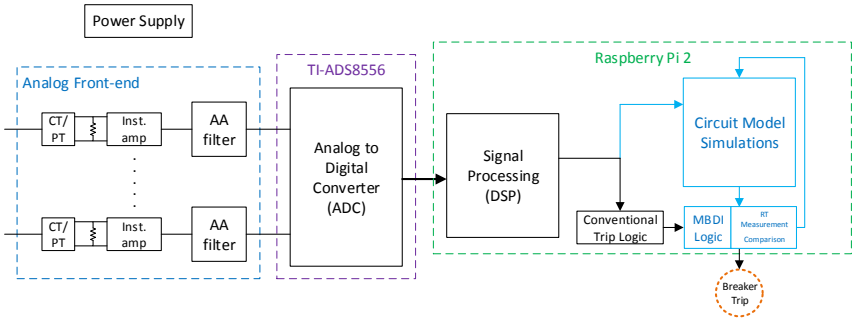

Figure 4.2: Block diagram of proposed MBDI relay design. Conventional relay architecture is shown with black outline. Proposed modules to be integrated are shown in light blue outline.

4.2 Relay Input Signals and Processing

Operation of the distance relay is triggered based on apparent impedance at the relay location. The relay only actually measures instantaneous voltage and current, but estimates the phasor $V_{LL}\angle\phi_z$ for line-to-line impedance by the following calculation. Voltage and current are sampled at a specified multiple of the fundamental frequency component, n_s samples/cycle. Next the fast Fourier transform (FFT) is applied on a 16-sample window. The FFT outputs the magnitude and phase angle of the fundamental frequency phasor (60 Hz). The rms phasors of voltage and current are used to calculate the line-to-line impedance phasor $\bar{Z}_{ab}$ as follows:

$$\bar{Z}_{ab} = \frac{\bar{V}_a - \bar{V}_b}{\bar{I}_a - \bar{I}_b} = \frac{\bar{V}_a}{\bar{I}_a} \tag{4.1}$$

where $(\bar{V}_a, \bar{I}_a)$ and $(\bar{V}_b, \bar{I}_b)$ are the rms phasors of phase A and B voltage and current.

4.2.1 Analog-to-Digital Conversion

This section describes the simultaneous sampling of voltage and current needed by the relay. At most, 6 channels will be required: three voltage and three current measurements. Analog-to-Digital conversion is accomplished with the TI ADS1256. In order to meet potential future requirements to observe high frequency components, the sampling frequency is chosen at $f_s = 10.240$ kHz or 170.66 samples/cycle. The Serial Peripheral Interface (SPI) is used for communication between the ADC and microcontroller. The protocol is also known as the synchronous serial interface (SSI), and utilizes a common clock signal to synchronize transmission between two devices. One device acts as the master and the remaining devices as the slaves, with the master device generating the clock signal. Four wires are utilized for communication: Sck (serial clock), MOSI (master out slave in), MISO (master in slave out),

and SS (slave select, usually active low).

4.3 Distributed Power Flow Solver

The power flow solver used in this implementation is based the solver utilized in OpenDSS. As discussed in the previous section, the system size is expected to be no larger than the adjacent zone 3 buses, with Thevenin equivalent circuits approximating the system past these buses. For this reason, the fixed-point iteration method for solving a system of equations utilized by OpenDSS and described in [49] is implemented in the Raspberry Pi. An overview of the power flow algorithm is briefly described below. The power flow for a given network is computed by solving the system of equations $I_{inj} = YV$ or,

$$\begin{bmatrix} \\ I_{inj} \\ \\ \end{bmatrix} = \begin{bmatrix} \\ Y \\ \\ \end{bmatrix} \begin{bmatrix} \\ V \\ \\ \end{bmatrix} \tag{4.2}$$

where I_{inj} is the node injection currents, Y is the $n \times n$ admittance matrix, and V is the node voltages with respect to ground. The node injection current represents the current injected into a node from outside the network represented by the admittance matrix Y. For example, injection currents will be nonzero for nodes that include current sources, voltage sources, nonlinear loads, or generator models. For a given system state, the vector I_{inj} is known and admittance matrix Y is known. Therefore, Eq. (4.2) is directly solved using the KLU sparse linear system solver [50]. The KLU algorithm is implemented in the Raspberry Pi and is written in C with modifications from [50] and [34].

The distributed solver implementation is tested by solving the power flow 1000 times for each particular test feeder, with results shown in Table 4.1 [34]. It can

Table 4.1: Average solution times for selected test feeders

Test Feeder	Avg. Solution Time [μs]
IEEE 13 node	136.3
IEEE 34 node	544.0
IEEE 37 node	508.9
IEEE 123 node	1049.3
IEEE 8500 node	37413.0

be observed that even for very large systems, e.g., IEEE 8500 node test feeder, the implementation in the Raspberry Pi has average solution times less than 40 ms. For systems representative of the size utilized by the MBDI algorithm, solution times are less than 1 ms. The accuracy of the solution is demonstrated by comparing the distributed implementation solution with the off-line OpenDSS solution for the IEEE 37 node test feeder. There are a total of 117 nodes over all three system phases and the total mean squared error over all nodes between the off-line and distributed solution is 1.34×10^{-12}. The overall results indicate that the distributed power flow solution in the Raspberry Pi is capable of producing accurate power flow results within the desired timing requirements.

4.4 Power System Test Bed

The MDBI relay prototype will be tested on a test bed representing a scaled model of a 5-bus power system. The test bed incorporates a table-top three-phase power system model, real-time monitoring and control system, and several locations to apply faults. A schematic of the test bed is shown in Fig. 4.3 and photos of the completed model are shown in Fig. 4.4. The power system model is built upon a 4 ft. by 8 ft. platform, with transmission line parameters designed to be representative of a 100-mi, 5-bus, 345kV system. The transmission lines are separated into 20-mi nominal-pi circuit segments, consisting of inductors and capacitors. The model

system includes both transmission and distribution circuits and operates at a scaled-down 208V and 41.6V, respectively. The system is powered through step-up and step-down transformers, supplying resistive load banks totaling 3kVA. The overall scale of the model is over 500 lbs. and has over 2000 connection points. Additionally, a real-time monitoring and control system, comprised of Arduino and the Raspberry Pi microcontrollers, measures and displays voltage, current, and harmonic content at each system bus. The model construction was completed as part of a senior design project by Team WISE in Spring 2015. In addition, short-circuit faults are safely applied through a specially designed enclosure shown in Fig. 4.5, allowing application of multiple fault conditions. Fault current is limited by a power resistor in series with fault connection.

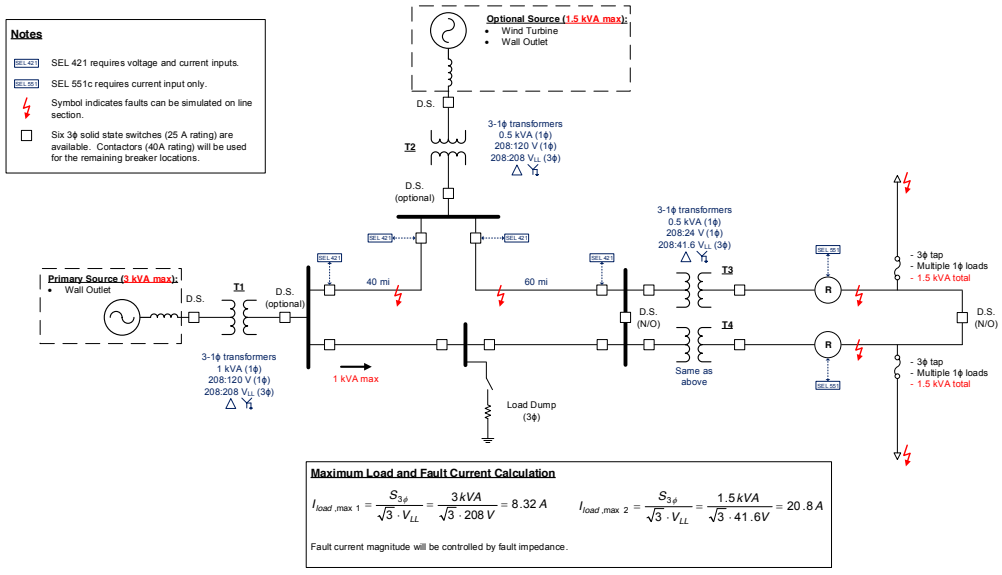

Figure 4.3: Schematic of power system test bed.

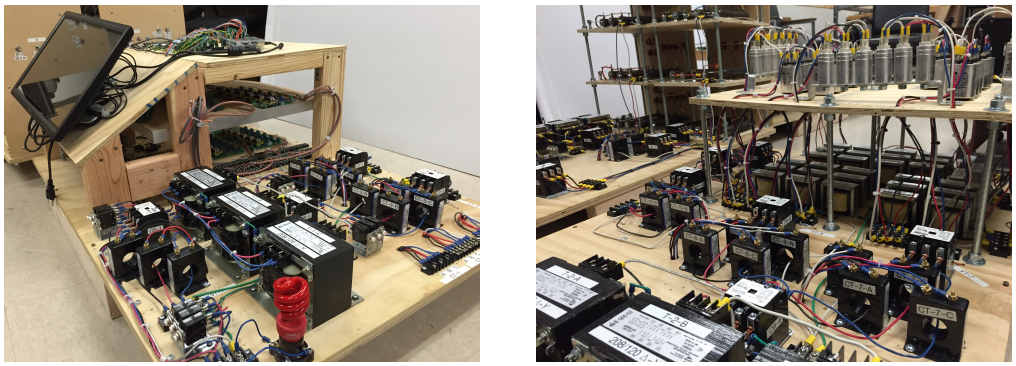

(a) (b)

Figure 4.4: Power system test bed developed at the University of Texas at Austin.

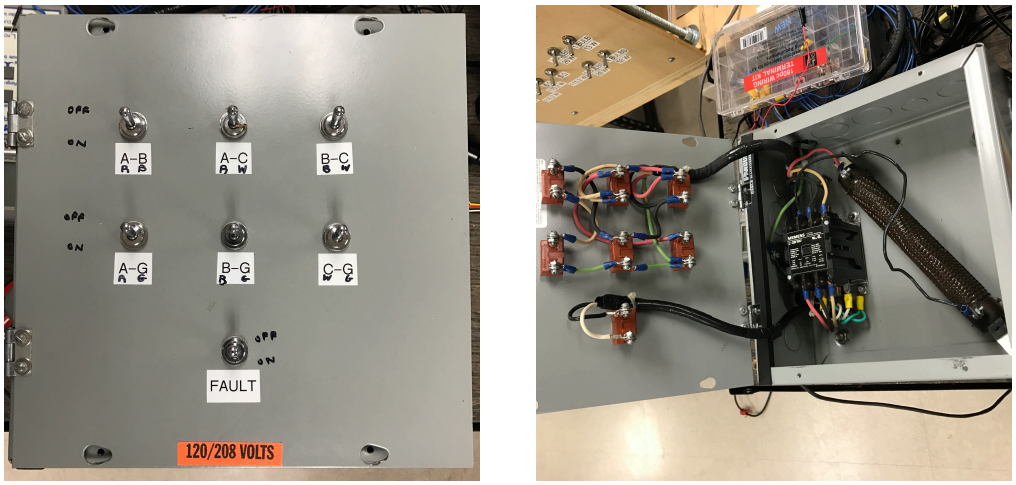

(a) (b)

Figure 4.5: Fault application enclosure for safely applying various fault conditions to the experimental power grid.

4.5 Experimental Results

In this section, an application of the proposed embedded real-time simulator and MBDI algorithm is described. The objective of the MBDI relaying framework is to supervise and secure the operation of remote backup protection elements. It is first

initiated when the apparent impedance of the relay enters distance elements Zones 2 or 3. In parallel with the conventional time-delay setting, the potential fault scenarios are simulated in the relay using the embedded real-time simulator. Considering a Zone2 fault for example, MBDI logic first simulates candidate faults using the apparent impedance data at the relay location. The output of the embedded fault simulation returns expected rms voltages at each bus for each candidate fault scenario. By comparing the embedded simulator solution with the measured real-time bus voltages at adjacent buses, the MBDI logic can confirm or reject whether a fault condition is present.

A simple experimental-scale physical power system test-bed is utilized to demonstrate the integrated MBDI/embedded real-time simulator prototype. A representative scenario is described below. The fault current on the transmission sections are limited to 6.7A, with a nominal load current of 1.4 A. A single line-to-ground fault is then applied at 100% of the representative 100 mi. transmission line section (shown in Fig. 4.4), corresponding to a Zone 2 fault. The top waveform captured in Fig. 4.7 shows the measured fault current scaled through a current transducer (CT) and the bottom waveform shows the output of the MBDI logic confirming the fault condition. The results show that after the fault is detected, the proposed embedded real-time simulator is able to simulate candidate fault scenarios. The simulation output for the adjacent bus voltage magnitudes match the corresponding measured values, allowing the MBDI logic to correctly send a supervisory confirmation of the Zone 2 fault. The results further demonstrate that the proposed embedded real-time simulator can help facilitate implementation of advanced protection concepts, such as MBDI, and other applications where distributed real-time simulation is required.

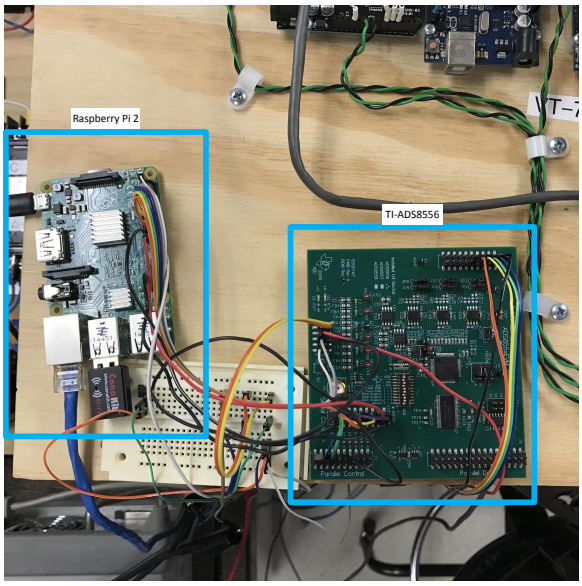

Figure 4.6: Raspberry Pi 2 and TI ADC used to implement prototype.

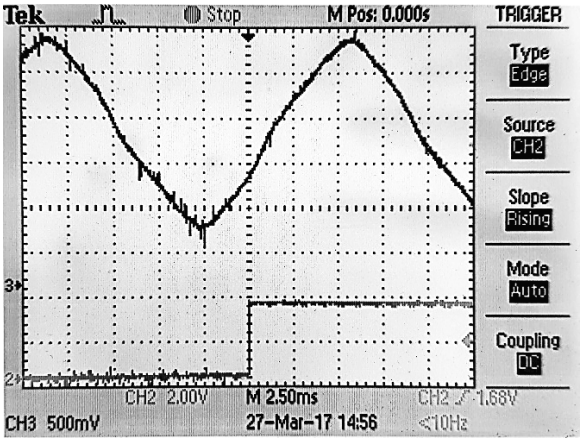

Figure 4.7: Fault current and MBDI supervisory signal captured for a Zone 2 fault at 100% line impedance.

Chapter 5

Supervised Learning for Symmetrical Fault Detection During Power Swings

In Chapters 2 and 3, a framework was developed for supervising remote backup relay operations using circuit model simulations. The approach is effective in remote backup zones, such as Zone 2 and Zone 3, because the time delays ranging from 50-300 ms allow sufficient time for the simulations and measured signals to converge. However, for instantaneous zones operating without intentional delay, improving security during power swings using another approach is investigated. During a power swing, load impedance can enter into zone 1 or zone 2 of a distance relay, appearing as a symmetrical fault and causing an unintentional line trip. Therefore, distance relay operation during power swing conditions should be blocked in order to prevent unnecessary line trips leading to the formation of unplanned islands and the propagation of disturbances. Although there are many power system quantities that can be monitored, such as rate of change of power, phase angle difference across a transmission line, swing-center voltage, etc., most modern distance relays provide a function for power swing blocking (PSB) which operates based on rate of change

of positive sequence impedance. However, this method may still fail to block if the impedance moves too fast during the power swing [43]. This approach fundamentally relies on the signal, rate of change of impedance, to discriminate symmetrical faults from power swings, conditioned on impedance being close to protected line. While it allows for great interpretability, e.g. it is straightforward to interpret a decision threshold specifying swing speeds greater than 6 Hz are classified as faults, the approach suffers from two key challenges: setting the appropriate threshold for rate of change of impedance and the detection of symmetrical faults after PSB has been activated.

During power swing conditions, the instantaneous voltage and current signals typically exhibit distinct characteristics from symmetrical faults. As a result, several approaches have been proposed to augment conventional PSB [51–53] using additional signals, such as high-frequency components or remote terminal measurements. In particular, machine learning, data mining, and statistical pattern recognition approaches have gained attention due to their ability to accurately detect patterns in high-dimensional data sets and ability to detect faults in scenarios where discrimination is not straightforward. For example, [54–56] apply classification models to detect high-impedance faults and faults on series compensated lines. Detection of symmetrical faults during power swings using classification methods is shown in [57–60] with good results. However, in these prior works, the primary focus has been to achieve high classification rates with only a minor emphasis on investigating the trade-off between accuracy and interpretability.

Therefore, in this chapter an alternative machine learning based approach using an effective feature selection criteria is proposed to augment discrimination of symmetrical faults during power swings. The approach seeks to maintain the performance of high-dimensional classifiers in the least amount of features and to provide

intuitive understanding with visualization and evaluation methods. The following classifiers are compared and evaluated: support vector machine, random forest, gradient tree boosting, CART decision tree, and k-nearest neighbors. The contribution of the approach is a systematic and interpretable approach resulting in the training of classifiers that maintains high classification rates. The approach is evaluated on power swing and fault scenario data from the IEEE 9-Bus system in PSCAD/EMTDC, consisting of scenarios where power swings enter zone 1 and where conventional relays are likely to fail. The results show excellent classification and true-positive rates, while minimizing false-positives. Furthermore, the analysis shows ensemble approaches using decision tree classifiers, such as random forest and gradient tree boosting, have better performance than other classifiers presented in literature. The approach further emphasizes analyzing the classifier's predicted probabilities and trade-offs between true-positive and false-positive rates instead of relying solely on the binary decision, resulting in a more interpretable model with similar or better performance.

5.1 Proposed Classification Approach

5.1.1 Generating Training Data

The IEEE 9-bus system is considered as a test system for studying the effectiveness of the proposed method. The system is modeled in PSCAD/EMTDC, with lines modeled as nominal pi sections and generators modeled with one axis flux decay dynamics and their exciters are represented by the IEEE Type-1 model [61]. The line parameters and the dynamic data of the generators are obtained from [62] and the exciter parameters are taken from [61]. The distance relay with mho characteristics in line 7-5 at bus 7 is selected for this study [57]. This distance relay is set to cover

85%, 120% and full length of adjacent line for zones 1, 2 and 3, respectively. When a power swing is detected, the distance relay elements are blocked for a preset power swing blocking period which is typically set as 1.5-2.5 cycles [63]. The choice of zones to be blocked depends upon the utility practice. The utility can configure the distance relays to block all the distance zones or block zone 2 and higher while allowing zone 1 to trip upon detection of a power swing [42]. When all the distance zones are blocked, a symmetrical fault cannot be detected during the power swing blocking period.

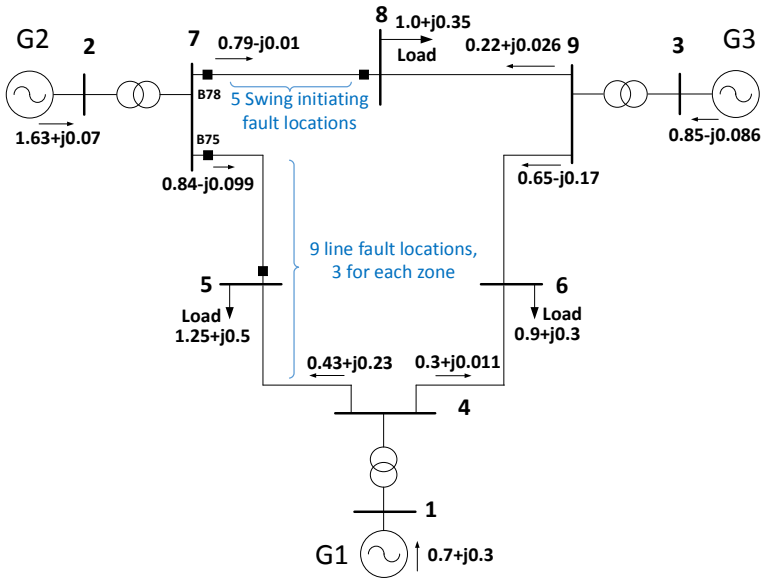

Figure 5.1: Single line diagram of WSCC 9-Bus system showing steady state power flow solution and location of fault simulations.

In order to generate a data set considering possible power swings of varying slip frequency and intensity, the simulation methodology in [57] is closely followed. This further allows for comparison of results as the data sets are similar. Power swings of varying slip frequencies are generated by varying the characteristics of an initiating three-phase-to-ground fault in line 7-8 as shown in Fig. 5.1. Five different locations on the line are considered, in addition to varying the fault resistance from

Table 5.1: Feature sets

Feature	Definition
x_1	Change in bus voltage magnitude (dV)
x_2	Change in bus voltage angle ($d\delta_V$)
x_3	Change in line current magnitude (dI)
x_4	Change in line current angle ($d\delta_I$)
x_5	Apparent impedance (resistance) (R)
x_6	Apparent impedance (reactance) (X)
x_7	Change in apparent impedance (resistance) (dR)
x_8	Change in apparent impedance (reactance) (dX)
x_9	Real power demand (P)
x_{10}	Reactive power demand (Q)
x_{11}	Change in real power demand (dP)
x_{12}	Change in reactive power demand (dQ)

0.01-45 Ω, fault duration from 200-350 ms, and time instant of occurrence at each quarter-cycle. This fault is cleared by opening breakers at both ends of the line. After the power swing is initiated, a three-phase-to-ground fault is simulated in relay B75's protected zones on lines 7-5 and 5-2 with varying fault location and varying fault resistance from 0.01-45 Ω.

The resulting data set consists of 17,280 different scenarios–each consisting of a power swing observed by relay B75, followed by a symmetrical fault in a protected zone. The duration of each simulated scenario is 3 s, with a resolution of 32 samples / cycle. After initiation, power swing waveform characteristics for 2 s are observed before the symmetrical fault is applied. The 2 s duration allows for the possibility of many slip cycles to be observed with the impedance rate of change increasing after the first slip cycle [42]. Therefore, the training data includes both stable and unstable power swings with very fast impedance rate of change. This ensures that the data includes scenarios where discrimination between symmetrical fault and power swing is very difficult.

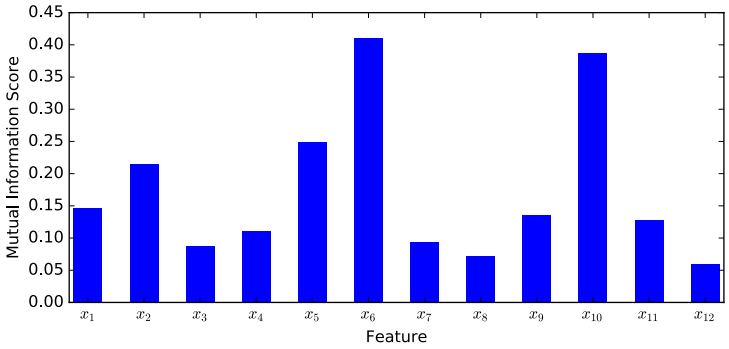

Figure 5.2: Mutual information score for 12 features described in Table I.

5.1.2 Feature Importance Ranking by Mutual Information

Prior works have shown that a wide range of signals, including measurements from remote buses, can be used as input to classification models for symmetrical fault detection during power swings. These include: rate of change of power swing center voltage $(d|V_s|cos\phi)/dt$, real and reactive power, dP/dt and dQ/dt, dR/dt, discrete wavelet transform, dV/dt and dI/dt. High frequency features can be sensitive to other switching events and also require a high sampling rate. Therefore, in this work high frequency features and remote end measurements are not considered. The considered features are shown in Table 5.1. Note that rate of change is computed by comparing the consecutive samples in time. A scatter plot matrix is shown in Fig. 5.3 for all twelve figures, illustrating the relationship between each pair of features, with power swings shown in blue and symmetrical faults shown in red. The histogram along the diagonal indicates the separation between each class for each 2-dimensional feature pair.

In order to improve transparency and understanding, a systematic method of selecting the most important features from the larger set of possible features is required. Mutual information has been shown to be an effective feature selection

criteria [64] and is applied in this work. It is defined in [65] as follows.

$$I(x,y) = \sum_{x,y} p(x,y) \ln \frac{p(x,y)}{p(x)p(y)} \tag{5.1}$$

where $p(x)$ is the probability distribution of X. Mutual information therefore represents the reduction in uncertainty of random variable x resulting from a new observation of random variable y. In this application, $I(x,y)$ is calculated between each feature vector x_i and the target variable y, with results shown in Fig. 5.2. It can be observed that reactive power and positive sequence reactance have the highest scores.

5.1.3 Classification Models

Numerous algorithms for the supervised learning classification problem have been shown to be effective in diverse data sets. In general, the problem considers n samples of training data belonging to two or more classes and tries to predict the class of a new unlabeled data sample. Prior work for symmetrical fault detection during power swings has been treated as a two-class classification problem and primarily focuses on the effectiveness of support vector machines (SVM). Although SVM classifiers can provide good accuracy, other classifiers can provide similar performance. In this study, the five classifiers chosen to be evaluated and are listed in Table 5.2. Each model's performance is tuned by finding optimal parameters through 5-fold grid-search cross-validation, with resulting tuned parameters shown in Table 5.2.

A brief description of the model and parameters follows below, with complete details of each classification model provided in [66] and [65]. All classification models are implemented with the *Scikit-learn* library [67]. First, the CART algorithm [66] is utilized to generate a single decision tree. The parameters considered for tuning include maximum depth n_{depth}, maximum number of samples per leaf n_{samples}, and

Table 5.2: Tuned parameters for each classifier

Classifier	Parameters
decision tree	$n_{\text{depth}} = 4$, $n_{\text{samples}} = 50$, $n_{\text{nodes}} = 20$
k-nearest neighbors	$k = 3$
support vector machine	$C = 4096$, $\gamma = 8$
random forest	$n_{\text{trees}} = 50$
gradient tree boosting	$n_{\text{trees}} = 500$, $\lambda = 0.1$

maximum nodes per leaf n_{nodes}. Next, the k-nearest neighbor classification model predicts the class of a new sample based on the distance to the k closest data points in the training sample. The parameter k is tuned with data points weighted by the inverse of their distance to the new sample. The SVM is implemented with the radial basis function kernel and regularization parameter C and kernel parameter γ chosen to be the same as in [57]. The random forest algorithm combines the predictions of multiple de-correlated decision trees in order to reduce the variance in the predictive model; the parameter for the number of trees, n_{trees}, is tuned to balance performance and training speed. Boosting is the process of sequentially training weak predictive models, where each successive model is trained on modified data where each successive model focuses on observations that were most difficult for the previous model to predict. The number of iterations in the algorithm and subsequently number of trees, n_{trees}, is tuned, along with the learning rate λ.

5.2 Model Evaluation and Case Study

In order to estimate the predictive performance of each model, three metrics are considered: cross-validation accuracy, test set accuracy, and area under receiver operating characteristic (AUROC). Note that training set accuracy is not considered as it can lead to over-fitting. Furthermore, only the five most important features based on (5.1) and Fig. 5.2 are considered. The approach first holds out a test

set which is generated by randomly sampling 20% of the total data set without replacement; the remaining data is used as a training set. The data is approximately evenly split between fault and power swing classes. Five-fold cross-validation is performed by splitting the training data into five random subsets, training on four of the subsets, and validating on the remaining subset. This is repeated for each of the five folds and the average is taken as the cross-validation score. The classification accuracy for cross-validation and the test set are shown in Table 5.3.

Table 5.3: Classification accuracy using five features with highest mutual information

Classifier	5-fold CV (%)	Test Set (%)
decision tree	92.06	93.41
k-nearest neighbors	93.23	94.67
support vector machine	93.67	94.71
random forest	97.83	97.84
gradient tree boosting	98.10	98.29

Classification accuracy alone, in general, is not a sufficient measure of a predictive model's performance. Most classifiers return predicted class probabilities in addition to binary class predictions and have a default threshold of 50%. It is therefore important to further consider the true-positive (TPR) and false-positive rates (FPR) as the classification threshold is varied, which is not captured in the classification accuracy score alone. In particular, power system protection is designed for high security and is largely averse to false-positive misoperation of relays (where faults are the positive class). Typically a trade-off has to be made between TPR and FPR. The receiver operating characteristic (ROC) and area under the curve is an appropriate method to summarize both types of errors [66]. The ROC plots the FPR versus TPR as the classification threshold is varied and is shown for the five classifiers in Fig. 5.4. The ROC curves for random forest (rf) and gradient tree

boosting (gbc) show a significant advantage for maintaining a high TPR without incurring larger FPR.

An illustrative power swing scenario is held out from the training data and is shown in Fig. 5.5. The time-domain voltage and current waveforms of phase A show a power swing occurring 1.8 to 2.7 s, after which a symmetrical fault is observed. The impedance trajectories observed by relay at B75 and corresponding output from the random forest classifier are also shown. It can be observed that the predicted class transitions from 1 to 0 accurately when the fault occurs. The predicted probability of fault also rises sharply. The susceptibility to false-positive can be further tuned by adjusting the classification threshold above 50% probability.

5.3 Summary

Supervised learning classification models can have excellent performance in finding decision boundaries in high-dimensional spaces that minimize the classification error rate. However, there is an inherent trade-off between predictive model performance and interpretability of the model and results. Fig. 5.6 further illustrates that additional relevant features can greatly improve classification rates. Including all 12 features can achieve accuracy over 99%. On the other hand, a model utilizing only two features such as R and X (as in conventional distance relays) is greatly interpretable. Even with machine learning models, often considered as black boxes, it allows for novel visualizations that makes the results more intuitive and understandable. For example, a random forest classifier is trained only using R and X as features, with the training data for both power swings and symmetrical faults plotted in Fig. 5.7. The predicted class probabilities from the model are plotted as contours, with the scale shown at right. It can be observed that the visualization provides great intuition and provides confidence for predictions on unseen

data. Even with only two features, accuracy is greater than 90%. To conclude, a supervised learning approach for detecting faults during power swings and focused on both interpretability and performance has been presented. Results indicate performance of classifiers on par with prior models, while providing intuitive evaluation and visualization methods.

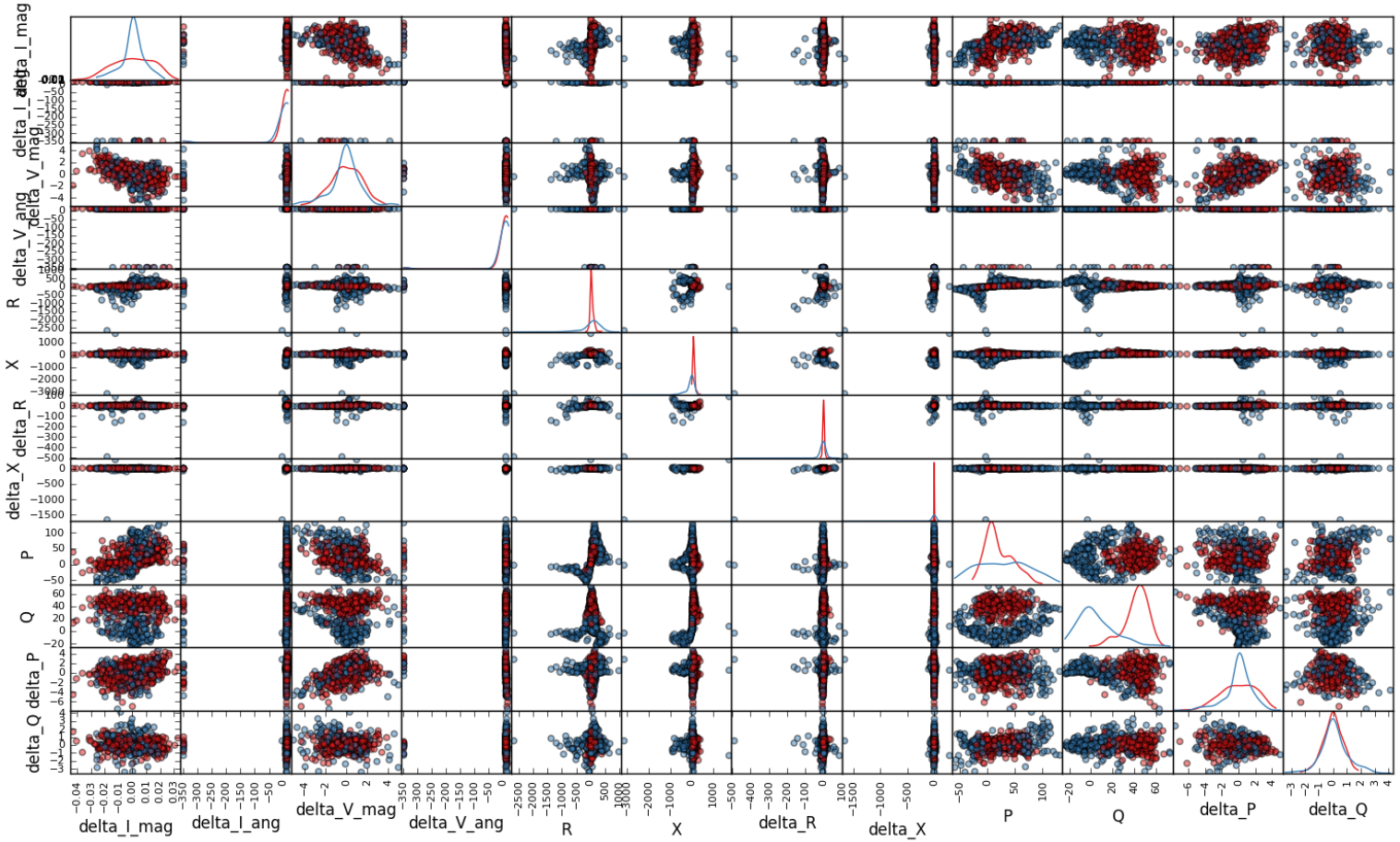

Figure 5.3: Scatter matrix comparing 12 features for both power swings and faults. Power swings are shown in blue and symmetrical faults in red.

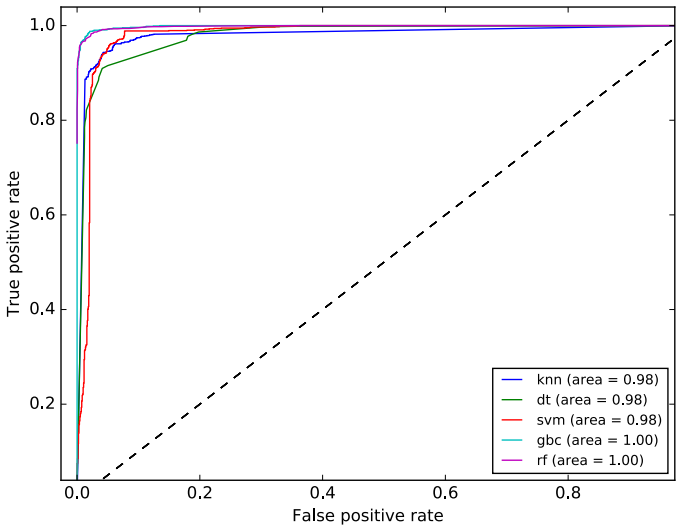

Figure 5.4: ROC and AUROC comparing effectiveness of each classifier.

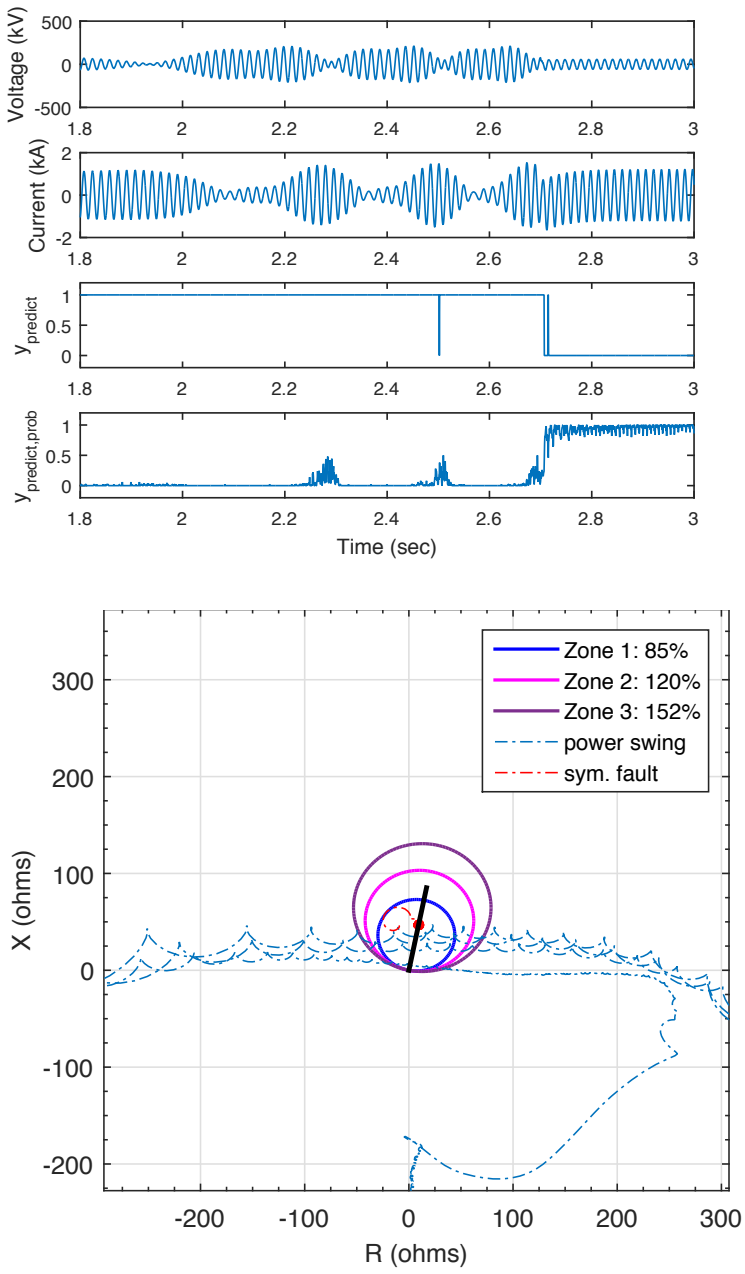

Figure 5.5: Classifier output for one power swing scenario. Voltage and current waveforms, predicted class, and predicted probability shown in (a). Corresponding impedance plane trajectories shown in (b).

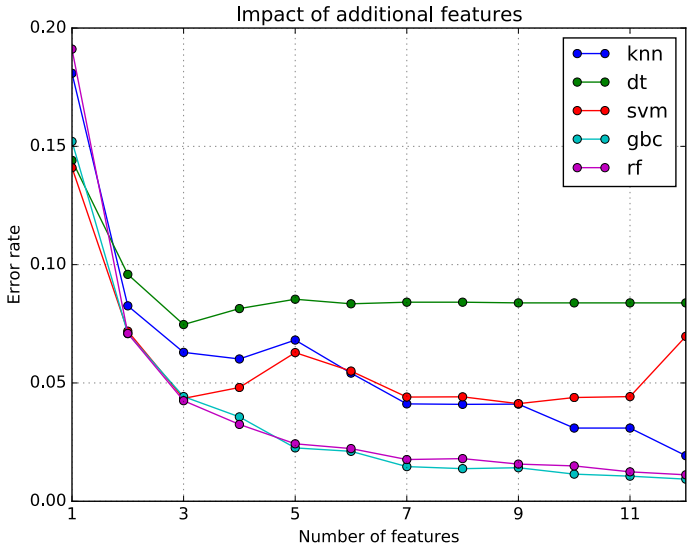

Figure 5.6: Classification error rate on test set as a function of the number of input features. Features are added sequentially in order of decreasing importance.

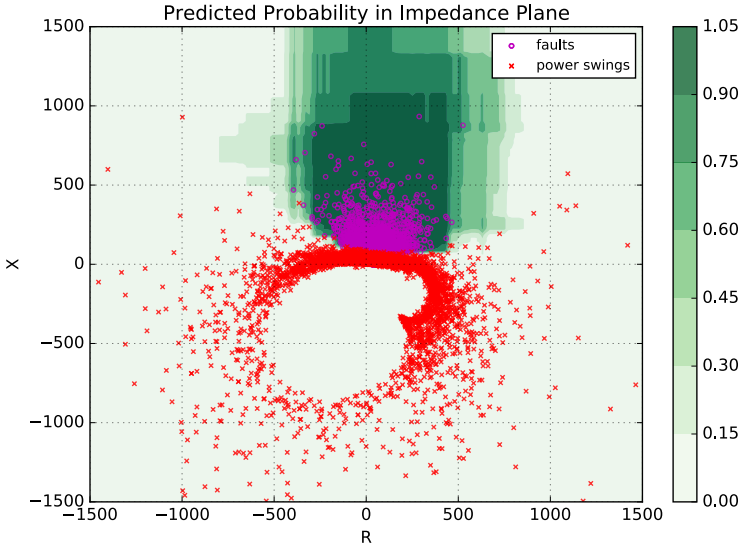

Figure 5.7: Predicted probability contours for random forest classifier. Data for faults and power swings are shown from training set.

Chapter 6

Stochastic Optimization of Discrete Overcurrent Relay Characteristics

This chapter develops the calculation of relay operating settings formulated as a stochastic optimization problem. In classical distribution networks, the system is designed for unidirectional power flow in radial feeders. Distributed generators introduce variable output sources that can impact fault current levels observed by protective relays, causing loss of coordination and unwanted operations. As penetration of DGs increases in the distribution system, a more complex protection system is required to ensure secure and reliable operation. At present, most utilities in North America require that DGs downstream of protection be de-energized when the protective relay senses a disturbance and opens a circuit breaker [17]. This ensures that DGs have minimal impact on existing protection schemes. However, fast reclosing schemes for temporary faults introduce additional challenges. Proper coordination is required so that the recloser waits long enough to allow downstream DGs to disconnect (known as anti-islanding detection) before the breaker is reclosed [68].

Overcurrent relays typically follow an inverse time operating characteristic that

allows for coordination between primary and backup relays. Coordination is achieved by delaying relays that are further upstream with some minimum amount of time delay, called the coordination time interval (CTI). The CTI represents uncertainty in the exact time a relay should open and captures the lack of precision due to factors such as current transformer errors, dc offset, fault impedance, and primary breaker failure. Operation of relays closest to the substation, however, can become slow if there are multiple relays needing coordination to accommodate CTIs and breaker operating times between each relay.

Furthermore, distribution systems are conventionally designed for unidirectional power flow with radial feeders. A high penetration of distributed generators (DGs) can affect fault current levels, contributing to protection coordination issues in fault detection and loss of selectivity [69–71]. The severity depends on the type and location of DGs, with synchronous DGs having the most impact. The impact to protection coordination from inverter-based DGs is less significant due of the ability to limit fault current and disconnect during faults. However, large photovoltaic (PV) generation on a distribution feeder can still cause varying fault current levels observed by protective relays and affect relay operating times [72–74]. For example, the ability of relays to sense faults can be affected on long branches with large DG generation due to reduced current at the substation breaker when downstream DGs are feeding the fault.

Several approaches have been proposed to improve the performance of protective relays in distribution systems. The conventional practice is to perform a relay coordination study of the worst-case fault scenarios and set each relay sequentially until full coordination is achieved in the system. This goal can be formulated as an optimization problem, where the objective is to minimize the sum of all relay operating times in the system with constraints to enforce coordination and selectivity.

This approach was introduced in [27], where the objective function minimizes the weighted sum of all relay operating times over possible time-dial and pickup settings. This framework is further developed in [28], where an adaptive scheme is introduced. A heuristic approach is presented in [75] combining a genetic algorithm (GA) with a linear program subproblem for increased computational efficiency. In [76], a meta-heurstic and linear programming algorithm is introduced to optimize coordination of directional overcurrent relays considering grid and islanded operation. In [77] a fuzzy-based GA is proposed for overcurrent relay coordination in interconnected networks and [78] considers DG location with optimal relay coordination using GA. In [79], a communications-based protection algorithm using blocking schemes is proposed. An adaptive scheme is proposed in [80] with settings depending on the grid connected or islanded mode of operation. In general, results have shown improvement in protection system speed and performance by minimizing fault clearing times.

Prior formulations to optimize overcurrent relay coordination, however, have applied an objective function minimizing the total sum of operating times for near and far end faults. These approaches, while effective, are further restrained to relay tripping times following the shape of the specified characteristic equation. In this work, a stochastic mixed-integer linear program (MILP) is formulated to minimize a relay's tripping time at discrete fault current intervals and considers the cost of tripping a relay as the objective function. The formulation takes into account the probabilistic nature of the fault current observed at each relay, which can be impacted by fault location, fault resistance, breaker failure, and DG output. Monte Carlo simulation is used to determine the empirical probabilities of each relay observing a particular fault current. Linear constraints are formulated for multiple relays to require selective and coordinated operation with downstream devices. The

concept is illustrated in Fig. 6.1 where the characteristic of relay i is determined by optimizing tripping time t_{ij} for each jth current interval. The resulting MILP is solved with the commercial solver CPLEX [81] and is shown to have fast solution times even for large systems and thousands of fault scenarios. The fast solution time further allows for the capability of adaptive relaying to change tripping characteristics based on fault current probabilities. Compared to prior approaches, the proposed method results in an optimal solution with a decrease in expected energy disconnected due to faults by over 11% for 10 000 Monte Carlo fault scenarios. The remainder of this chapter is organized as follows. The proposed stochastic MILP formulation is described in Section 6.1. The proposed approach is then applied to a simple radial test system in Section 6.2 to demonstrate its performance in comparison with conventional approaches. Scenarios with probabilistic models for DG are then studied in Section 6.3. The results are discussed in Section 6.4 and final conclusions in Section 6.5.

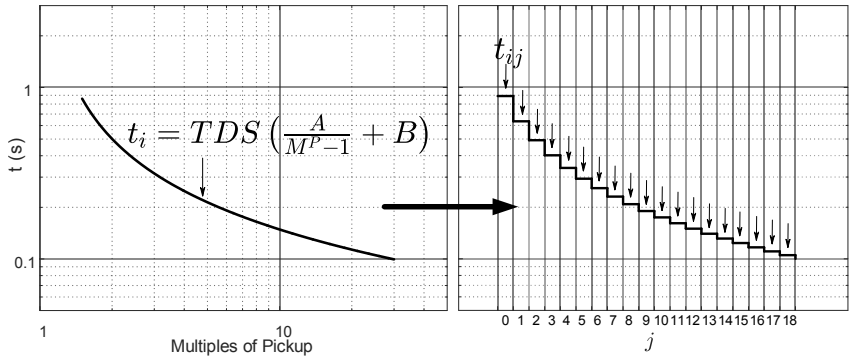

Figure 6.1: Conceptual illustration with conventional curve on left and proposed approach on right where the characteristic of relay i is determined by optimizing tripping time t_{ij} for each jth current interval.

6.1 Proposed Stochastic Optimization Formulation

6.1.1 Problem Formulation

In each of the prior methods discussed previously, the time-delayed tripping characteristic is defined by an analytic function that continuously maps measured fault current to a time-delay. The proposed approach, rather than trying to find an optimal curve, instead seeks to directly find an optimal operating time, t_{ij}, associated with each possible value of fault current j for every relay i in the network. To simplify the problem, the continuous space of possible fault currents, j, is discretized into m discrete levels. The problem is then formulated as a stochastic MILP whose objective is to minimize expected energy loss for customers and distributed generators in the network due to faults. The solution of this problem yields an optimal set of operating times $\{t^{\star}_{ij}\}$ for all possible fault currents and defines a piecewise constant function specifying each relay's tripping characteristic.

The MILP is first formulated and applied to a simple radial distribution feeder. The feeder is protected by a total of n relays, with each relay protecting one of n discrete sections. Aggregated customer load and distributed generation is connected to each bus. The system load current and the fault contribution of distributed generation will change over time. Therefore, the optimal tripping times are determined at each relay such that only the nearest relay trips for any fault on the feeder. The notation is defined below.

Sets:

$\omega \in \Omega$	set of fault scenarios
$i \in I$	set of line-sections, $I = \{1, 2, ..., n\}$
$j \in J$	set of discretized current levels, $J = \{1, 2, ..., m\}$

Data:

$(i^\omega, j^\omega, R^\omega)$	fault scenario ω
i^ω	is the faulted line-section in scenario ω, $i^\omega \in I$
j^ω	the observed fault-current level in scenario ω, $j^\omega \in J$
R^ω	the set of line-sections that have functional relays that observe the fault in scenario ω, $R^\omega \subseteq I$
ρ^ω	the probability of observing the fault scenario ω, $\omega \in \Omega$
DG_i	distributed generation in line-section i, $i \in I$
$Cust_i$	aggregated customer load connected to line-section i, $i \in I$
C_i	the total customer load and distributed generation in MVA on line-section i, where $C_i = DG_i + Cust_i$, $i \in I$
δ	time duration a breaker stays open to clear fault if reclosing is deployed
γ	sum of relay sense time and breaker operating time. Relay sense time is time a relay needs to identify a fault. Breaker operating time is the mechanical operating time of the breaker.
ϕ_{ij}	discretized melting time for a fuse in line-section i on observing a fault-current level j
χ	scalar parameter for controlling conservativeness of the relay characteristics
M	a sufficiently large constant

Variables:

t_{ij}	the operating time for relay in line-section i on observing a fault-current level j
L^{ω}	the energy loss associated with a fault scenario ω
V^{ω}	the shortest operating time of all functional relays observing a fault, $V^{\omega} = min_{r \in R^{\omega}} t_{r,j^{\omega}}$
y_i^{ω}	is a binary variable that equals 1 if the relay in line-section i has a minimal operating time for fault scenario ω, and equals 0 otherwise
x_i^{ω}	is a binary variable that equals 1 if the customers in line-section i lose power under fault scenario ω, and 0 otherwise
f_{ij}	discretized melting time for a fuse in line-section i on observing a fault-current level j

The model is formulated as follows:

$$\min_{t_{ij}} \sum_{\omega} \rho^{\omega} \cdot L^{\omega} \tag{6.1}$$

$$\text{s.t.} \quad L^{\omega} = (V^{\omega} + \delta) \sum_{a=i^{\omega}}^{n} C_a + \delta \sum_{a=0}^{i^{\omega}-1} x_a^{\omega} C_a \qquad \forall \omega \in \Omega \tag{6.2}$$

$$t_{ij^{\omega}} \geq V^{\omega} \qquad \forall \omega \in \Omega, \forall i \in R^{\omega} \tag{6.3}$$

$$t_{ij^{\omega}} \leq V^{\omega} + (1 - y_i^{\omega}) \cdot M \qquad \forall \omega \in \Omega, \forall i \in R^{\omega} \tag{6.4}$$

$$\sum_{i \in R^{\omega}} y_i^{\omega} \geq 1 \qquad \forall \omega \in \Omega, \forall i \in R^{\omega} \tag{6.5}$$

$$y_i^{\omega} \leq x_i^{\omega} \qquad \forall \omega \in \Omega, \forall i \in R^{\omega} \tag{6.6}$$

$$x_{i-1}^{\omega} \leq x_i^{\omega} \qquad \forall \omega \in \Omega, \forall i \in I - \{0\} \tag{6.7}$$

$$V^{\omega} - t_{ij^{\omega}} + \chi(\gamma + \phi_{ij^{\omega}}) \leq x_i^{\omega} \chi(\gamma + \phi_{ij^{\omega}}) \qquad \forall \omega \in \Omega, \forall i \in R^{\omega} \tag{6.8}$$

$$f_{ij} = \phi_{ij} \qquad \forall j \in J, \forall i \in I \tag{6.9}$$

$$t_{ij} + \gamma \leq t_{i-1j} \qquad \forall j \in J, \forall i \in I - \{0\} \tag{6.10}$$

$$x_i^{\omega} \in \{0, 1\} \qquad \forall \omega \in \Omega, \forall i \in R^{\omega} \tag{6.11}$$

$$y_i^{\omega} \in \{0, 1\} \qquad \forall \omega \in \Omega, \forall i \in R^{\omega} \tag{6.12}$$

Faults are considered to occur with randomly distributed fault impedance, location, and pre-fault system loading. Therefore the faulted line-section, i, and observed fault current, j, are random variables to model this behavior. In radial systems, sequential relays provide a backup functionality when the primary relay fails to clear a fault by time-grading its operation. To model this functionality, for each fault at location i and fault current j, circuit breakers at each relay location may be considered to be malfunctioning, resulting in a stochastic set of line-sections with functional relays that observe the fault, R. The term *fault scenario* describes

all these factors and many fault scenarios are possible. A particular fault scenario, denoted by ω, is defined as $\omega = \{i^\omega, j^\omega, R^\omega\}$.

Let t_{ij} be the operating time for relay in line-section i on observing a fault-current level j in a radial system. The objective is to obtain an optimal operating time for each relay considering varying output of distributed generators and loads while aiming to minimize the expected value of the energy loss, L^ω, corresponding to each potential fault scenario ω. The loss function L^ω defines the energy disconnected in each fault scenario. Energy disconnected due to relay operations is a natural choice for the loss function as it corresponds to typical reliability indices, such as SAIDI and CAIDI [82].

6.1.2 Explanation of Constraints

Constraints (6.2) - (6.12) link the relay operating time t_{ij} and the loss function L^ω by requiring that relays operate in a coordinated and selective manner. Constraint (6.2) indicates that L^ω can be split into two summands: 1) the amount of load and generation in the line-sections downstream to the fault, and 2) the amount of load and generation in the line-sections upstream to the fault. The first summand in constraint (6.2) indicates that load and generation downstream to the fault will lose power during the fault and clearing time. The second summand indicates that load and generation upstream to the fault will lose power only during fault clearing time. The binary variables x_a^ω indicate whether line-section a loses power.

Constraint (6.3) indicates that V^ω is smaller than or equal to the operating time of all the functional relays observing the fault current. Constraint (6.4) indicates that if the relay at line-section i in scenario ω trips, the operating time of that relay is the shortest operating time of all the relays observing the fault current. If the relay does not trip, (6.4) becomes a redundant constraint. The purpose of constraint

(6.3) and (6.4) is to guarantee that V^{ω} is the shortest operating time of all the relays observing the fault current. Constraint (6.5) indicates that for each scenario, there is at least one relay tripping. Constraint (6.6) requires that if $y_i^{\omega} = 1$ (i.e., the relay of line-section i in scenario ω trips), then $x_i^{\omega} = 1$, and the customers at line-section i in scenario ω lose power. Constraint (6.7) ensures that if line-section i loses power, so do any line-sections downstream from i. Constraint (6.8) ensures that relays whose trip time is within $\chi(\gamma + \phi_{ij^{\omega}})$ of the minimum trip time for a scenario also trip and requires that relays operate slower than the downstream fuses, allowing them to clear the fault first.

If $V^{\omega} - t_{ij^{\omega}} + \chi(\gamma + \phi_{ij^{\omega}}) > 0$, then x_i^{ω} must equal one to satisfy the constraint. Otherwise, if $V^{\omega} - t_{ij^{\omega}} + \chi(\gamma + \phi_{ij^{\omega}}) \leq 0$, then x_i^{ω} can be zero. Constraint (6.9) simulates the TCC curve of the fuse and constraint (6.10) requires a backup relay to operate slower than a primary relay by a duration of γ. Constraints (6.11) and (6.12) require x_i^{ω} and y_i^{ω} to be binary variables. The scalar parameter χ allows adjustment of the overall speed of the characteristics without violating other constraints in model (6.1). Increasing χ will increase the operating time, t_{ij}, in the regions of j where fault current distributions overlap and allows for control of the conservativeness of relay characteristics or further coordination with fixed-characteristic devices such as fuses. This model is applicable to any radial distribution topology.

6.2 Case Study: Simple Radial Test System

The simple radial system shown in Fig. 6.2 is used to demonstrate performance of the proposed approach in comparison with conventional and parameter optimization approaches. The simple test system is a three-bus system with data from [41], shown in Table 6.1. The relays are coordinated with minimum CTI = 0.3 s and breaker operating time of 5 cycles (0.083 s). Only three-phase and single line-to-ground

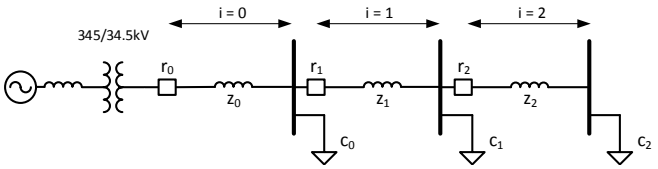

Figure 6.2: Single-line diagram of a simplified radial distribution system.

faults are considered.

Table 6.1: System Data

Bus	Max Load (MVA)	Max I_f (A)
0	11	3000
1	4	2000
2	6	1000

6.2.1 Illustrative Example

An illustrative example is first presented to provide intuition on how the model calculates optimal tripping times. Assume only two fault scenarios ($\omega = \{0, 1\}$) are possible for the three line-sections ($i = \{0, 1, 2\}$) corresponding to Fig. 6.2. The fault current observed by relays $r_0, r_1,$ and r_2 is discretized into three levels ($j = \{0, 1, 2\}$) as follows, where I_f is given in amperes:

$$j = \begin{cases} 0, & 500 \leq I_f \leq 1000 \\ 1, & 1000 < I_f \leq 2000 \\ 2, & 2000 < I_f \leq 3000 \end{cases} \tag{6.13}$$

The fault scenario data for this example is listed in Table 6.2. In scenario 0, a fault occurs in the most downstream line-section, $i = 2$, resulting in the lowest fault current level 0 with $i^0 = 2$ and $j^0 = 0$. All three relays are functional and observe the fault current, $R^0 = \{0, 1, 2\}$. In scenario 1, a fault occurs in line-section

$i = 1$, resulting in fault current level 0 with $i^1 = 1$ and $j^1 = 0$. Relays 0 and 1 are functional and observe the fault current, so $R^1 = \{0, 1\}$. Finally, assume that scenario 0 is more likely to occur than scenario 1 and so different probabilities are assigned for each scenario: $\rho^0 = 0.75$, $\rho^1 = 0.25$.

Table 6.2: Two fault scenario data

Scenario, ω	i^ω	j^ω	R^ω	ρ^ω
0	2	0	0, 1, 2	0.75
1	1	0	0,1	0.25

The maximum load in each line-section is considered from Table 6.1, with $C_0 =$ 11 MVA, $C_1 = 4$ MVA, $C_2 = 6$ MVA. The amount of time required to clear the fault is $\delta = 1$ s and the sum of relay sense time and breaker operating time is $\gamma = 0.2$ s. The parameter $\chi = 1$ and no fuses are in the system. By solving the MILP model, the optimal relay operating times are found to be $t_{00} = 0.4$ s, $t_{10} = 0.2$ s and $t_{20} = 0$ s. V^ω can be obtained for each scenario by choosing the shortest relay operating time in the scenario. $V^0 = min(t_{00}, t_{10}, t_{20}) = min(0.4, 0.2, 0) = 0$ s. Similarly, $V^1 = 0.2$ s.

The constraints (6.5) - (6.12) restrict relays to operate in a selective and coordinated manner. For example, consider scenario 0, where $y_\cdot^0 = (0, 0, 1)$ and $x_\cdot^0 = (0, 0, 1)$. This indicates that the relay in line-section 2 is the one that clears the fault, and that only line-section 2 loses power. Similarly, for scenario 1, $y_\cdot^1 = (0, 1, 0)$ and $x_\cdot^1 = (0, 1, 1)$ indicates that the relay in line-section 1 clears the fault, and only line-sections 1 and 2 lose power. Given the values of the x^ω and V^ω variables, it is straightforward to calculate the expected energy loss in each scenario through constraint (6.2). For scenario 0, it is $L^0 = 6(V^0 + 1) + 11x_0^0 + 4x_1^0 = 6$. Similarly, for scenario 1, it is $L^1 = (V^1 + 1) \times (4 + 6) + 11x_0^1 = 12$. The overall objective function value is then $\rho^0 L^0 + \rho^1 L^1 = 0.75 \times 6 + 0.25 \times 12 = 7.5$. This result matches with the optimal objective function value.

Note that in this illustrative example, there are only two scenarios and one current level. Without scenarios for current levels 1 and 2, the model effectively treats faults at these current levels as having probability zero. As such, the model does not compute relay operating times for these current levels. In other words, in order to compute optimal tripping times for a particular current level, scenarios with faults at that current level must be present in the data.

6.2.2 Comparison with Conventional Settings

In this section, performance of the proposed approach is compared with conventional TCC curves. The relays in the system are specified as operating on the standard inverse time-current characteristic curve and the trip time t_{trip} in seconds can be expressed as specified in (6.14) for $M > 1$

$$t_{trip} = \mathrm{TDS}\left(\frac{\mathrm{A}}{\mathrm{M^P} - 1} + \mathrm{B}\right), \tag{6.14}$$

where TDS is the time dial setting, I_{pickup} is the relay pickup setting, M is the measured current in multiples of I_{pickup}, and {P, A, B} are constants chosen to emulate specific TCC curve shapes [41]. The analytic equation implemented by microprocessor relays and conforming to the IEEE C37.112-1996 Standard Inverse Time Characteristic Equations is utilized for the TCC curve, with A = 5.95, B = 0.18, and P = 2 in (6.14). Setting each relay with coordination for maximum fault current, the time-dial setting (TDS) and tap-setting (TS) are determined, with the results shown in Table 6.3.

For the comparison, all 18 possible fault scenarios are simulated for relays operating with both conventional settings and optimized tripping times. The scenario data is shown in Table 6.4. The aggregated load at each bus, C_i, is given in units of MVA with values as specified in Table 6.1. In this example, all possible com-

Table 6.3: Relay Data

Relay	Curve	CT Ratio	TS	TDS
r_0	CO-8	400:5	5	3
r_1	CO-8	200:5	5	2
r_2	CO-8	200:5	3	1/2

binations of fault location, fault current, and functional relays are chosen. The maximum expected fault current at each bus is specified in Table 6.1 and fault current is discretized into three levels as in the illustrative example.

The probability of observing each fault scenario, ρ^{ω}, is calculated with the following assumptions. Circuit breaker failure is modeled as a failure to open. In this study, the circuit breaker failure rate, λ_{cb}, is considered to be once per 50 000 commands to open [83]. Relay failure is modeled as failure to trip and the numerical relay failure rate, λ_r, is considered to be 0.018 [84]. Therefore, the probability of protection failure at each relay location $\lambda_i = 1-(1-\lambda_{cb})(1-\lambda_r)$. In the context of relay coordination, a backup relay should operate only if the primary relay or circuit breaker fails to open during a fault. It is also assumed that the line-sections are of equal length and therefore have equal exposure to faults and equal probability for each line-section [85].

Using the settings in Table 6.3 and the maximum I_f for each current level, the operating relay and associated operating times, t_{trip}, are obtained for each fault scenario. Note that the maximum continuous current I_f in each discrete current level is chosen to provide a comparison of the conventional settings at its fastest operating time, for each current level j. The operating times are then inserted into the cost function, L^{ω}, to compute the expected energy loss for the conventional settings. This value is calculated to be 20.070. The same scenarios are then used as data for the MILP formulation given by model (6.1). The problem is solved with a

Table 6.4: Simplified fault scenario data

Scenario, ω	i^ω	j^ω	Functional Relays, R^ω	ρ^ω
1	2	0	0, 1, 2	0.076002
2	2	1	0, 1, 2	0.253339
3	2	2	0, 1, 2	0
4	2	0	0, 1	0.001370
5	2	1	0, 1	0.004565
6	2	2	0, 1	0
7	2	0	0	0.000025
8	2	1	0	0.000082
9	2	2	0	0
10	1	0	0, 1	0
11	1	1	0, 1	0.109780
12	1	2	0, 1	0.219561
13	1	0	0	0
14	1	1	0	0.001978
15	1	2	0	0.003956
16	0	0	0	0
17	0	1	0	0
18	0	2	0	0.329341

total solution time of 0.032 s. The value of the objective function at the optimum is 13.998. The optimal coordinated relay operating times, t_{ij}, are plotted in Fig. 6.3 as $t_{i,op}$ where i corresponds to relay r_i.

First, it can be observed that the proposed approach improves upon the expected loss, reducing it from 20.070 to 13.998 (see Table 6.6). This is a direct result of finding shorter relay tripping times, t_{ij}, at all current levels. Next, it can be observed that the solution defines an inverse step function, which follows intuition as time-grading facilitates coordination between relays. The constraints defined in model (6.1) force the relay operations to be coordinated for all fault scenarios. It is observed that the relay r_2 at the end of the feeder operates nearly instantaneously. Because relay r_2 is protecting the end of the line, if any fault current is observed, the relay should operate without any intentional time-delay. Similarly for relays r_1

and r_0, the tripping operation is only delayed enough to give the primary relay time to operate. If fault current is observed past this delay, the relay no longer needs to wait and will trip. In comparison with conventional TCC curves at all fault current levels, there is no excess delay beyond what is required for the downstream relay and breaker to operate. It is observed in Fig. 6.3 that as the TDS values increase, large delays are incurred for smaller fault currents due to the shape of the TCC curve. The proposed approach, therefore, eliminates these excess delays while taking into account the necessary uncertainties.

6.2.3 Comparison With Parameter Optimization Approach

In this section the proposed approach is compared with a relay parameter optimization formulation to minimize the sum of relay operating times for all near-end faults [28]. The simplified formulation is provided in model (6.15).

$$\min_{\mathrm{TDS}_i} \sum_{i=1}^{n} w_i t_i \tag{6.15}$$

$$\text{s.t.} t_j - t_i \geq \mathrm{CTI} \quad \forall (i,j) \in \Omega \tag{6.16}$$

$$t_i = a_i \times \mathrm{TDS}_i \tag{6.17}$$

$$a_i = \frac{k}{(I_{mpu})^n - 1} \tag{6.18}$$

where t_i = time delay of relay i for a near-end fault, n = number of relays, and w_i = likelihood a fault occurs in a given zone (set to one). The coordination constraints are specified in (6.16) and ensure that the delay between primary and backup relays are greater than the CTI. Constraints (6.17) and (6.18) restrict the relay to operate on a specified TCC curve. The problem reduces to a linear program by considering a_i as a constant for specific near-end fault current, I_{mpu}.

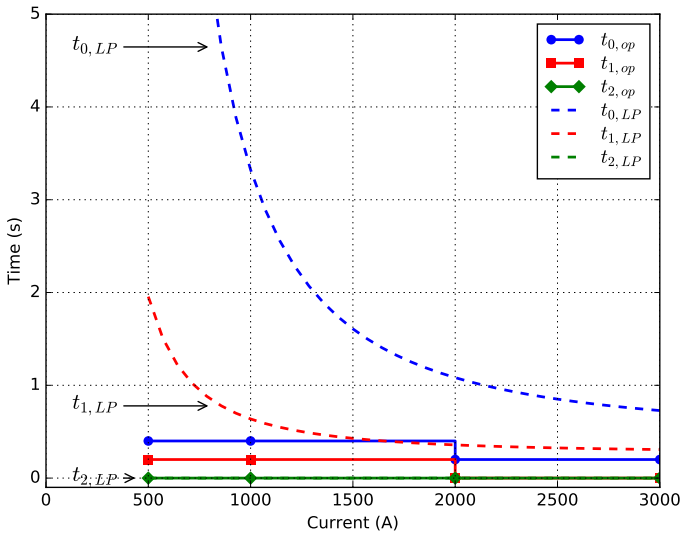

Figure 6.3: Comparison of proposed optimal tripping characteristic with parameter optimization of TCC curves approach. The proposed approach provides faster operating times for all fault currents.

The parameter optimization approach is then solved for the same test system as both a linear program and as an integer program (IP) by considering discrete values of TDS. The solution to this model minimizes the sum of all relay operating times. By inserting the $t_i = a_i \mathrm{TDS_i}$ values obtained from the parameter optimization model into the objective function (6.1), it is shown that the result is only marginally better than the conventional relay settings. A comparison of the conventional TDS solution with that of the parameter optimization approach is shown in Table 6.5. It can be observed that if the parameter optimization model is solved as an integer program, the solution, TDS_{IP}*, is nearly identical to the conventional setting approach. The linear program solution, TDS_{LP}*, provides only marginally faster operating times. The objective function value of each approach is compared in Table 6.6 and operating times from the linear program solution are compared in Fig. 6.3, shown as $t_{i,LP}$ for each relay.

Table 6.5: Comparison of Optimal Settings

Relay	Curve	TS	TDS_{conv}	TDS_{IP}*	TDS_{LP}*
r_0	inverse	5	3	3	2.530
r_1	inverse	5	2	2	1.489
r_2	inverse	3	1/2	0	0

Table 6.6: Total Expected Energy Loss From Relay Operations

Relay Setting Approach	Objective Function Value
Conventional TCC	20.070
Parameter Optimization, IP	19.856
Parameter Optimization, LP	18.540
Proposed Approach	13.998

6.3 Case Study: IEEE 34-Node Feeder

In this section, the IEEE 34-Node radial distribution feeder is used to demonstrate the proposed approach in the presence of uncertainty due to DG output. The test feeder is specifically chosen for its topology, availability of load and short-circuit data, and DG integration studies [86–89]. The feeder can be characterized as long and lightly loaded, supplied from a 69kV/24.9kV substation transformer that operates on a 2.5 MVA base. The total load on the feeder is 1.769 MW. The single-line diagram of the test feeder is shown in Fig. 6.4 with locations for overcurrent relays and DG modified from [86] and [87].

6.3.1 Probabilistic Fault Scenarios with DG

Renewable-based DG can impact the available fault current levels and result in bidirectional flows on the feeder. In such cases, directional overcurrent relays (DOCRs) can be utilized to maintain sensitivity and selectivity. The proposed approach is readily applied with DOCR schemes in radial systems simply by applying model

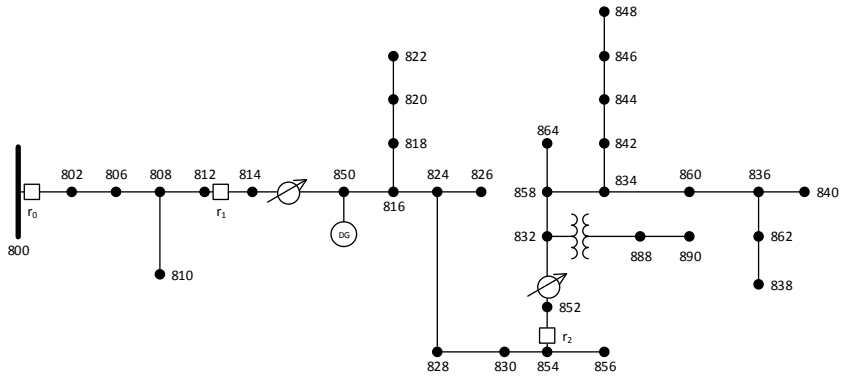

Figure 6.4: IEEE 34-node test feeder with modified protection and DG locations.

(6.1) to the set of relays looking in the same direction. For example, if the relays shown in Fig. 6.4 are considered to be looking in the forward direction, model (6.1) is applied only to these relays and separately to solve for the coordinated characteristics of the set of relays looking in the reverse direction. In this section, a solar PV generation plant is connected to the three-phase node 850 and is modeled using the methodology in [87]. The PV plant is sized at 700 kW, corresponding to 40% penetration, to study the impact to the optimal characteristics. PV output for the next hour is modeled by a Beta distribution function [90] and two scenarios are considered for maximum solar irradiance:

1. low irradiance, corresponding to a maximum of 14%

2. full irradiance, corresponding to a maximum of 100%

The scenarios represent probability distributions corresponding to solar irradiance for different times of day or forecasted weather conditions.

Furthermore, fault location is considered to be uniformly distributed with respect to the length of each line-section and the relay locations are chosen to approximately equalize the probability of faults on the resulting zones. Fault resistance is characterized by a high probability of small resistance and a maximum resistance of 40

Ω [91]. It can be modeled as a discrete or continuous random variable following a Beta and Weibull distribution functions; the Weibull distribution is chosen to model fault resistance. The system is modeled in OpenDSS [92] and probabilistic fault scenarios are simulated resulting in a distribution of fault currents at each relay location. The distributions of fault current observed at each relay over 10 000 Monte Carlo simulations are shown in Fig. 6.5a and Fig. 6.5b with mean μ and standard deviation σ, respectively for both irradiance scenarios.

6.3.2 Optimal Tripping Characteristics

The simulation data is then input to the model (6.1) to solve for optimal relay tripping times. With more data available for this test system, the number of current discretization levels is chosen as 20 uniformly sized bins in fault current. The size of the resulting optimization problem is much larger compared to the simple radial test system in Section 6.2. The number of current levels has increased from 3 to 20 and the number of scenarios has increased from 18 to 10 000. However, the problem is solved in a reasonable time, with an optimal solution found in 8.77 s. The resulting optimal characteristics are shown in Fig. 6.5c and 6.5d.

It is first observed from Fig. 6.5a and Fig. 6.5b that the mean of the distribution for relay 1 decreases due to the DG downstream and the mean of the distribution for relay 2 increases due to the DG upstream. Although the changes in fault current are relatively small, an average decrease of less than 1 A for relay 1 and an average increase of less than 10 A for relay 2, the overlap between distributions has increased as shown in Fig. 6.5b. The result corresponds to more uncertainty in whether the fault is located in the primary relay's protected zone. The subsequent optimal tripping characteristics in Fig. 6.5d show that as the uncertainty (i.e., the overlap between distributions) increases, the tripping time becomes more conservative. This

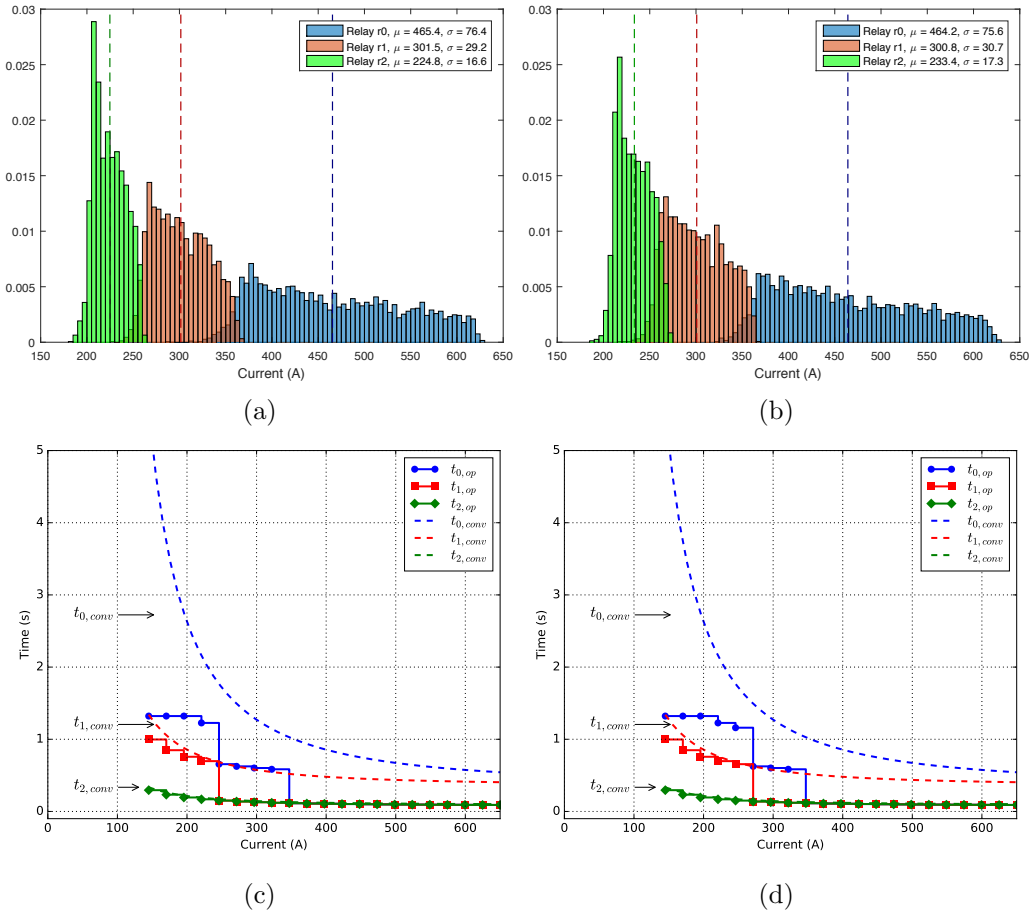

Figure 6.5: Distribution of fault currents observed at each relay for 10 000 Monte Carlo fault scenarios are shown for (a) 14% and (b) 100% maximum irradiance scenarios for a 700 kW distributed generator at node 850. The corresponding optimal characteristics are shown with $\chi = 1.5$. in (c) and (d), respectively.

can be observed in the characteristics for relay 1 where the tripping time for fault currents in the range 250 to 275 A has increased, exactly the range where there is more overlap with faults located downstream of relay 2. The proposed model produces an optimal solution for this data, allowing relay 2 to clear faults in its protected zone with increased fault current due to the DG. Conversely, when the fault current contribution from DG is expected to be low as in Fig. 6.5a, the proposed model finds faster optimal characteristics.

In comparison with the conventional approaches, the optimal characteristics provide faster operating times for all current levels. The resulting objective function value over all 10 000 scenarios for conventional TCC, LP parameter optimization, and the proposed approach is 2.058, 1.816, and 1.707, respectively. The proposed approach therefore provides a 6% decrease in expected energy loss compared to the fastest TCC characteristics provided by the LP parameter optimization approach. Additional performance gains up to 11.5% can be achieved by further reducing the conservativeness parameter χ to 1.

6.4 Discussion

The results in Sections 6.2 and 6.3 demonstrate that the proposed approach finds optimal tripping characteristics for fast to instantaneous operation at high fault currents and reduced tripping times at lower fault currents. The proposed approach is also demonstrated as an adaptive scheme by considering sets of probability distributions for different operating conditions. The probability of each fault scenario ω depends upon the fault location i^{ω}, observed fault-current level j^{ω} and the reliability of the protective relays R^{ω}. Therefore, different fault scenario probability distributions can be considered for seasonal changes, imminent storm conditions, or based on forecasted DG output [93]. Even for large data sets, the proposed MILP can be solved quickly, providing the capability for relay tripping characteristics to be updated on a reasonable time-horizon, such as every hour. Ideally for a large distribution network the protection system should minimize the loads disconnected due to any fault clearing operation. Therefore, another benefit is to potentially allow more relays to be coordinated in a distribution network. Relays operating with existing TCC curves, however, may be limited by unacceptable time-delays introduced from multiple devices coordinated in series.

Practical issues for implementation also need to be considered as the proposed approach requires microprocessor-based overcurrent relays to operate on a characteristic different than existing TCC curves. It is shown in Sections 6.2 and 6.3 that the solution of the proposed MILP results in an optimal operating characteristic that is an inverse piecewise constant function mapping observed fault current to an optimal tripping time. Consequently, programming of relays to operate on this optimal characteristic will not require more computational power than what is presently utilized in existing relays.

Another consideration regarding implementation is with respect to the fault scenario data. An example of the data required to solve the proposed optimization model is provided in Table 6.4. Monte Carlo simulations can be run off-line to generate the necessary input to the proposed model. Historical or vendor provided data can be used to estimate the circuit breaker failure rates and fault incidence per mile. As updated estimates of fault probabilities and load profiles are made available, the fault scenario probabilities ρ^{ω} can be updated accordingly. The proposed approach can thus take advantage of more information as it becomes available in the future.

6.5 Summary

In summary, this chapter proposes a stochastic mixed-integer linear program to determine optimal tripping characteristics for overcurrent relays in radial distribution systems. The objective is to minimize the expected value of load and generation disconnected due to relay operations. Case studies are performed on a three-bus radial distribution feeder and performance is compared with conventional approaches. Case studies with distributed generation are preformed on the IEEE 34-Node Test Feeder. Results show that the proposed approach finds faster operating times and maintains coordination without needing communication between relays.

Chapter 7

Optimal Allocation of Protective Devices in Distribution Systems

The location of protective devices and isolating switches is a key factor impacting the reliability performance of distribution networks. Devices such as circuit breakers, reclosers, sectionalizers, and fuses operate automatically to detect and clear faults. Isolating and tie switches (ISs and TSs) operate to allow healthy sections of the circuit to be restored either manually or automatically. In general, as more devices are installed, network reliability improves as faults impact fewer customers. However, the trade-off is the installation and maintenance cost of each device. Distributed generators (DGs) connected through tie switches can further improve reliability if intentional islanding is allowed [94–96].

Therefore, the allocation of protective devices and switches can be formulated as an optimization problem to minimize the expected total reliability cost, which is typically composed of a cost-based reliability index and the cost of the devices themselves. However, prior work has often made simplifications to consider a relaxed problem. For example, the allocation of reclosers, fuses, and sectionalizers are often

considered as an independent problem from isolating switch allocation [97–99]. Furthermore, sectionalizers have been considered functionally identical to reclosers. As a result, the models do not capture the full interaction between devices and therefore do not fully account for the impact to reliability. A second simplification is to divide a feeder into main line and lateral sections while aggregating loads on the secondary circuit instead of considering the full system topology [97, 98]. The simplification restricts the solution by reducing the number of possible device locations.

A third simplification is to ignore the impact of momentary interruptions and the trade-off between momentary/sustained interruptions [97–102]. There is an increasing need to incorporate the economic losses of customers due to momentary interruptions and other power quality events [103]. Depending on the frequency of temporary faults and the sensitivity of electronic equipment in the system, this cost can be significant. A fourth simplification is to ignore the capability for distributed generators to sustain temporary islands while the faulted section is repaired. This practice is not yet commonly applied, but as distributed generators become more prevalent, it is important to consider this possibility [97–99, 101, 102]. Lastly, several models use a non-linear formulation to describe the dependencies between protective devices and their impact to reliability indices. The problem can be solved with heuristic algorithms, however, they cannot guarantee optimality and may be slow to converge for large systems [100, 101, 104].

In this chapter, a new formulation is presented that comprehensively considers the key factors impacting reliability in distribution networks without making the above simplifications. The formulation relies on representing the full distribution network as a directed graph to consider the complete interactions between devices. The specific impact of each protection device type (circuit breaker, recloser, sectionalizer, fuse) and isolating switch is further modeled, e.g., momentary interruptions

caused by reclosers are considered. As the number of network nodes becomes larger, however, the optimization problem becomes more difficult to solve. The proposed approach addresses this challenge by applying efficient graph search algorithms on the directed graph representation to pre-process the network data for each node. The approach facilitates the formulation of a mixed-integer linear program (MILP), which is significant because the global optimal solution can be computed in a reasonable time. It further allows for practical comparison of solutions for multiple scenarios of DG location and capacity.

7.1 Notation and Data Preprocessing

In this section, the mathematical notation for the sets, parameters, and decision variables used in the MILP formulation are first defined. A description of the process for translating device models and distribution system data for graph representation is then presented. Finally, the process of determining feasible nodes for isolating switches performing downstream restoration operations is described.

7.1.1 Notation

Sets:

I	set of nodes in the tree
U_i	set of nodes upstream to i, including i, $i \in I$
D_i	set of nodes downstream to i, including i, $i \in I$
B_{ik}	set of nodes downstream to k and upstream to i, $B_{ik} = D_k \cap U_i$, $i \in I, k \in U_i$
B'_{ik}	set of nodes downstream to k but not downstream to i, $B'_{ik} = D_k \cap D_i^c$, $i \in I, k \in U_i$
ML	set of nodes on the main line
O	source node of the network system
V	set of devices: reclosers (R), fuse-blowing fuses (F^γ), fuse-saving fuses (F^λ), sectionalizers (S), isolating switches (IS) and circuit breaker (CB). $V = \{R, F^\gamma, F^\lambda, S, IS, CB\}$, where the circuit breaker is used and only used in the source node

Parameters:

γ_i	probability of temporary fault in i, $i \in I$
λ_i	probability of permanent fault in i, $i \in I$
C_i^λ	sustained outage cost per load per unit time in i, $i \in I$
C_i^γ	momentary outage cost per load per unit time in i, $i \in I$
r^γ	momentary outage time
$r_{ik}^{F^\gamma}$	outage time if the fault in i is cleared by fuse-blowing fuse in k, $i \in I$, $k \in U_i$

$r_{ik}^{F^\lambda}$ outage time if the permanent fault in i is cleared by fuse-saving fuse in k, $i \in I$, $k \in U_i$

$r_{ik}^{v^\gamma}$ outage time if the temporary fault in i is cleared by device v in k, $i \in I$, $k \in U_i$, $v \in \{R, CB\}$

$r_{ik}^{v^\lambda}$ outage time if the permanent fault in i is cleared by device v in k, $i \in I$, $k \in U_i$, $v \in \{R, CB\}$

r_c^v replacement time of device v, $v \in \{F^\gamma, F^\lambda, CB\}$

N_i number of customers in node i, $i \in I$

L_i amount of energy consumption (kW) in node i, $i \in I$

m number of times the recloser trips

n_v number of available device v, $v \in V$

C_v unit cost of device v, $v \in V$

B budget for devices

a_i^v equals 1 if there is device v in node i, 0 otherwise, $v \in \{TS, DG\}$, $i \in I$

DG_i DG capacity in node i, $i \in I$

u utilization of DG

Variables:

$ECOST$ system expected interruption cost

C_D device cost

C_T expected cost due to temporary fault

C_P expected cost due to permanent fault

x_k^v equals 1 if a device v is placed in k, 0 otherwise, $k \in I$, $v \in V$

$y_{ik}^{\gamma v}$ equals 1 if temporary fault in i is cleared by device v in k, 0 otherwise, $i \in I$, $k \in U_i$, $v \in \{R, F^\gamma, CB\}$

$y_{ik}^{\lambda v}$ equals 1 if permanent fault in i is cleared by device v in k, 0 otherwise, $i \in I$, $k \in U_i$, $v \in \{R, F^{\gamma}, F^{\lambda}, CB\}$

S_{ikj}^{v} equals 1 if the permanent fault in i is cleared by the recloser in k, there's a device v in j, and v is working to keep some customers from losing power, 0 otherwise, $i \in I$, $k \in U_i$, $j \in B_{ik}$, $v \in \{S, F^{\gamma}, F^{\lambda}\}$

T_{ikj}^{v} equals 1 if the permanent fault in i is cleared by a device v in k, there is an IS in j, and the IS operates with a TS, 0 otherwise, $i \in I$, $k \in U_i$, $j \in D_i$, $v \in \{R, F^{\gamma}, F^{\lambda}, CB\}$

G_{ikj}^{v} equals 1 if the permanent fault in i is cleared by a device v in k, there is an IS in j, and the IS operates with a DG, 0 otherwise, $i \in I$, $k \in U_i$, $j \in D_i$, $v \in \{R, F^{\gamma}, F^{\lambda}, CB\}$

From this point forward, the following notation will be used for brevity: $\forall(i,k)$ will be used to mean $\forall i \in I, \forall k \in U_i$.

7.1.2 Protection Capabilities of Each Device

Each protective device has a specific role or function for system protection and therefore different impact to overall reliability. Table 7.1 is provided to indicate the fault clearing and restoration operations that are modeled for each protective device type. The mathematical model for reliability of each device and coordination with other devices is further discussed in Section 7.2.

7.1.3 Graph Representation of Distribution Systems

In a conventional radial distribution feeder topology, power flows unidirectionally from the substation to the loads. The structure can be described by a tree graph with nodes representing distribution line segments and edges representing the physical

Table 7.1: Protection Capabilities of Devices

Operation	CB	R	S	F^{γ}	F^{λ}	IS
temporary fault clearing	x	x	-	x	-	-
permanent fault clearing	x	x	-	x	x	-
automatic reclosing	-	x	-	-	-	-
upstream restoration	-	-	x	-	-	x
downstream restoration, tie switch	-	-	-	-	-	x
downstream restoration, islanding	-	-	-	-	-	x

connection between nodes. The graph representation allows for efficient preprocessing of the data and formulation of the optimal allocation problem as a mixed-integer linear program.

In order to model protective device operations as an MILP, the sets of nodes impacted in each fault scenario due to protective device operations must be generated. In each fault scenario, a fault occurs at node i. Different nodes and customers are isolated depending on which protection devices operate to clear the fault. Four sets of nodes are defined to aid the formulation in the objective function. These four sets, U_i, D_i, B_{ik}, and B'_{ik}, are illustrated in Fig. 7.1.

Set U_i is simply the set of nodes between the fault at node i and the feeder source. These nodes describe possible locations of protective devices that can clear the fault. Set D_i is the set of nodes downstream of and including faulted node i and represents customers in outage due to the fault. Set B_{ik} is the set of nodes downstream of a recloser at k and upstream of a fault at i and represents possible locations for sectionalizing devices that coordinate with the recloser. Therefore, nodes not in the shortest path between k and i are not included in B_{ik}. Similarly, set B'_{ik} is the set of nodes downstream to protective device in k but not downstream of node i and these nodes represent customers impacted by recloser momentary operations. Therefore, nodes in all connected branches are included in B'_{ik}, unlike in B_{ik}.

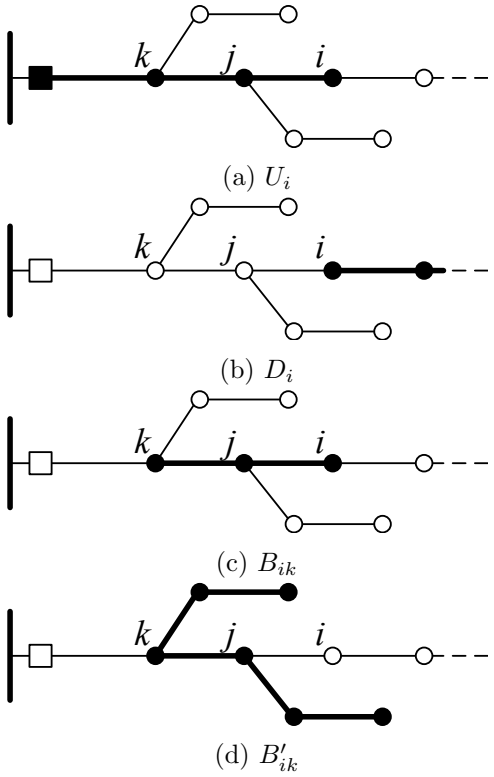

Figure 7.1: For a fault at node i in an example radial feeder, the four sets of nodes shown in (a)-(d) are used to model the impact of protective device operations. Shaded nodes are included in the set.

7.1.4 Feasible Sets for Restoration Operations

After a fault is cleared, healthy sections of the distribution feeder may be automatically restored from TS and DG islanding operations. Prior to solving the optimization problem, the set of feasible nodes for location of isolating switches are first determined where such operations satisfy conditions for coordination with DGs and TSs. For restoration from an alternate feeder, there has to be at least one TS downstream to the IS. For restoration from intentional islanding with DGs, a strategy similar to [104] is followed. First there must be at least one DG downstream of IS, and the product of the sum of DG capacities downstream to the IS and the

utilization should be greater than the sum of the loads in corresponding nodes. The proposed formulation considers a fixed location of DGs and TSs, and the approach pre-processes the system data to determine feasible locations for ISs meeting the above conditions.

7.2 Proposed Formulation

The objective function (7.1) considers monetary costs incurred to customers from momentary and sustained interruptions resulting from both permanent and temporary faults, in addition to installation and maintenance costs of the protection devices and ISs. The formulation aims to determine the type and location of protective devices, sectionalizers, and ISs that minimize the sum of costs to customers and the utility. Permanent interruption costs to customers are calculated by the reliability index ECOST and momentary interruption costs are calculated by $\text{MAIFI}_\text{e} \times \$/\text{interruption}$.

7.2.1 Objective Function

The objective function (7.1) is composed of $E[C_T]$, the expected cost due to temporary faults, $E[C_P]$, the expected cost due to permanent faults, and C_D, the cost due to device installation and maintenance. Binary decision variables x_k^v equal one if a device v is installed in node k and zero otherwise. Decision variables y_{ik}^v, S_{ikj}^v, T_{ikj}^v and G_{ikj}^v are introduced to model device operations based on their location specified by x_k^v.

$$\min \quad E[C_T] + E[C_P] + C_D \tag{7.1}$$

The costs of temporary faults are first modeled. When a temporary fault occurs, it can be cleared by a CB, recloser or fuse-blowing fuse. Therefore, the expected cost due to temporary faults, C_T, is composed of three components as shown below in (7.2).

$$E[C_T] = \sum_{i \in I} \gamma_i \left[b_i^{CB} + b_i^R + b_i^{F^\gamma} \right] \tag{7.2}$$

where,

$$b^{CB} = \sum_{k \in U_i} y_{ik}^{\gamma CB} \Big(\sum_{j \in D_k} C_j^\lambda(r^\gamma) N_j \Big) \tag{7.3a}$$

$$b^R = \sum_{k \in U_i} y_{ik}^{\gamma R} \Big(\sum_{j \in D_i} C_j^\gamma(r^\gamma) N_j + \sum_{j \in B'_{ik}} C_j^\gamma m N_j \Big) \tag{7.3b}$$

$$b^{F^\gamma} = \sum_{k \in U_i} y_{ik}^{\gamma F^\gamma} \sum_{j \in D_k} C_j^\lambda(r_{ik}^{F^\gamma}) N_j \tag{7.3c}$$

(7.3a) indicates if a temporary fault in node i is cleared by a CB in node k, then all the customers downstream to the CB will suffer permanent outage. Equation (7.3b) illustrates that for a temporary fault at i, if a recloser is located in U_i and clears the fault, customers downstream to the recloser in B'_{ik} have momentary outage. Equation (7.3c) illustrates that when the temporary fault is cleared by a fuse-blowing fuse in U_i, customers downstream to the suffer sustained outage.

For permanent faults, clearing can be accomplished by either a CB, recloser, or fuse, after which automatic sectionalizing or restoration can occur. Therefore, the expected cost due to permanent faults, C_P, is expressed in (7.4).

$$E[C_P] = \sum_{i \in I} \lambda_i \left[c_i^{dev} - c_i^{sec} - c_i^{res} \right] \tag{7.4}$$

The cost of a device clearing a permanent fault c^{dev} is defined in (7.5).

$$c^{dev} = \sum_{k \in U_i} y_{ik}^{\lambda CB} \sum_{j \in D_k} C_j^{\lambda}(r_{ik}^{CB^{\lambda}}) N_j \tag{7.5a}$$

$$+ \sum_{k \in U_i} y_{ik}^{\lambda R} \left(\sum_{j \in B'_{ik}} C_j^{\gamma} m N_j + \sum_{j \in D_k} C_j^{\lambda}(r_{ik}^{R^{\lambda}}) N_j \right) \tag{7.5b}$$

$$+ \sum_{k \in U_i} y_{ik}^{\lambda F^{\lambda}} \sum_{j \in D_k} C_j^{\lambda}(r_{ik}^{F^{\lambda}}) N_j \tag{7.5c}$$

$$+ \sum_{k \in U_i} y_{ik}^{\lambda F^{\gamma}} \sum_{j \in D_k} C_j^{\lambda}(r_{ik}^{F^{\gamma}}) N_j \tag{7.5d}$$

Similar to (7.2), for every fault in node i, devices that can clear the fault must be located in U_i. Therefore, (7.5a) through (7.5d) indicate when a permanent fault is cleared by a CB, all the customers downstream to CB suffer from permanent outage. When a permanent fault is cleared by a recloser, all customers downstream to the recloser have sustained outage, and customers between the recloser and fault also have momentary outage. When a permanent fault is cleared by a fuse-saving fuse, customers downstream to the fuse-saving fuse have sustained outage. When a permanent fault is cleared by fuse-blowing fuse, customers downstream to the fuse-blowing fuse have sustained outage.

Note that the cost in (7.5) does not include the outage costs saved due to sectionalizing and restoration operations. The outage costs saved due to sectionalizing operation are defined in (7.6).

$$c^{sec} = \sum_{k \in U_i} \sum_{j \in B_{ik}} S^{S}_{ikj} \Big(\sum_{l \in B'_{jk}} C^{\lambda}_{l}(r^{R^{\lambda}}_{ik}) N_l \Big) \tag{7.6a}$$

$$+ \sum_{k \in U_i} \sum_{j \in B_{ik}} S^{F^{\lambda}}_{ikj} \Big(\sum_{l \in B'_{ij}} C^{\gamma}_{l} m N_l + \sum_{l \in D_k} C^{\lambda}_{l}(r^{R^{\lambda}}_{ik}) N_l \Big) \tag{7.6b}$$

$$+ \sum_{k \in U_i} \sum_{j \in B_{ik}} S^{F^{\gamma}}_{ikj} \Big(\sum_{l \in B'_{ij}} C^{\gamma}_{l} m N_l + \sum_{l \in D_k} C^{\lambda}_{l}(r^{R^{\lambda}}_{ik}) N_l \Big) \tag{7.6c}$$

(7.6a) through (7.6c) show that if the permanent fault is cleared by a recloser, and there is a sectionalizer between the recloser and the fault, then customers downstream to the recloser but not downstream to sectionalizer will be protected. When a permanent fault is cleared by a recloser and by a fuse between the recloser and fault, then customers downstream to the recloser can be protected.

The outage costs saved due to downstream restoration from alternate feeders and

intentional islanding operations are defined in (7.7).

$$
\begin{aligned}
c^{res} = \sum_{k\in U_i}\sum_{j\in D_i}\Bigg(& T^{CB}_{ikj}\sum_{l\in D_j} C^{\lambda}_{l}(r^{CB^{\lambda}}_{ik} - r^{CB}_{c})N_l \\
& + T^{R}_{ikj}\sum_{l\in D_j} C^{\lambda}_{l}(r^{R^{\lambda}}_{ik})N_l \\
& + T^{F^{\gamma}}_{ikj}\sum_{l\in D_j} C^{\lambda}_{l}(r^{F^{\gamma}}_{ik} - r^{F^{\gamma}}_{c})N_l \\
& + T^{F^{\lambda}}_{ikj}\sum_{l\in D_j} C^{\lambda}_{l}(r^{F^{\lambda}}_{ik} - r^{F^{\lambda}}_{c})N_l\Bigg) \qquad (7.7a) \\
& + \sum_{k\in U_i}\sum_{j\in D_i}\Bigg(G^{CB}_{ikj}\sum_{l\in D_j} C^{\lambda}_{l}(r^{CB^{\lambda}}_{ik} - r^{CB}_{c})N_l \\
& + G^{R}_{ikj}\sum_{l\in D_j} C^{\lambda}_{l}(r^{R^{\lambda}}_{ik})N_l \\
& + G^{F^{\gamma}}_{ikj}\sum_{l\in D_j} C^{\lambda}_{l}(r^{F^{\gamma}}_{ik} - r^{F^{\gamma}}_{c})N_l \\
& + G^{F^{\lambda}}_{ikj}\sum_{l\in D_j} C^{\lambda}_{l}(r^{F^{\lambda}}_{ik} - r^{F^{\lambda}}_{c})N_l\Bigg) \qquad (7.7b)
\end{aligned}
$$

(7.7a) indicates if a permanent fault is cleared, there is an IS downstream to the permanent fault, and there is at least one TS downstream to IS, then customers downstream to the IS will be restored. (7.7b) means if a permanent fault is cleared, there is an IS downstream to the permanent fault, and there are working DGs downstream to the IS, then customers downstream to the IS will be restored.

The remaining component of the objective function is the device cost C_D, shown in (7.8). The device cost consists of the cost for reclosers, fuse-blowing fuses, fuse-saving fuses, sectionalizers, ISs and CBs.

$$C_D = C_R \sum_{k \in I} x_k^R + C_{F^\gamma} \sum_{k \in I} x_k^{F^\gamma} + C_{F^\lambda} \sum_{k \in I} x_k^{F^\lambda} + C_S \sum_{k \in I} x_k^S + C_{IS} \sum_{k \in I} x_k^{IS} + C_{CB} \sum_{k \in I} x_k^{CB} \tag{7.8}$$

7.2.2 Constraints

Coordination of protective devices, sectionalizers, and restoration actions is enforced through the constraints detailed below. Constraint (7.9a) shows a CB is always placed in the root node to protect the system. Constraints (7.9b) and (7.9c) indicate fuses should not be used on the main line.

$$x_O^{CB} = 1 \tag{7.9a}$$

$$x_i^{F^\gamma} = 0 \qquad \forall i \in ML \tag{7.9b}$$

$$x_i^{F^\lambda} = 0 \qquad \forall i \in ML \tag{7.9c}$$

Constraints (7.10a) and (7.10b) indicate that devices must be placed in a node in order to clear faults downstream of that node.

$$y_{ik}^{tv} \leq x_k^v \qquad \forall (i,k), t \in \{\gamma, \lambda\}, v \in \{R, F^\gamma, CB\} \tag{7.10a}$$

$$y_{ik}^{\lambda F^\lambda} \leq x_k^{F^\lambda} \qquad \forall (i,k) \tag{7.10b}$$

Constraint (7.11) ensures the most downstream recloser upstream to a fuse also operates for a permanent fault.

$$y_{ij}^{\lambda v} \leq y_{ik}^{\lambda R} + (1 + \sum_{l \in B_{jk} - \{k\}} x_l^R - x_k^R)$$
$$\forall (i,k), j \in B_{ik}, v \in \{F^\gamma, F^\lambda\} \tag{7.11}$$

Constraint (7.12a) forces each permanent fault to be cleared by at least one device (CB, recloser, fuse-blowing fuse or fuse-saving fuse) and constraint (7.12b) forces each temporary fault to be cleared by a CB, recloser, or fuse-blowing fuse.

$$\sum_{k \in U_i} y_{ik}^{\lambda R} + \sum_{k \in U_i} y_{ik}^{\lambda F^\gamma} + \sum_{k \in U_i} y_{ik}^{\lambda F^\lambda} + \sum_{k \in U_i} y_{ik}^{\lambda CB} \geq 1 \quad \forall (i,k) \tag{7.12a}$$

$$\sum_{k \in U_i} y_{ik}^{\gamma R} + \sum_{k \in U_i} y_{ik}^{\gamma F^\gamma} + \sum_{k \in U_i} y_{ik}^{\gamma CB} = 1 \quad \forall (i,k) \tag{7.12b}$$

Constraint (7.13a) allows at most one device in each node. Constraints (7.13b) and (7.13c) control the total device cost and the total number of devices of each type, respectively.

$$x_i^R + x_i^{F^\gamma} + x_i^{F^\lambda} + x_i^S + x_i^{IS} + x_i^{CB} \leq 1 \quad \forall i \tag{7.13a}$$

$$\sum_{i \in I} \sum_{v \in V} C_v x_i^v \leq B \tag{7.13b}$$

$$\sum_{i \in I} x_i^v \leq n_v \quad \forall v \in V \tag{7.13c}$$

Constraints (7.14a)–(7.14c) control sectionalizing device operations and coordination with other devices. Constraints (7.14a) to (7.14b) indicate that only when a

sectionalizer or fuse is placed in node j, and the recloser in node k clears the fault in node i, can S_{ikj} be nonzero. Constraint (7.14c) requires that only if the permanent fault in i is cleared by a fuse in j, can S_{ikj} be nonzero.

$$S^v_{ikj} \leq x^v_j \qquad \forall (i,k), j \in B_{ik}, v \in \{S, F^\gamma, F^\lambda\} \tag{7.14a}$$

$$S^v_{ikj} \leq y^{\lambda R}_{ik} \qquad \forall (i,k), j \in B_{ik}, v \in \{S, F^\gamma, F^\lambda\} \tag{7.14b}$$

$$S^v_{ikj} \leq y^{\lambda v}_{ij} \qquad \forall (i,k), j \in B_{ik}, v \in \{F^\gamma, F^\lambda\} \tag{7.14c}$$

Constraints (7.15a) and (7.15b) control IS locations and coordination with other devices for downstream restoration from TSs. (7.15a) and (7.15b) make sure that only when there is an IS in j and a permanent fault in i is cleared by a recloser or fuse in k, can T_{ikj} be nonzero.

$$T^v_{ikj} \leq x^{IS}_j \quad \forall (i,k), j \in D_i, v \in \{R, F^\gamma, F^\lambda, CB\} \tag{7.15a}$$

$$T^v_{ikj} \leq y^{\lambda v}_{ik} \quad \forall (i,k), j \in D_i, v \in \{R, F^\gamma, F^\lambda, CB\} \tag{7.15b}$$

Constraints (7.16a) and (7.16b) control IS locations and coordination with other devices for downstream restoration from intentional islanding. (7.16a) and (7.16b) ensure only when there is an IS in j and a permanent fault in i is cleared by a recloser or fuse in k, can G_{ikj} be nonzero.

$$G^v_{ikj} \leq x^{IS}_j \quad \forall (i,k), j \in D_i, v \in \{R, F^\gamma, F^\lambda, CB\} \tag{7.16a}$$

$$G^v_{ikj} \leq y^{\lambda v}_{ik} \quad \forall (i,k), j \in D_i, v \in \{R, F^\gamma, F^\lambda, CB\} \tag{7.16b}$$

Constraints (7.17a)–(7.17c) requires that only one sectionalizing switch operates per restoration operation after a fault. Constraint (7.17a) indicates that for a permanent fault in i and a reacting recloser in k, there can be at most one operating sectionalizer or fuse in each path between the recloser and permanent fault. Constraint (7.17b) indicates that in each branch downstream to a permanent fault, there can be at most one IS working with a TS. (7.17c) indicates that in each branch downstream to a permanent fault, there can be at most one IS working with an intentional island.

$$S^{v}_{ikj} \leq 1 - S^{v'}_{ikd}$$
$$\forall (i,k), j \in B_{ik}, d \in B_{ij} - \{j\}, v, v' \in \{S, F^{\gamma}, F^{\lambda}\} \tag{7.17a}$$
$$T^{v}_{ikd} \leq 1 - T^{v}_{ikj}$$
$$\forall (i,k), j \in D_i, d \in D_j - \{j\}, v \in \{R, F^{\gamma}, F^{\lambda}, CB\} \tag{7.17b}$$
$$G^{v}_{ikd} \leq 1 - G^{v}_{ikj}$$
$$\forall (i,k), j \in D_i, d \in D_j - \{j\}, v \in \{R, F^{\gamma}, F^{\lambda}, CB\} \tag{7.17c}$$

Constraints (7.18a) and (7.18b) require that if a fuse at k is the closest protective device upstream to a fault at i, then the fuse at k clears the fault at i, unless the fuse is fuse-saving and the fault is temporary.

$$y^{\lambda F^{\lambda}}_{jk} \geq y^{\lambda F^{\lambda}}_{ik} - \sum_{l \in B_{jk} - \{k\}} \sum_{v \in \{R, F^{\lambda}, F^{\gamma}\}} x^{v}_{l}$$
$$\forall (i,k), j \in D_i \tag{7.18a}$$
$$y^{tF^{\gamma}}_{jk} \geq y^{t'F^{\gamma}}_{ik} - \sum_{l \in B_{jk} - \{k\}} \sum_{v \in \{R, F^{\gamma}\}} x^{v}_{l}$$
$$\forall (i,k), j \in D_i, t, t' \in \{\gamma, \lambda\} \tag{7.18b}$$

Constraint (7.19) restricts all variables to be binary.

$$x, y, S, T, G \in \{0, 1\} \tag{7.19}$$

The proposed formulation is derived such that additional constraints or operating conditions can be modeled similarly to the constraints shown above if required.

7.3 Case study: 10-node feeder

The first case study is performed on a small modified 10-node system with data such as overhead line failure rates and average connected load, from [97]. There is a TS to an alternate feeder in node 41 and a 800kW DG in node 32. The costs are scaled and are set as follows: $C_{CB} = 0.5$, $C_R = 20$, $C_{F^\gamma} = C_{F^\lambda} = 0.5$, $C_S = 10$ and $C_{IS} = 5.5$. The number of devices available is unlimited, except that only one CB is allowed.

The following assumptions are made. First, the switching time of automated sectionalizing devices is 5 min. Next, the component failure rate of overhead lines is taken to be 0.065 (f/yr/km). Further, the repair time of all overhead lines are considered to be 5 hrs. and fuse repair times are 1.1 hrs. After a fault is detected and cleared, the sectionalizer can open and the breaker reclose to allow restoration of all points between the supply and the sectionalizer. This is considered to be the switching time. The temporary failure rate is assumed to be 4 times that of the permanent failure rate.

7.3.1 Example Solution and Analysis

An example solution using the proposed formulation is shown in Fig. 7.2 with the budget is set to $B = 45$. It can be observed that a CB is placed at the root node 11 and a recloser in node 12. Fuse-blowing fuses are placed in node 21 and 22 and a fuse-saving fuse coordinated with the upstream recloser is placed in node 31. Isolating switches are placed in 14 and 32, allowing restoration from alternate feeders and intentional islands, respectively. A sectionalizer is placed in node 13 allowing coordination with the recloser for automatic upstream restoration. An analysis of the MILP model for this solution follows below.

The y variables indicate that a temporary fault in node 11 is cleared by the CB in 11. The temporary faults in node 21 and 22 are cleared by fuse-blowing fuses in node 21 and 22, respectively. The temporary faults in all the other nodes are cleared by the recloser in node 12. For permanent faults, the CB in node 11 clears the fault in its own node. The recloser in node 12 clears the permanent faults in all the nodes except 11. fuse-blowing fuses in node 21 and 22 clear the permanent fault in node 21 and 22 respectively. The fuse-saving fuse in node 31 detects the permanent fault in node 31 and 32. The S variables show that the sectionalizer and all the fuses are working with the recloser in node 12 if the permanent fault is in the node where the fuse (or sectionalizer) is located or in the downstream nodes without a fuse (or sectionalizer).

The x variables show that ISs are placed in node 14 and 32. The T variables control operation of these ISs for restoration from alternate feeders and indicate that for permanent upstream faults in nodes 11, 12, 13 and 14 cleared by the CB in node 11 or the recloser in node 12, the IS in node 14 can restore downstream nodes from the tie switch in node 41. Furthermore, the G variables control operation of ISs for restoration from intentional islands. There is an 800 kW DG in node 32, with

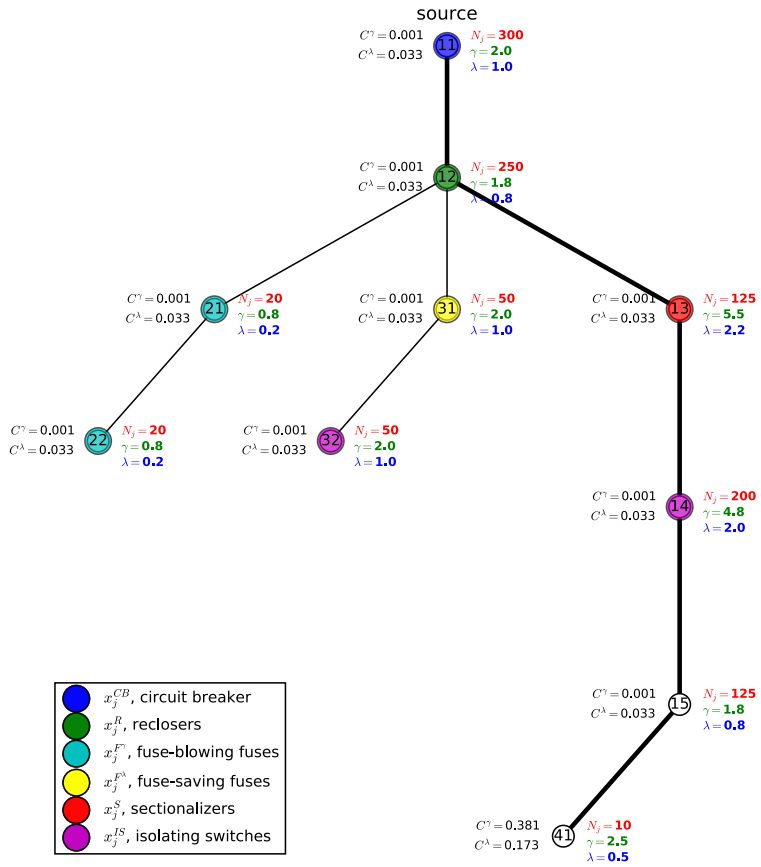

Figure 7.2: Solution of modified 10-node example with budget of 45 units.

a utilization $u = 0.8$, and a load in node 32 of 100 kW. Therefore, the IS in node 32 can be opened after fault clearing by devices in node 11, 12 and 31 allowing restoration by the DG in node 32, as $100 < 800 \times 0.8$. The final result shows the device cost is 43, fault cost is 503.74, and the total cost is 546.74.

7.3.2 Impact of Varying Budget

In this section, the proposed formulation is solved with same data as in the previous sections, except with a varying budget. The objective is to find the relationship between the device cost and fault cost, and to further explore how device cost, fault

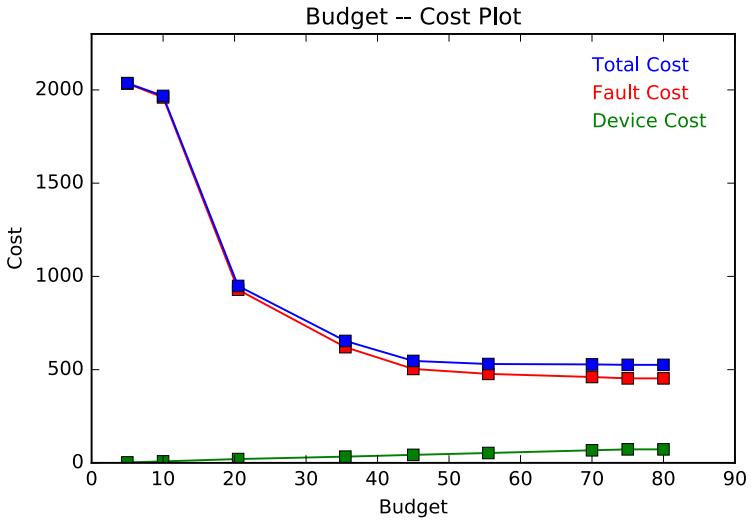

Figure 7.3: Cost – Budget Plot of modified 10-node system.

cost, and total cost change with the budget. Fig. 7.3 shows the expected costs due to faults decreases as more devices are allowed in the system resulting in increasing device costs. This is an intuitive result indicating that as more protective devices are allocated, the fewer loads are isolated from fault clearing operations. Fig. 7.3 also indicates that as the budget increases, the total expected cost of reliability (the sum of device cost and fault cost) will decrease. The higher budget enables larger expenditures on protective devices, thus reducing the fault cost. Furthermore, higher budget can be interpreted as a looser constraint, which will lead to a better objective function value.

7.3.3 Impact of DG Location and Capacity

Larger DG installations in any particular node will allow more loads to be restored by islanding after a fault clearing operation. However, the location and capacity of the DG will alter the optimal solution for placement of protective devices. In this section, the impact of DG location and capacity on the expected total cost of

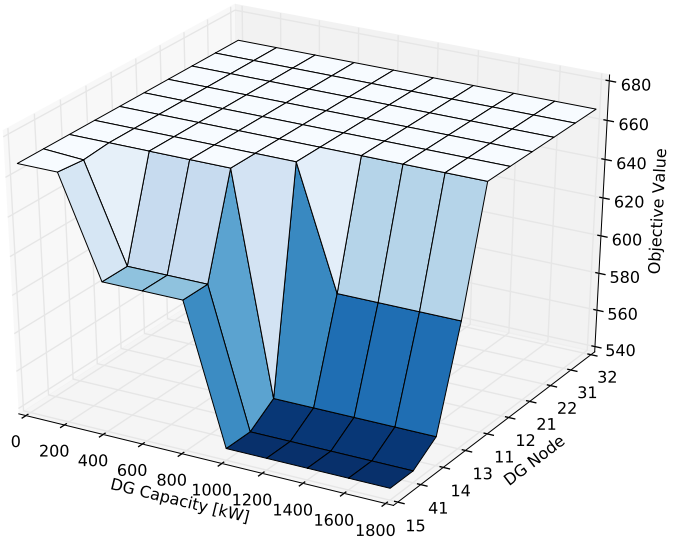

Figure 7.4: Impact of the capacity and location of a single DG on the objective function, total expected cost of reliability.

reliability is explored.

First, the budget is fixed at $B = 45$, corresponding to the example solution in Section 7.3.1, except with the TS in node 41 removed so that downstream restoration can only be supplied by DGs. The objective function value for the optimal solution at this baseline case is 666.28. A DG sized at a specific capacity is then added to a single node, and the optimization is solved obtaining a new optimal solution of protective device and switch allocations and a new objective function value. The same DG is then moved to a different node and the procedure is repeated sequentially for all nodes and DG capacities ranging from 0 to 1800 kW. The objective function value is then plotted against DG capacity and node location in Fig. 7.4.

It can be observed that in some nodes, e.g., nodes 13, 14, 15 and 41, the expected total cost of reliability decreases monotonically with DG capacity. In node 15 for example, placing a DG of only size 400 kW can lower the objective at the optimal solution by approximately 8%. This result indicates that having larger capacity of

DGs in these particular nodes can have a positive impact on the optimal reliability allocation, even for a fixed protection budget. It can also be observed in Fig. 7.4, that for some nodes the objective function value at the optimal solution does not change and is fixed at the baseline value of 668.28. For example, consider a DG placed in node 31. With large enough capacity, an island can be formed by placing an IS in upstream node 12. However, the proposed formulation determines that it is optimal to have a recloser in 12 instead. This result is intuitive as the recloser can clear all temporary faults downstream of node 12. Therefore, the optimal solution will not change even if DG capacities in such nodes are very large.

Finally, a similar study is performed locating DGs of the same capacity in three nodes simultaneously. For this 10-node system, there are subsequently 120 combinations of three node triplets. It can be observed from Fig. 7.5 that the objective can be significantly reduced by placing three DGs of 500 kW in the appropriate nodes. As with the single node case, placing DGs in some node triplets will not result in an improved optimal device allocation. The results in this section show the advantages of the proposed MILP formulation, allowing efficient comparison of multiple DG scenarios.

7.4 Case Study: 58-Node RBTS System

In this section, a case study is performed on a larger system for the 58-Node RBTS system to compare the solutions with prior formulations. The system contains 51 possible device locations, 7 possible CB locations, and 67 line segments or edges. It represents a substation supplying 7 radial feeders. Loads are connected at 38 different load points for a total of 4779 customers. The system data, such as interruption costs to customers, device costs, the probability of faults in each node, is provided in [102, 105–107].

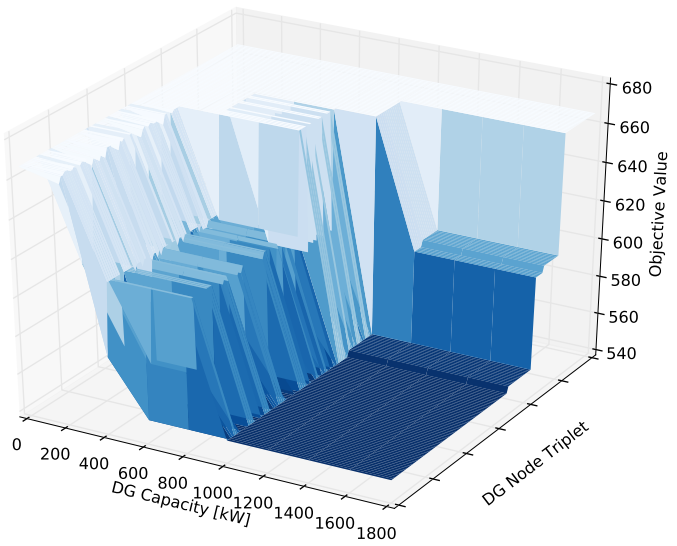

Figure 7.5: Impact of the capacity and location of three DGs of the same size on the total expected cost of reliability. A total of 120 node triplets are shown.

7.4.1 Comparison of Solutions

The proposed approach is first solved using the same device constraints as in prior works, i.e., allowing only a specified number of circuit breakers and isolating switches. The optimal solution is computed with an objective function value of 1762.27, device cost of 70, and fault cost of 1692. In comparison with the proposed approach, referred to as MILP*, solutions from prior works are shown in Table 7.2. For example, in comparison with the solution in [105], which uses metahueristic search approaches particle swarm optimization (PSO) and simulated annealing (SA), the proposed approach finds an improved solution. All methods shown in the comparison use a formulation with ECOST as the reliability metric in their respective objective functions.

The proposed formulation is solved again to show the impact to momentary interruptions by now allowing reclosers and sectionalizers. It should be noted that the

Table 7.2: Comparison with prior solutions For 58-Node System

Method	Switches	Total Cost	Fault Cost	Device Cost
MILP [106]	12	1875.71	1805	70
PSO [105]	12	1854.70	1784	70
SA [105]	14	1801.04	1720	81
MILP [99]	12	1786.24	1716	70
MILP [99]	14	1775.42	1694	81
MILP*	12	1762.27	1692	70
MILP**	12	671.03	487	183

prior formulations in Table 7.2 do not have this capability. The results are shown in Fig. 7.6 and Table 7.2, as MILP**, for the allocation of seven reclosers and twelve IS or sectionalizers. The size of each node is proportional to the product of the cost of permanent faults, load, and probability of faults. The optimal solution from the proposed algorithm is shown in the shaded circles. For comparison, the solution from [99] using an MILP formulation is shown with the cross markings to the right of each node.

It can be observed that many of the device locations are similar, however, circuit breakers have been replaced by reclosers for each feeder. Further, the proposed formulation includes the cost of both temporary and permanent faults in addition to considering sectionalizers. The result is a lower objective function value and a better allocation of switches and sectionalizers at nodes where costs are high. It can be observed that the ISs are placed in the nodes with the highest cost, allowing downstream restoration. For example, the prior solution places ISs at nodes 6, 31, and 39, however, the total cost at each load is relatively low. The proposed formulation more appropriately places ISs in 30 and 40, in addition to a sectionalizer at node 47, allowing upstream restoration.

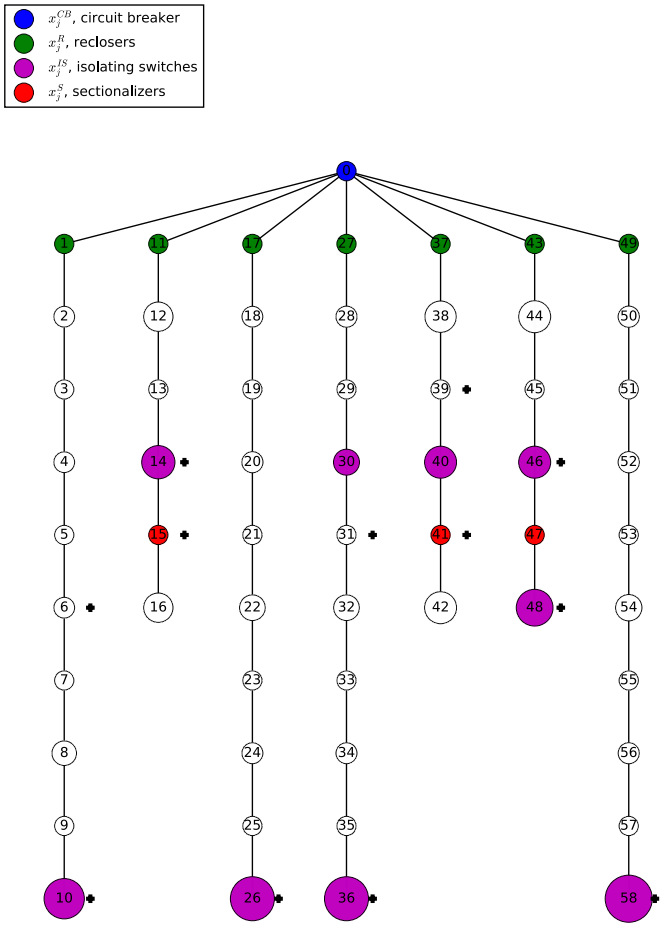

Figure 7.6: MILP** solution in RBTS Bus 4 test system allowing for circuit breakers, reclosers, sectionalizers, and ISs. A maximum of 12 ISs or sectionalizers are allowed and the device budget constraint has been removed. The comparison with a prior solution is shown with a plus sign next to each node.

7.5 Summary

An MILP formulation for protective device and switch allocation in distribution systems considering intentional islanding with distributed generation has been presented. The contribution is a formulation modeling the specific impact of each protection device (circuit breaker, recloser, sectionalizer, fuse) and isolating switch

type. The proposed approach is facilitated by representing the distribution system as a directed graph allowing efficient pre-processing of the network data. Numerical tests are performed on 10-node and 58-node feeders and shows computation of the optimal solution with improved objective function values. Furthermore, formulation as an MILP allows efficient computation of optimal solutions for multiple DG scenarios.

Chapter 8

Conclusions

Protective relays continue to play a critical role in the power system at all levels, including generation, transmission, and distribution. Because these devices control the actuation of circuit breakers, relays must operate with high reliability and selectively isolate faulted sections. Furthermore, power systems are growing in complexity and operating with additional uncertainty from increasing renewable generation. The research presented in this dissertation aims to improve power system protection under uncertainty while leveraging the increased computational power available to relays. The work focuses on both transmission and distribution protection. In this final chapter, the key results and contributions are summarized.

- *Model-Based Relaying Framework*

  A new framework has been proposed for supervising protective relay decisions by integrating the capability to quickly run circuit model simulations at the local relay level. The proposed method works in parallel with and supervises conventional distance relaying algorithms to improve discrimination between 3-phase faults and stressed conditions. Utilizing measurements of bus voltage magnitudes from adjacent buses, the proposed algorithm compares measured values with possible fault scenarios. The relay's trip or block decision is super-

vised and validated by real-time simulation results to maintain coordination with other relays. Simulation results in PSCAD demonstrate that the proposed framework has the potential to prevent undesired operation of remote backup relays during load encroachment, voltage instability, and power swings. A hardware prototype has been developed and tested a power system test-bed, demonstrating the capability of the approach.

- *Supervised Learning for Symmetrical Fault Detection During Power Swings*
  A supervised learning approach using effective feature selection criteria is proposed to augment discrimination of symmetrical faults during power swings. The approach is evaluated on power swing and fault scenario data from the IEEE 9-Bus system in PSCAD/EMTDC, consisting of scenarios where power swings enter zone 1 and where conventional relays are likely to fail. The analysis shows ensemble approaches using decision tree classifiers, such as random forest and gradient tree boosting, have better performance than other classifiers presented in literature. The approach further emphasizes analyzing the classifier's predicted probabilities and trade-offs between true-positive and false-positive rates instead of relying solely on the binary decision, resulting in a more interpretable model with similar performance.

- *Stochastic Optimization of Discrete Overcurrent Characteristics*
  A stochastic mixed-integer linear program (MILP) is proposed to minimize a relay's tripping time at discrete fault current intervals. The formulation takes into account the probabilistic nature of the fault current observed at each relay, which can be impacted by fault location, fault resistance, breaker failure, and DG output. Monte Carlo simulation is used to determine the empirical probabilities of each relay observing a particular fault current. The resulting MILP is shown to have fast solution times even for large systems

and thousands of fault scenarios. This allows for adaptive relaying to change tripping characteristics based on fault current probabilities. Compared to prior approaches, the proposed method results in an optimal solution with an average decrease of 10% in expected energy disconnected due to faults for 10,000 Monte Carlo fault scenarios.

- *Optimal Allocation of Protective Devices in Distribution Systems*

  A new MILP formulation is developed for allocating protective devices in distribution systems that comprehensively considers factors impacting reliability. The contribution includes improved computational tractability for large networks and allocation of multiple device types. The specific impact of each protection device (circuit breaker, recloser, sectionalizer, fuse) and isolating switch type is modeled, and the impact of residential distributed generators are modeled to allow islanding. Numerical tests are performed on 10-node and 58-node feeders and shows computation of the optimal solution with improved objective function values. Furthermore, formulation as an MILP allows efficient computation of optimal solutions for multiple DG scenarios.

Bibliography

[1] M. V. Venkatasubramanian, M. Kezunovic, and V. Vittal, "Detection, prevention and mitigation of cascading events," Power Systems Engineering Research Center, Tech. Rep., 2008.

[2] D. Novosel, G. Bartok, G. Henneberg, P. Mysore, D. Tziouvaras, and S. Ward, "Ieee psrc report on performance of relaying during wide-area stressed conditions," *Power Delivery, IEEE Transactions on*, vol. 25, no. 1, pp. 3–16, Jan 2010.

[3] M. Vaiman, P. Hines, J. Jiang, S. Norris, M. Papic, A. Pitto, Y. Wang, and G. Zweigle, "Mitigation and prevention of cascading outages: Methodologies and practical applications," in *2013 IEEE Power and Energy Society General Meeting (PES)*, July 2013, pp. 1–5.

[4] D. Tziouvaras, "Relay performance during major system disturbances," in *60th Annual Conference for Protective Relay Engineers, 2007.*, March 2007, pp. 251–270.

[5] CERC, "Report on the grid disturbance on 30th july 2012 and grid disturbance on 31st july 2012," Tech. Rep., 2012.

[6] "Final report on the august 14, 2003 blackout in the united states and canada: Causes and recommendations," U.S.-Canada Power System Outage Task Force, Tech. Rep., 2004.

[7] G. Andersson, P. Donalek, R. Farmer, N. Hatziargyriou, I. Kamwa, P. Kundur, N. Martins, J. Paserba, P. Pourbeik, J. Sanchez-Gasca, R. Schulz, A. Stankovic, C. Taylor, and V. Vittal, "Causes of the 2003 major grid blackouts in north america and europe, and recommended means to improve system dynamic performance," *IEEE Trans. on Power Systems*, vol. 20, no. 4, pp. 1922–1928, Nov 2005.

[8] UTCE, "Final report: System disturbance on november 2006," Tech. Rep., 2007.

[9] C. Li, Y. Sun, and X. Chen, "Recommendations to improve power system security: Lessons learned from the europe blackout on november 4," in *42nd International Universities Power Engineering Conference, 2007. UPEC 2007*, Sept 2007, pp. 529–533.

[10] M. Lwin, H. Padullaparti, and S. Santoso, "Transmission line protection for enhanced security: Including circuit models in relays," EPRI, Tech. Rep., 2014.

[11] "Performance of relaying during wide-area stressed conditions," IEEE Power Systems Relaying Committee, Tech. Rep., 2008.

[12] J. De La Ree, Y. Liu, L. Mili, A. Phadke, and L. Dasilva, "Catastrophic failures in power systems: Causes, analyses, and countermeasures," *Proceedings of the IEEE*, vol. 93, no. 5, pp. 956–964, May 2005.

[13] "Misoperations report," NERC Protection System Misoperations Task Force, Tech. Rep., 2013.

[14] 20% wind energy by 2030: Increasing wind energy's contribution to u.s. electricity supply. U.S. Department of Energy. [Online]. Available: http://www1.eere.energy.gov/wind/pdfs/41869.pdf

[15] U.s. wind industry third quarter 2014 market report. American Wind Energy Association. [Online]. Available: http://www.awea.org/Resources/Content.aspx?ItemNumber=6865

[16] Solar industry data. Solar Energy Industries Association. [Online]. Available: http://www.seia.org/research-resources/solar-industry-data

[17] G. Antonova, M. Nardi, A. Scott, and M. Pesin, "Distributed generation and its impact on power grids and microgrids protection," in *2012 65th Annual Conference for Protective Relay Engineers*, April 2012, pp. 152–161.

[18] S. Das, S. Santoso, and A. Maitra, "Effects of distributed generators on impedance-based fault location algorithms," in *2014 IEEE PES General Meeting*, July 2014, pp. 1–5.

[19] T. Boutsika and S. Santoso, "Quantifying short-term wind power variability using the conditional range metric," *IEEE Trans. on Sustainable Energy*, vol. 3, no. 3, pp. 369–378, July 2012.

[20] "Use of synchrophasor measurements in protective relaying applications," IEEE Power Systems Relaying Committee, Tech. Rep., 2013.

[21] J. L. Blackburn and T. J. Domin, *Protective Relaying Principles and Applications*, 4th ed. CRC Press, 2014.

[22] S. H. Horowitz and A. G. Phadke, *Power System Relaying*, 4th ed. Wiley, 2014.

[23] "Application of overreaching distance relays," IEEE Power Systems Relaying Committee, Tech. Rep., 2009.

[24] P. Nayak, A. Pradhan, and P. Bajpai, "Secured zone 3 protection during stressed condition," *IEEE Trans. on Power Delivery*, vol. 30, no. 1, pp. 89–96, Feb 2015.

[25] M. Jin and T. S. Sidhu, "Adaptive load encroachment prevention scheme for distance protection," *Electric Power Systems Research*, vol. 78, no. 10, pp. 1693 – 1700, 2008. [Online]. Available: http://www.sciencedirect.com/science/article/pii/S0378779608000722

[26] E. Bernabeu, J. Thorp, and V. Centeno, "Methodology for a security/dependability adaptive protection scheme based on data mining," *Power Delivery, IEEE Trans. on*, vol. 27, no. 1, pp. 104–111, Jan 2012.

[27] A. Urdaneta, R. Nadira, and L. Perez Jimenez, "Optimal coordination of directional overcurrent relays in interconnected power systems," *IEEE Trans. on Power Delivery*, vol. 3, no. 3, pp. 903–911, Jul 1988.

[28] B. Chattopadhyay, M. Sachdev, and T. Sidhu, "An on-line relay coordination algorithm for adaptive protection using linear programming technique," *Power Delivery, IEEE Trans. on*, vol. 11, no. 1, pp. 165–173, Jan 1996.

[29] H. Abyaneh, M. Al-Dabbagh, H. Karegar, S. Sadeghi, and R. Khan, "A new optimal approach for coordination of overcurrent relays in interconnected power systems," *Power Delivery, IEEE Transactions on*, vol. 18, no. 2, pp. 430–435, April 2003.

[30] C. So and K. Li, "Time coordination method for power system protection by evolutionary algorithm," *Industry Applications, IEEE Transactions on*, vol. 36, no. 5, pp. 1235–1240, Sep 2000.

[31] A. Noghabi, H. Mashhadi, and J. Sadeh, "Optimal coordination of directional overcurrent relays considering different network topologies using interval linear programming," *IEEE Trans. on Power Delivery*, vol. 25, no. 3, pp. 1348–1354, July 2010.

[32] M. Lwin, H. Padullaparti, and S. Santoso, "Model-based relaying supervision for mitigation of cascading outages," in *IEEE Power and Energy Society General Meeting*, July 2016, pp. 1–5.

[33] ——, "Supervision of power swing blocking using model-based distributed intelligence relaying framework," in *North American Power Symposium*, Sept 2016, pp. 1–6.

[34] M. Hernandez *et al.*, "Advances in embedded real-time simulation for power distribution systems," *IET Generation, Transmission & Distribution*, in Review.

[35] M. Lwin, H. Padullaparti, and S. Santoso, "Symmetrical fault detection during power swings: An interpretable supervised learning approach," in *IEEE Power and Energy Society General Meeting*, July 2017.

[36] M. Lwin, J. Guo, N. Dimitrov, and S. Santoso, "Stochastic optimization for discrete overcurrent relay tripping characteristics and coordination," *IEEE Trans. Smart Grid*, in Review.

[37] ——, "Protective device and switch allocation for reliability optimization with distributed generators," *IEEE Trans. Sustain. Energy*, in Review.

[38] J. Rao and A. Pradhan, "Logic-based supervised zone 3 decision using wide area information," in *Power Systems Conference (NPSC), 2014 Eighteenth National*, Dec 2014, pp. 1–6.

[39] P. Navalkar and S. Soman, "Secure remote backup protection of transmission lines using synchrophasors," *Power Delivery, IEEE Transactions on*, vol. 26, no. 1, pp. 87–96, Jan 2011.

[40] P. Kundu and A. Pradhan, "Synchrophasor-assisted zone 3 operation," *Power Delivery, IEEE Transactions on*, vol. 29, no. 2, pp. 660–667, April 2014.

[41] J. Glover, M. Sarma, and T. Overbye, *Power System Analysis and Design*, 4th ed. Thomson, 2008.

[42] "Power swing and out-of-step considerations on transmission lines," Power Systems Engineering Research Center, Tech. Rep., 2005.

[43] S. Lotfifard, J. Faiz, and M. Kezunovic, "Detection of symmetrical faults by distance relays during power swings," *IEEE Trans. Power Del.*, vol. 25, no. 1, pp. 81–87, Jan 2010.

[44] E. Kimbark, *Power System Stability*. John Wiley & Sons, 1995, no. vol. 1-3.

[45] J. Berdy, "Application of out-of-step blocking and tripping relays," GER-3180, Tech. Rep.

[46] "Protection system response to power swings," NERC, Tech. Rep., 2013.

[47] A. G. Phadke and J. S. Thorpe, *Computer Relaying for Computer Systems*. Wiley, 2009.

[48] K. Gadgil, "A numerical protection relay solution," Texas Instriuments, Tech. Rep., 2010.

[49] R. C. Dugan and T. E. McDermott, "An open source platform for collaborating on smart grid research," in *2011 IEEE Power and Energy Society General Meeting*, July 2011, pp. 1–7.

[50] T. A. Davis and E. P. Natarajan, "Sparse matrix methods for circuit simulation problems," in *Scientific Computing in Electrical Engineering SCEE 2010*. Springer, 2012, pp. 3–14.

[51] B. Mahamedi and J. G. Zhu, "A novel approach to detect symmetrical faults occurring during power swings by using frequency components of instantaneous three-phase active power," *IEEE Trans. Power Del.*, vol. 27, no. 3, pp. 1368–1376, July 2012.

[52] J. G. Rao and A. K. Pradhan, "Differential power-based symmetrical fault detection during power swing," *IEEE Trans. Power Del.*, vol. 27, no. 3, pp. 1557–1564, July 2012.

[53] ——, "Power-swing detection using moving window averaging of current signals," *IEEE Trans. Power Del.*, vol. 30, no. 1, pp. 368–376, Feb 2015.

[54] A. R. Sedighi, M. R. Haghifam, O. P. Malik, and M. H. Ghassemian, "High impedance fault detection based on wavelet transform and statistical pattern recognition," *IEEE Trans. Power Del.*, vol. 20, no. 4, pp. 2414–2421, Oct 2005.

[55] N. Perera and A. D. Rajapakse, "Recognition of fault transients using a probabilistic neural-network classifier," *IEEE Trans. Power Del.*, vol. 26, no. 1, pp. 410–419, Jan 2011.

[56] Z. Moravej, M. Pazoki, and M. Khederzadeh, "New pattern-recognition method for fault analysis in transmission line with UPFC," *IEEE Trans. Power Del.*, vol. 30, no. 3, pp. 1231–1242, June 2015.

[57] K. Seethalekshmi, S. N. Singh, and S. C. Srivastava, "A classification approach using support vector machines to prevent distance relay maloperation under power swing and voltage instability," *IEEE Trans. Power Del.*, vol. 27, no. 3, pp. 1124–1133, July 2012.

[58] A. Swetapadma and A. Yadav, "Data-mining-based fault during power swing identification in power transmission system," *IET Science, Measurement Technology*, vol. 10, no. 2, pp. 130–139, 2016.

[59] N. G. Chothani, B. R. Bhalja, and U. B. Parikh, "New support vector machine-based digital relaying scheme for discrimination between power swing and fault," *IET Generation, Transmission Distribution*, vol. 8, no. 1, pp. 17–25, Jan 2014.

[60] T. Guo and J. V. Milanović, "Online identification of power system dynamic signature using pmu measurements and data mining," *IEEE Trans. Power Syst.*, vol. 31, no. 3, pp. 1760–1768, May 2016.

[61] P. Kundur, N. J. Balu, and M. G. Lauby, *Power system stability and control*. McGraw-Hill.

[62] P. M. Anderson and A. A. Fouad, *Power system control and stability*. Iowa State University Press.

[63] N. Fischer *et al.*, "Tutorial on power swing blocking and out-of-step tripping," in *39th Annual Western Protective Relay Conference*, 2012, pp. 108–119.

[64] H. Peng, F. Long, and C. Ding, "Feature selection based on mutual information criteria of max-dependency, max-relevance, and min-redundancy," *IEEE Trans. Pattern Anal. Mach. Intell.*, vol. 27, no. 8, pp. 1226–1238, Aug 2005.

[65] C. M. Bishop, *Pattern Recognition and Machine Learning*. Springer.

[66] T. Hastie, R. Tibshirani, and J. Friedman, *The Elements of Statistical Learning*. Springer.

[67] F. Pedregosa *et al.*, "Scikit-learn: Machine learning in Python," *Journal of Machine Learning Research*, vol. 12, pp. 2825–2830, 2011.

[68] F. Trindade, K. do Nascimento, and J. Vieira, "Investigation on voltage sags caused by dg anti-islanding protection," *IEEE Trans. on Power Delivery*, vol. 28, no. 2, pp. 972–980, April 2013.

[69] EPRI, "High-penetration PV integration handbook for distribution engineers," Tech. Rep., 2016.

[70] R. A. Walling *et al.*, "Summary of distributed resources impact on power delivery systems," *IEEE Trans. Power Del.*, vol. 23, pp. 1636–1644, July 2008.

[71] A. Girgis and S. Brahma, "Effect of distributed generation on protective device coordination in distribution system," in *2001 Large Engineering Systems Conf. on Power Engineering*, pp. 115–119.

[72] M. E. Baran, H. Hooshyar, Z. Shen, and A. Huang, "Accommodating high PV penetration on distribution feeders," *IEEE Trans. Smart Grid*, vol. 3, no. 2, pp. 1039–1046, June 2012.

[73] H. Yazdanpanahi, Y. W. Li, and W. Xu, "A new control strategy to mitigate the impact of inverter-based DGs on protection system," *IEEE Trans. Smart Grid*, vol. 3, no. 3, pp. 1427–1436, Sept 2012.

[74] N. Rajaei and M. M. A. Salama, "Management of fault current contribution of synchronous DGs using inverter-based DGs," *IEEE Trans. Smart Grid*, vol. 6, no. 6, pp. 3073–3081, Nov 2015.

[75] A. Noghabi, J. Sadeh, and H. Mashhadi, "Considering different network topologies in optimal overcurrent relay coordination using a hybrid ga," *IEEE Trans. on Power Delivery*, vol. 24, no. 4, pp. 1857–1863, Oct 2009.

[76] E. Dehghanpour, H. Karegar, R. Kheirollahi, and T. Soleymani, "Optimal coordination of directional overcurrent relays in microgrids by using cuckoo-linear optimization algorithm and fault current limiter," *IEEE Trans. Smart Grid*, vol. PP, no. 99, pp. 1–1, 2016.

[77] D. S. Alkaran, M. R. Vatani, M. J. Sanjari, G. B. Gharehpetian, and M. S. Naderi, "Optimal overcurrent relay coordination in interconnected networks by using fuzzy-based GA method," *IEEE Trans. Smart Grid*, vol. PP, no. 99, pp. 1–1, 2016.

[78] H. Zhan *et al.*, "Relay protection coordination integrated optimal placement and sizing of distributed generation sources in distribution networks," *IEEE Trans. Smart Grid*, vol. 7, no. 1, pp. 55–65, Jan 2016.

[79] I. Xyngi and M. Popov, "An intelligent algorithm for the protection of smart power systems," *IEEE Trans. Smart Grid*, vol. 4, no. 3, pp. 1541–1548, Sept 2013.

[80] P. Mahat, Z. Chen, B. Bak-Jensen, and C. L. Bak, "A simple adaptive overcurrent protection of distribution systems with distributed generation," *IEEE Trans. Smart Grid*, vol. 2, no. 3, pp. 428–437, Sept 2011.

[81] IBM ILOG CPLEX Optimizer 12.6.2.0. [Online]. Available: https://www-01.ibm.com/software/commerce/optimization/cplex-optimizer/

[82] S. Santoso, *Fundamentals Of Electric Power Quality*, Winter ed., 2012.

[83] A. Janssen, D. Makareinis, and C. E. Sölver, "International surveys on circuit-breaker reliability data for substation and system studies," *IEEE Trans. Power Del.*, vol. 29, pp. 808–814, April 2014.

[84] H. Kameda *et al.*, "Estimation of replacement of numerical relay systems from reliability analysis," in *2011 Int. Conf. on Advanced Power System Automation and Protection*, vol. 1, pp. 114–119.

[85] T. A. Short, *Electric Power Distribution Handbook*, 2nd ed. CRC Press.

[86] H. B. Funmilayo, J. A. Silva, and K. L. Butler-Purry, "Overcurrent protection for the IEEE 34-node radial test feeder," *IEEE Trans. Power Del.*, vol. 27, pp. 459–468, April 2012.

[87] D. S. Kumar, D. Srinivasan, and T. Reindl, "A fast and scalable protection scheme for distribution networks with distributed generation," *IEEE Trans. Power Del.*, vol. 31, pp. 67–75, Feb 2016.

[88] Y. Wang *et al.*, "Online overvoltage prevention control of photovoltaic generators in microgrids," *IEEE Trans. Smart Grid*, vol. 3, pp. 2071–2078, Dec 2012.

[89] W. H. Kersting, "Radial distribution test feeders," in *2001 IEEE Power Engineering Society Winter Meeting.*, vol. 2, pp. 908–912 vol.2.

[90] Y. M. Atwa *et al.*, "Optimal renewable resources mix for distribution system energy loss minimization," *IEEE Trans. Power Syst.*, vol. 25, pp. 360–370, Feb 2010.

[91] A. dos Santos and M. C. de Barros, "Stochastic modeling of power system faults," *Electric Power Systems Research*, vol. 126, pp. 29–37, Sep 2015.

[92] OpenDSS 7.6.5. [Online]. Available: https://sourceforge.net/projects/electricdss/

[93] E. Lorenz *et al.*, "Irradiance forecasting for the power prediction of grid-connected photovoltaic systems," *IEEE J. Sel. Topics Appl. Earth Observ. in Remote Sens.*, vol. 2, pp. 2–10, March 2009.

[94] P. M. de Quevedo *et al.*, "Contingency assessment and network reconfiguration in distribution grids including wind power and energy storage," *IEEE Trans. Sustain. Energy*, vol. 6, no. 4, pp. 1524–1533, Oct 2015.

[95] K. Zou *et al.*, "An analytical approach for reliability evaluation of distribution systems containing dispatchable and nondispatchable renewable dg units," *IEEE Trans. Smart Grid*, vol. 5, no. 6, pp. 2657–2665, Nov 2014.

[96] Y. M. Atwa and E. F. El-Saadany, "Reliability evaluation for distribution system with renewable distributed generation during islanded mode of operation," *IEEE Trans. Power Syst.*, vol. 24, no. 2, pp. 572–581, May 2009.

[97] F. Soudi and K. Tomsovic, "Optimized distribution protection using binary programming," *IEEE Trans. Power Del.*, vol. 13, no. 1, pp. 218–224, Jan 1998.

[98] R. Billinton and S. Jonnavithula, "Optimal switching device placement in radial distribution systems," *IEEE Trans. Power Del.*, vol. 11, no. 3, pp. 1646–1651, Jul 1996.

[99] A. Abiri-Jahromi, M. Fotuhi-Firuzabad, M. Parvania, and M. Mosleh, "Optimized sectionalizing switch placement strategy in distribution systems," *IEEE Trans. Power Del.*, vol. 27, no. 1, pp. 362–370, Jan 2012.

[100] V. F. Martins and C. L. T. Borges, "Active distribution network integrated planning incorporating distributed generation and load response uncertainties," *IEEE Trans. Power Syst.*, vol. 26, no. 4, pp. 2164–2172, Nov 2011.

[101] E. Zambon *et al.*, "A novel nonlinear programming model for distribution protection optimization," *IEEE Trans. Power Del.*, vol. 24, no. 4, pp. 1951–1958, Oct 2009.

[102] J.-M. Sohn, S.-R. Nam, and J.-K. Park, "Value-based radial distribution system reliability optimization," *IEEE Trans. Power Syst.*, vol. 21, no. 2, pp. 941–947, May 2006.

[103] M. F. McGranaghan, "Quantifying reliability and service quality for distribution systems," *IEEE Trans. Ind. Appl.*, vol. 43, no. 1, pp. 188–195, Jan 2007.

[104] A. Pregelj, M. Begovic, and A. Rohatgi, "Recloser allocation for improved reliability of dg-enhanced distribution networks," *IEEE Trans. Power Syst.*, vol. 21, no. 3, pp. 1442–1449, Aug 2006.

[105] A. Moradi and M. Fotuhi-Firuzabad, "Optimal switch placement in distribution systems using trinary particle swarm optimization algorithm," *IEEE Transactions on Power Delivery*, vol. 23, no. 1, pp. 271–279, Jan 2008.

[106] A. Heidari, V. G. Agelidis, and M. Kia, "Considerations of sectionalizing switches in distribution networks with distributed generation," *IEEE Trans. Power Del.*, vol. 30, no. 3, pp. 1401–1409, June 2015.

[107] R. N. Allan, R. Billinton, I. Sjarief, L. Goel, and K. S. So, "A reliability test system for educational purposes-basic distribution system data and results," *IEEE Transactions on Power Systems*, vol. 6, no. 2, pp. 813–820, May 1991.

Vita

Min Naing Lwin was born in Macomb, Illinois on April 10, 1986. He received the B.S. degree from the University of Illinois at Urbana-Champaign in 2008 and the M.S.E. degree from the University of Texas at Austin in 2013, both in electrical engineering. From 2008 to 2011, he worked as an Associate Electrical Engineer at Sargent & Lundy in Chicago. His research interests include power system protection, discrete optimization, and machine learning.

Permanent address: m.lwin@utexas.edu